Compressive Sensing for Multi-channel and Large-scale MIMO Networks

Sinh L. H. Nguyen

A Thesis

in

The Department

of

Electrical and Computer Engineering

Presented in Partial Fulfillment of the Requirements

for the Degree of Doctor of Philosophy at

Concordia University

Montreal, Quebec, Canada

August 2013

CONCORDIA UNIVERSITY

SCHOOL OF GRADUATE STUDIES

This is to certify that the thesis prepared

By: **Sinh L. H. Nguyen**

Entitled: **Compressive Sensing for Multi-channel and Large-scale MIMO Networks**

and submitted in partial fulfillment of the requirements for the degree of

DOCTOR OF PHILOSOPHY (Electrical & Computer Engineering)

complies with the regulations of the University and meets the accepted standards with respect to originality and quality.

Signed by the final examining committee:

_____ Chair
Dr. B. Jaumard

_____ External Examiner
Dr. H. Leib

_____ External to Program
Dr. X. Zhou

_____ Examiner
Dr. W. Hamouda

_____ Examiner
Dr. M.R. Soleymani

_____ Thesis Supervisor
Dr. A. Ghrayeb

Approved by _____
Dr. A.R. Sebak, Graduate Program Director

August 23, 2013

_____
Dr. Christopher W. Trueman, Interim Dean
Faculty of Engineering and Computer Science

Abstract

Compressive Sensing for Multi-channel and Large-scale MIMO Networks

Sinh L. H. Nguyen, Ph.D.

Concordia University, 2013

Compressive sensing (CS) is a revolutionary theory that has important applications in many engineering areas. Using CS, sparse or compressible signals can be recovered from incoherent measurements with far fewer samples than the conventional Nyquist rate. In wireless communication problems where the sparsity structure of the signals and the channels can be explored and utilized, CS helps to significantly reduce the number of transmissions required to have an efficient and reliable data communication. The objective of this thesis is to study new methods of CS, both from theoretical and application perspectives, in various complex, multi-channel and large-scale wireless networks. Specifically, we explore new sparse signal and channel structures, and develop low-complexity CS-based algorithms to transmit and recover data over these networks more efficiently.

Starting from the theory of *sparse vector approximation* based on CS, a compressive multiple-channel estimation (CMCE) method is developed to estimate multiple sparse channels simultaneously. CMCE provides a reduction in the required overhead for the estimation of multiple channels, and can be applied to estimate the composite channels of two-way relay channels (TWRCs) with sparse intersymbol interference (ISI). To improve end-to-end error performance of the networks, various iterative estimation and decoding schemes based on CS for ISI-TWRC are proposed, for both modes of cooperative relaying: *Amplify-and-Forward* (AF) and *Decode-and-Forward* (DF). Theoretical results including the *Restricted Isometry Property* (RIP) and low-coherent condition of the discrete pilot signaling matrix, the performance guarantees, and the convergence of the schemes are

presented in this thesis. Numerical results suggest that the error performances of the system is significantly improved by the proposed CS-based methods, thanks to the awareness of the sparsity feature of the channels.

Low-rank matrix approximation, an extension of CS-based sparse vector recovery theory, is then studied in this research to address the channel estimation problem of large-scale (or massive) multiuser (MU) multiple-input multiple-output (MIMO) systems. A low-rank channel matrix estimation method based on nuclear-norm regularization is formulated and solved via a dual quadratic semi-definite programming (SDP) problem. An explicit choice of the regularization parameter and useful upper bounds of the error are presented to show the efficacy of the CS method in this case. After that, both the uplink channel estimation and a downlink data precoding of massive MIMO in the interference-limited multicell scenarios are considered, where a CS-based rank-q channel approximation and multicell precoding method are proposed. The results in this work suggest that the proposed method can mitigate the effects of the pilot contamination and intercell interference, hence improves the achievable rates of the users in multicell massive MIMO systems. Finally, various low-complexity greedy techniques are then presented to confirm the efficacy and feasibility of the proposed approaches in practical applications.

To my parents,

who have constantly loved and supported me.

Acknowledgements

I would like to gratefully thank my research supervisor, Professor Ali Ghrayeb for giving me the opportunity of pursuing my doctoral program under his supervision at Concordia University, for his inspiration, consistent guidance, and generous support throughout my doctoral studies. I have learned greatly from his remarkable knowledge and research enthusiasm. He has also helped me in critically reviewing this thesis and vastly enriching it with his very helpful comments.

I am grateful to my thesis committee members and examiners: Professor Reza Soleymani and Professor Walaa Hamouda (ECE Department, Concordia University), Professor Xiaowen Zhou (Mathematics Department, Concordia University), and Professor Harry Leib (ECE Department, Mcgill University), for their time of reading and reviewing my Ph.D. work, for their very valuable and constructive comments for the thesis.

I would like to gratefully acknowledge Concordia University, Natural Sciences and Engineering Research Council of Canada (NSERC), and Qatar Foundation, for the financial supports during this research work.

I am grateful for the beautiful time spent with my friends in Montreal, for being surrounded by wonderful colleagues and staff in the ECE Department at Concordia University, during these past four years.

Lastly, I want to thank Mom and Dad, my brother and my sister, for their constant love, encouragement and support in all my pursuits. Without their support and encouragement, the accomplishment of this thesis would not have been possible.

Contents

List of Figures

List of Tables

List of Acronyms

AF	Amplify-and-Forward
AoA	Angle of Arrival
APP	A Posteriori Probability
AWGN	Additive White Gaussian Noise
BER	Bit-Error Rate
BPDN	Basic Pursuit Denoising
BPSK	Binary Phase Shift Keying
BS	Base Station
CF	Compress-and-Forward
CMCE	Compressive Multi-Channel Estimation
CoSaMP	Compressive Sampling Matching Pursuit
CRB	Cramér-Rao Bound
CS	Compressive Sensing
CSCE	Compressive Single-Channel Estimation
CSI	Channel State Information

DE	Density Evolution
DF	Decode-and-Forward
FRI	Finite Rate of Innovation
IBI	Inter-Block Interference
IHT	Iterative Hard Thresholding
I.I.D.	Independent and Identically Distributed
ISI	Intersymbol Interference
LDPC	Low-Density Parity Check
LLR	Log-Likelihood Ratio
LS	Least Squares
LTE	Long Term Evolution
MAC	Multiple Access Channel
MAP	Maximum A Posteriori
MCP	Multi-Cell Processing
MIMO	Multiple-Input Multiple-Output
MMSE	Minimum Mean-Squared Error
MP	Message Passing
MRI	Magnetic Resonance Imaging
MS	Mobile Station
MSE	Mean-Squared Error

MUD	Multiuser Detection
NNM	Nuclear Norm Minimization
OFDM	Orthogonal Frequency Division Multiplexing
OMP	Orthogonal Matching Pursuit
ORC	Oracle
PA	Pilot-Assisted
PAPR	Peak-to-Average Power Ratio
RA	Radio Frequency
RE	Restricted Eigenvalue
RIP	Restricted Isometry Property
SC/MMSE	Soft-Cancellation Minimum Mean Square Error
SCS	Sparse Common-support Scenario
SDP	Semi-Definite Programming
SISO	Soft-Input Soft-Output
SNR	Signal-to-Noise Ratio
SVP	Singular Value Projection
TWRC	Two-Way Relay Channel
UT	User Terminal

Chapter 1

Introduction

1.1 Compressive Sensing

In recent years, there has been a growing interest in reconstructing sparse signals from a small number of incoherent linear measurements. This method, referred to in the literature as *compressive sensing* (CS) or *compressed sampling* [1], [2], has proven, under suitable conditions, to be superior to traditional signal reconstruction techniques. The rationale behinds CS is that certain classes of sparse or compressible signals in some basis, where most of their coefficients are zero or small and only a few are large, can be exactly or sufficiently accurately reconstructed with high probability (w.h.p.). The measurement process projects the signals onto a small set of vectors, or dictionary, which is incoherent with the sparsity basis. The reconstruction of the entire signals is then done by using some optimization algorithm or greedy-based techniques that, from these projections, find the sparsest representation consistent with the acquired measurements.

CS was first proposed as a new low-rate image and signal acquisition method, which operates at a rate significantly lower than the Shannon-Nyquist rate [3]. It is then developed as a novel and efficient tool to solve a class of more general under-determined inverse problems. The main advantage of CS is that it potentially reduces the number of

measurements required to acquire sparse or compressible signals, or accurately solve the ill-posed, under-determined system of linear equations where the solution is sparse. This has a huge impact and completely changes the way we capture and communicate sparse signals, such as natural images or communication signals into a much more efficient way.

While its theory is being continually studied and developed by both mathematics and engineering societies, CS has been successfully applied to many topics ranging from image acquisition, machine learning, data communication, sampling physics, sensor networks and computational biology. For instance, CS has found its way in astronomy as an effective tool for enabling transmitting astronomical images with high accuracy [4]. The notion here is that the size of astronomical data is huge and it needs to be transmitted in a short period of time. CS theory helps in this regard by exploiting the sparsity in images, resulting in compressing images/signals at low rates while being able to reconstruct them at the receiver end with high accuracy. The same is true for medical imaging, with emphasis on dynamic magnetic resonance imaging (MRI) imaging [5]. Along similar lines, CS has proven effective in computational photography, which led to smaller, cheaper and more effective digital cameras [6]. Another distinct field that benefited from CS is DNA identification [7], whereby one can achieve accurate identification of large numbers of genetic sequences in an environment. Furthermore, CS has been shown to be beneficial for structure recovery in biological networks [8].

1.2 Compressive Sensing in Communications

More recently, albeit limited, CS has found its charm in the communications field as well [9–12]. The premise here is that CS allows for accurate system parameter estimation with less training, resulting in improved bandwidth efficiency and system performance. One of the immediate applications of CS in communications is the pilot-assisted (PA) sparse intersymbol interference (ISI) channel estimation, in which the channel impulse

response has a long delay spread but with only a small number of dominant taps. This type of channels occurs in many practical radio-frequency communication scenarios, such as underwater acoustic communications (as shown in Fig. 1.1), or communications taking place in rural areas. By exploring the sparsity models of the channels in the time or frequency domain, one can reduce significantly the number of pilot symbols needed to obtain a sufficiently accurate estimation, resulting in a throughput improvement of the system.

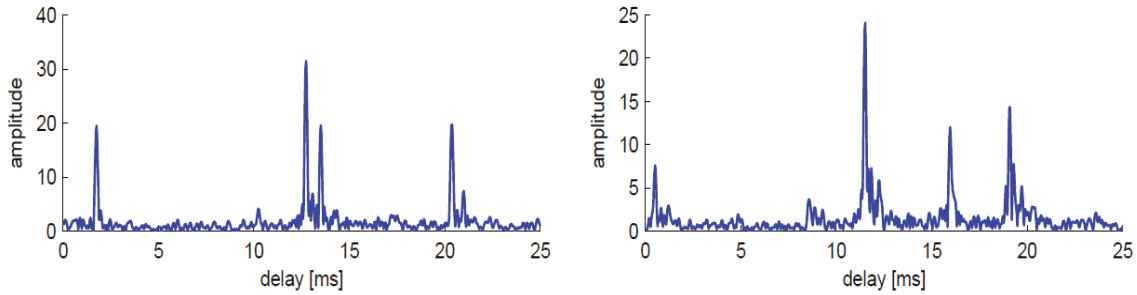

Figure 1.1: Example of sparse UWA channel [GLINT'08 Experiment].

CS techniques can also be applied to multi-user communications with a sparse active profile, i.e., when only a small subset of users actively communicate during any given time slot. Applications in this direction can be found in many topics including sparse event detection [13], reduced-dimensionality of multiuser detection (MUD) [14], cognitive spectrum sensing [15] and smart power grid [16]. In [13], based on the fact that in large wireless sensor networks, the events are relatively sparse compared with the number of sources due to the deployment cost, limited number of sensor and energy constraints, the authors formulate the sparse event detection as a CS problem. The CS-based detection scheme is then proposed using a Bayesian method heuristically, significantly reducing the sampling rate without sacrificing the system performance. A similar sparsity signal modeling is used in [14] by exploiting the fact that the number of active users is typically small relative to the total number of users in the system. Also, an analog CS algorithm is proposed to decrease the number of required correlation branches at the receiver front-

end, while still achieving performance similar to that of the conventional matched-filter bank. In [15], the sparsity model is introduced by the narrow-band nature of transmit power spectral densities relative to the broad swaths of usable spectrum and the sparsely located active radios in the operational space. A distributed spectrum sensing based on the least absolute shrinkage and selection operator (also called LASSO) algorithm [17] is used to detect the unknown positions of transmitting cognitive radios, and reduce spatial and frequency spectrum leakage by 15 dB relative to the least squares (LS) counterparts. The sparsity model in [16] is based on the fact that the number of smart meters is large and the data burst is sparse, i.e., only a small fraction of the smart meters report their power loads at the same time. The authors then use a CS technique to solve the smart wireless meter reading, allowing the active meters to be transmitted simultaneously using a random sequence, and still achieve the privacy and integrity of the system.

Recently, some connections between error correcting codes and CS are also exploited [18], where low-density parity check (LDPC) codes are used in the CS system, in which the message passing (MP) decoding algorithm can be used as the reconstruction algorithm. Specifically, the strictly-sparse signal reconstruction problem is formulated as a decoding problem over large finite alphabets in the high-rate regime, with the oversampling ratio of the codes is the number of measurements divided by the number of non-zero elements. The LDPC coded CS-based system with MP decoding then can be analyzed using density evolution (DE) analysis for the randomized reconstruction, or the stopping set analysis for the uniform (in probability) reconstruction.

Other communication applications that have benefited from CS include wireless sensor networks [19], UWA communications assuming orthogonal frequency division multiplexing (OFDM) [20], radar communication/imaging [21], wideband cognitive radio [22] and ultra wideband (UWB) communications [23].

1.3 Research Motivation and Objectives

Motivated by the great potential of CS, this thesis aims to develop new techniques and applications of CS in wireless communications. Specifically, we invoke CS into more complex multi-channel, cooperative and large-scale wireless communication networks, including the multiple access channel (MAC), two-way relay channels (TWRCs) [24–26], and multiple users and large multiple-input multiple-output (MIMO) systems [27, 28]. These wireless networks are underlying models of many on-going research topics, and are expected to play a major role towards achieving the target of high data rates that would be offered by future communication networks. Especially as the demand for data rate transmission is increasing, and the scarcity spectrum problem is becoming an important issue, the higher data rates, better link reliability, and better spectral-energy efficiency tradeoff that the considered systems bring are crucial.

There are many challenges for CS to be applied to the above communication problems. Firstly, different from the ones in traditional point-to-point scenarios, the problems of channel learning and exchanging in multiple channels and cooperative networks are more challenging, due to the large number of channel parameters resulting from the large dimensions of the problem. The problem becomes even more difficult for the case of large multiuser MIMO as the numbers of base station (BS) antennas and user terminals (UTs) grow beyond a hundred. The challenge here is that we need to estimate the channels, within a limited coherence time, with a minimum number of training signals to achieve the desired latency, energy constraints, and bandwidth efficiencies. Secondly, also different from most of the previous works on CS for point-to-point channels, it is hard to recognize the implicit sparsity model, to prove conditions required for CS to be applicable, as well as to derive the performance guarantee bounds for CS solutions. Thirdly, it not easy to find the most suitable CS algorithm for each of the problems that are required not only to provide good results but also to be done with affordable computational complexity. Finally, when considering the channel learning/estimation along with the data decod-

ing/detection for these channels using CS, we need to consider all of the complexity, error performance of the estimator, decoder, and precoder in a unified framework, and look for the overall improvement of the end-to-end performance.

The objective of this work is to directly address the above practical challenges. That is, we explore the new signal and channel structures in these system and channel models where CS can kick in. In several cases, we provide theoretical results of the sufficient conditions for the measurement process and the performance guarantee bounds using CS reconstruction methods. Furthermore, we propose new joint estimation and data detection schemes and analyze the end-to-end error performance of the proposed schemes. We also study various CS methods to find ones with modest computational complexities for each of the considered problems. Overall, we aim to show that recognizing these problems and finding good CS solutions is so important as in many cases it brings us favorable results, making such proposed methods appealing to be realized in practice.

1.4 Thesis Contributions

The technical contributions of the thesis are summarized into two main themes as follows.

1.4.1 Compressive Sensing based Sparse Channel Vector Estimation

a) We develop the theory of CS-based estimation to be able to estimate multiple sparse channels simultaneously. This compressive multi-channel estimation (CMCE) provides a reduction in the required overhead for the estimation of MAC as compared to the method that performs the estimation of the channels individually. We show that the resulting CMCE sensing matrix satisfies the *Restricted Isometry Property* (RIP) and low-coherent condition, making the extension from compressive single-channel estimation (CSCE) to CMCE possible. We then apply the result to the problem of estimation of sparse ISI-

TWRC, where the estimation of the composite channels can be formulated as a CMCE problem. We prove that for i.d.d. equally likely ± 1 Bernoulli pilots, the two above conditions for the sensing matrix hold for a CMCE method, and the improvement of the proposed method also confirmed via performance guarantee bounds.

b) We then consider the problem of joint estimation and data detection of the sparse ISI-TWRC under both modes of cooperative relaying: *Amplify-and-Forward* (AF) and *Decode-and-Forward* (DF). In AF mode, based on the result of channel estimation for composite channel using CMCE, we proposed a joint iterative compressive channel estimation and data detection to improve the end-to-end MSE and BER performance of the TWRC. In DF, where channel estimation and detection in the uplink is performed separate from the one in downlink, we propose a sparsity-aware receiver, where the sparsity feature of the channels is utilized not only in the estimation but also in the equalization process, and the soft-input soft-output (SISO) equalization is performed via the MP algorithm. Furthermore, an thresholding method to mitigate the error propagation due to relaying is proposed to further improve the end-to-end error performance of ISI-TWRC.

1.4.2 Compressive Sensing based Low-rank Channel Matrix Approximation

a) We propose a CS-based approach to address the channel estimation problem of a MU-MIMO system where both dimensions of the channel matrix grow large, with a physical propagation channel model. The research is based on more recent results in CS, where the idea of the sparsity model of the signal vector is generalized to the low-rank model of the matrix variable. CS based low-rank approximation has also been applied in diverse contexts in statistics and signal processing, but to the best of our knowledge, it has not been investigated in MIMO channel matrix estimation. Our main results include the formulation of the low-rank "massive" (or large-scale) MU-MIMO channel estimation problem as a convex nuclear norm minimization (NNM) under noisy setting, whose dual

problem can be represented as a quadratic semi-definite programming (SDP). By doing this, the problem can be conveniently solved by a SDP solver (in polynomial time). We also obtain an explicit choice of the regularization parameter and an useful upper bound of the Frobenius norm of the error for the case of Bernoulli training matrix. Since prior works in this bound have been done for continuous Gaussian ensembles, our results are useful for the MU-MIMO channel matrix estimation due to the discrete nature of the pilot signaling.

b) We then apply CS-based rank-q approximation to solve the pilot contamination and intercell interference problems in multicell multiuser massive MIMO systems. We are also interested in the end-to-end performance of the system including both uplink channel estimation and downlink data precoding and detection. The notion here is that, instead of estimating the global channel matrix, only the most dominant q singular subspaces of the global channel matrix are estimated. Hence we refer to this technique as rank-q channel approximation. We then use the estimate of the global channel matrix to design an intercell-interference-aware (IA) zero-forcing (ZF) downlink precoding vectors with the objective of mitigating both the intracell interference and intercell interference.

c) We derive a lower bound on the downlink achievable rate while assuming knowledge of the exact rank-q global channel matrix approximation assumption. This bound is used as a benchmark for the proposed techniques. Given the high computational complexity of the common SDP-based method used in the estimation process, which becomes prohibitively complex, we present two other low-complexity greedy techniques including Iterative Hard Thresholding (IHT) and Matrix Factorization. We show that the proposed techniques outperform the conventional method based on LS estimation and single-cell precoding, for the same training sequence length.

1.5 Thesis Organization

The rest of the thesis is organized as follows.

Chapter 2 presents some relevant background on topics pertaining to our proposed research. We begin with a brief review of CS techniques for sparse vector and low-rank matrix approximations, where we give the problem settings, the required conditions of the CS dictionaries, and major reconstruction algorithms along with guarantee performance bounds. We then cover the topics of wireless communications where CS has potential applications and will be studied in the following chapters. They include channel estimation, joint iterative estimation and decoding for ISI channels, TWRCs, and estimation and precoding for massive MIMO communications.

Chapter 3 studies the problem of CMCE. In this chapter, we extend the theory of CS for single sparse ISI channel estimation to estimating multiple sparse ISI channels simultaneously, leading to improvements in bandwidth efficiency due to savings in the required training. We consider the CMCE problem for the general case when the sparse channels do not necessary have the same support, where the channel observations are the superposition of the outputs of the individual ISI channels. We then apply the CMCE concept to the problem of channel estimation of a TWRC, which involves two source nodes and one relay node operating analog network coding. We provide several theoretical results on the RIP and low condition of the measurement matrix for both MAC and TWRC, and demonstrate the efficacy of the CS-based schemes over existing ones.

Chapter 4 is concerned with the problem of joint compressive channel estimation and data decoding for sparse ISI-TWRC, for both the AF and DF modes of relaying. In the AF mode, we propose an iterative receiver based on the CMCE technique for TWRC developed in Chapter 3, combined with a turbo decoding method. In the DF mode, we improve the end-to-end bit-error rate (BER) performance of the system via an iterative receiver that utilizes the sparsity of the channel structure in the channel estimation phase and the equalization process. We further improve the system performance by proposing

a thresholding method to mitigate the impact of the error propagation in the relaying process.

Chapter 5 studies the problem of CS-based channel estimation for massive MIMO systems via nuclear norm regularization. In this chapter, a new approach based on CS for the channel matrix estimation problem for massive MU-MIMO systems is proposed. The system model includes a BS equipped with a very large number of antennas communicating simultaneously with a large number of autonomous single-antenna UTs, over a realistic physical channel with finite scattering model. Based on the idea that the degrees of freedom of the channel matrix are smaller than its large number of free parameters, a low-rank matrix approximation based on CS is proposed and solved via a SDP. Our analysis and experimental results suggest that the proposed method outperforms the existing ones in terms of estimation error performance or training transmit power, without requiring any knowledge about the statistical distribution or physical parameters of the propagation channel.

Chapter 6 is concerned with the compressive rank-q channel sensing and precoding for massive MIMO systems. In this chapter, we present a framework based on compressive rank-q approximation for alleviating the impact of pilot contamination, as well as mitigating the intercell and intracell interference of the multicell massive MIMO. Specifically, we propose in the uplink training a rank-q channel approximation method based on CS to estimate the most dominant singular subspaces of the global multicell MIMO channel matrix with a modest training length. Then, the estimate of the global channel information is used to design an IA-ZF multicell precoding method in the downlink to mitigate not only the intracell interference but also the intercell interference of the channel. We analyze the achievable rate of the proposed method using the exact rank-q approximation, and present various compressive rank-q approximation techniques. We compare the proposed scheme with the conventional one using LS estimation and single-cell precoding, and we demonstrate significant improvements achieved by the proposed scheme in the achievable

rates for all users in the cells, particularly the cell-edge users.

Chapter 7 presents a summary of the thesis and suggests some potential problems for future studies.

1.6 Notation

Throughout the thesis, we adopt the following notations.

- Boldface lowercase and uppercase letters denote vectors and matrices, respectively.
- $\boldsymbol{I}_n$: $n \times n$ identity matrix.
- $\boldsymbol{A}^T$, $\boldsymbol{A}^H$, $\boldsymbol{A}^\dagger$, $\mathrm{Tr}(\boldsymbol{A})$: transpose, conjugate transpose, Moore-Penrose pseudo-inverse, and trace of matrix $\boldsymbol{A}$, respectively.
- $\boldsymbol{a}_k$: the k-th column of matrix $\boldsymbol{A}$.
- $\underline{\boldsymbol{A}}_{(k,:)}$: the k-th row of matrix $\boldsymbol{A}$.
- $\langle \boldsymbol{u}, \boldsymbol{v} \rangle$: the inner product of two vectors $\boldsymbol{u}$ and $\boldsymbol{v}$ having the same dimension.
- $[\boldsymbol{A}]_{(m,n)}$ or $\boldsymbol{A}_{m,n}$: the (m,n)-th item of matrix $\boldsymbol{A}$.
- $\|\boldsymbol{A}\|_F$, $\|\boldsymbol{A}\|_*$, and $\|\boldsymbol{A}\|_{\mathrm{op}}$: denote the Frobenius norm, the nuclear norm, and the operator norm of a matrix $\boldsymbol{A}$, respectively.
- $\|\boldsymbol{x}\|_p$: the ℓ_p-norm of vector $\boldsymbol{x}$.
- $(\cdot)_K$ takes the first K rows (entries) of the enclosed matrix (vector).
- $\mathbb{R}^n$ and $\mathbb{R}^{m \times n}$ denote the space of n-dimensional real-valued vectors, and $m \times n$ real-valued matrices, respectively.
- $\mathbb{C}^n$ and $\mathbb{C}^{m \times n}$ denote the space of n-dimensional complex-valued vectors, and $m \times n$ complex-valued matrices, respectively.

- $\mathrm{vec}(\boldsymbol{A})$: vectoring operator, stacking the columns of $\boldsymbol{A} \in \mathbb{C}^{m\times n}$ to form a column in $\mathbb{C}^{mn}$.
- $\mathrm{vec}^{-1}_{m,n}(\cdot)$: the inverse operator of $\mathrm{vec}(\cdot)$, converting the enclosed vector into a $m \times n$ matrix, where the (i, j) entry of the matrix is the $(i \times j)$-th entry of the vector.
- $\mathcal{A}(\cdot)$ denotes a linear operator on the enclosed variable.
- $\mathbb{E}\{\cdot\}$ denotes the expectation operator.
- $\mathbb{P}\{\cdot\}$ denotes the probability of the enclosed event.
- $\Re\{\cdot\}$ and $\Im\{\cdot\}$: the real and the imaginary parts of the enclosed, respectively.
- $\otimes$: Kronecker product.
- $\succeq$: generalized matrix inequality with respect to the Hermitian positive-semidefinite cone.

Chapter 2

Background and Literature Review

As mentioned in Chapter 1, the thesis research topics span a number of areas in applied mathematics, wireless communications and signal processing. In the following sections, we give a brief description of those topics, and the relevant background.

2.1 Compressive Sensing based Sparse Vector Estimation

2.1.1 Inverse Problems

Data acquisition and signal recovery are usually formulated as linear inverse problems. In order that the entire data or signal be reconstructed without error (or with small error in the noisy settings), the well-posed condition requires that the number of equations (i.e., the number of samples or observations) be at least as many as the number of unknowns. In many practical situations, this condition does not always hold, due to the cost of high sampling or the fact that the number of observations is limited. Observing that it is common in nature that many signals are sparse or approximately sparse, in many situations one can still recover the signal with an exact or sufficient accuracy using fewer measurements, given that some specific conditions hold. This has been shown possible by

using CS [1], [29], a novel and very efficient tool to reconstruct sparse signals. The CS process involves employing linear projections and then reconstructing the entire signals from these projections using a greedy technique or a convex optimization algorithm.

Suppose that we need to reconstruct an N-dimensional signal $\boldsymbol{x} \in \mathbb{R}^N$ from a lower-dimensional signal $\boldsymbol{y} \in \mathbb{R}^m$ $(m < N)$ via a linear measurement $\boldsymbol{\Phi}$, i.e.,

$$\boldsymbol{y} = \boldsymbol{\Phi}\boldsymbol{x}, \tag{2.1}$$

where $\boldsymbol{\Phi} \in \mathbb{R}^{m \times N}$ is a measurement matrix. A noisy version of (2.1) is

$$\boldsymbol{y} = \boldsymbol{\Phi}\boldsymbol{x} + \boldsymbol{w}, \tag{2.2}$$

where $\boldsymbol{w} \in \mathbb{R}^m$ is a vector of m additive white Gaussian noise (AWGN) samples.

We define $\boldsymbol{x}$ as a *S-sparse* signal if $\boldsymbol{x}$ has only S large coefficients $(S \ll N)$ and its other $N - S$ coefficients are zeros or approximately zeros. The assumption is referred to hard sparsity or soft sparsity if either exactly $N - S$ out of N coefficients are zeros or approximately zeros, respectively. (Note that if $\boldsymbol{x}$ is non-sparse in the considered basis, but has the *S-sparse* representation $\boldsymbol{s} \in \mathbb{R}^N$ in some other basis $\boldsymbol{\Psi} \in \mathbb{R}^{N \times N}$, then the following results are applied for a $m \times N$ measurement matrix $\boldsymbol{\Theta} = \boldsymbol{\Phi}\boldsymbol{\Psi}$). The CS theory states that the entire S-sparse signal $\boldsymbol{x}$ can be reconstructed with a sufficient accuracy with high probability from $\boldsymbol{y}$ if the measurement matrix $\boldsymbol{\Phi}$ satisfies the so-called RIP [1]. In short, the theory fundamentally relies on two conditions: *sparsity* and *RIP*. The main tasks require designing a stable measurement matrix $\boldsymbol{\Phi}$ satisfying the RIP, and designing an efficient reconstruction algorithm to reconstruct the signal from these measurements.

2.1.2 Sensing Dictionaries

From the RIP definition, the sensing/measurement matrix $\boldsymbol{\Phi}$ is said to satisfy the $RIP(S, \delta_S)$ if for any vector $\boldsymbol{v}$ sharing the same S non-zero elements as $\boldsymbol{x}$, the two following inequal-

ities hold for some $\delta_S > 0$

$$1 - \delta_S \leq \frac{\|\boldsymbol{\Phi v}\|_2}{\|\boldsymbol{v}\|_2} \leq 1 + \delta_S. \tag{2.3}$$

(Note that a less restrictive requirement for $\boldsymbol{\Phi}$, called *Restricted Eigenvalue (RE) Condition* [30], is also used in some works).

The RIP is related to the *incoherence* condition [2], which requires that the maximum (in absolute) value of all inner products between two different columns in $\boldsymbol{\Phi}$ is small (or the measurement basis $\boldsymbol{\Phi}$ and the representation basis $\boldsymbol{\Psi}$ are a low coherence pair in the case that $\boldsymbol{x}$ has the *S-sparse* representation $\boldsymbol{s}$ the transformed basis $\boldsymbol{\Psi}$, not the original basis $\boldsymbol{\Phi}$). It is proven that random measurement matrices, whose elements are drawn from an independent and identically distributed (i.i.d.) Gaussian distribution, have sufficiently small coherence. In practice, other measurement matrices have been considered, such as i.i.d. Bernoulli, random partial Fourier or scrambled block Hadamard ensembles, etc., again depending on the specific applications.

Another important property of $\boldsymbol{\Phi}$ that makes it a suitable candidate for a CS dictionary, closely related to the RIP, is the low-coherence between its columns. Defining the mutual coherence of $\boldsymbol{\Phi}$ as

$$\mu \triangleq \max_{l \neq j} |\langle \boldsymbol{\phi}_j, \ \boldsymbol{\phi}_l \rangle| \,, \tag{2.4}$$

which is the the largest off-diagonal entry (in the magnitude sense) of the Gram matrix of $\boldsymbol{\Phi}$, $\boldsymbol{G} \triangleq \boldsymbol{\Phi}'\boldsymbol{\Phi}$.

2.1.3 Reconstruction Algorithms

To reconstruct the signal $\boldsymbol{x}$ from the linear measurement $\boldsymbol{y}$, an optimization solver is run to find the solution of a regularized ℓ_0-minimization (ℓ_0-norm minimization) problem. ℓ_0-norm minimization is an NP-hard problem, and solving for the optimal solution requires an exhaustive search of all $\binom{N}{S}$ possible locations of the non-zero elements in $\boldsymbol{x}$. Fortunately, there are a variety of other reconstruction techniques that, provided hav-

ing a good CS dictionary, can efficiently solve for $\boldsymbol{x}$ with exact accuracy w.h.p by only $m \geq cS\log(N/S)$ measurements in a noiseless setting or with sufficient accuracy w.h.p with only $m \geq cS^2\log(N/S)$ measurements in a noisy setting, for some $c > 0$ [2], [29]. Those techniques can be categorized into two main groups [31]: greedy-based methods such as the IHT [32] and Orthogonal Matching Pursuit (OMP) [33]; and ℓ_p-based optimization methods including the ℓ_p-constrained minimization, error-constrained ℓ_p minimization, the relaxation version of ℓ_p-constrained minimization [34], and Danzig selector [17].

A) Greedy Methods

The class of greedy techniques have been widely used for sparse approximation thanks to theirs simplicity and efficiency. The idea behind the algorithms is to choose the columns of the dictionary in a greedy fashion. For example, the typical greedy-based algorithm, OMP, works as follows. At each iteration, the algorithm picks up the column that is most correlated with the residual, which is the remaining part of the observation after being subtracted by the contribution of the column in the previous iteration. In other words, the OMP greedily chooses the best columns of the dictionary representing the signal. Using Theorem 4 of [35], the performance guarantee for OMP in terms of the mean-squared error (MSE) is given as

$$\mathrm{MSE}_{\mathrm{OMP}} \leq 8(1+\alpha)S\sigma^2\log N, \tag{2.5}$$

with probability exceeding $1 - \left(N^{\alpha}\sqrt{\pi(1+\alpha)\log N}\right)^{-1}$ for some $\alpha > 0$, under the condition

$$|\boldsymbol{h}_{\min}| - (2S-1)\mu|\boldsymbol{h}_{\min}| \geq 2\sigma\sqrt{2(1+\alpha)\log N}. \tag{2.6}$$

The major weakness of the OMP is that the above performance guarantee only holds under (2.6), meaning that the magnitudes of all S non-zero coefficients of $\boldsymbol{h}$ are required somewhat to be above the noise level. If some of them are smaller than the noise level, the OMP, which is a greedy version of the LS method, may incorrectly define the support

set of $\boldsymbol{h}$ making its performance very poor.

B) ℓ_p-based Optimization Methods

Reconstruction from CS measurements using ℓ_p-based optimization methods are achieved by solving one of the three following minimization problems. The ℓ_p-constrained minimization problem, which is constrained by the sparsity budget S of the signal, reads

$$\min_{\boldsymbol{x}} \frac{1}{2} \|\boldsymbol{y} - \boldsymbol{\Phi x}\|_2^2 \text{ s.t. } \|\boldsymbol{x}\|_p \leq S. \tag{2.7}$$

The error-constrained ℓ_p minimization, which is based on the 2-norm error budget ϵ, reads

$$\min_{\boldsymbol{x}} \|\boldsymbol{x}\|_p \text{ s.t. } \frac{1}{2} \|\boldsymbol{y} - \boldsymbol{\Phi x}\|_2^2 \leq \epsilon. \tag{2.8}$$

The relaxation version of (2.8) reads

$$\min_{\boldsymbol{x}} \frac{1}{2} \|\boldsymbol{y} - \boldsymbol{\Phi x}\|_2^2 + \gamma \|\boldsymbol{x}\|_p, \tag{2.9}$$

where γ is the turning parameter.

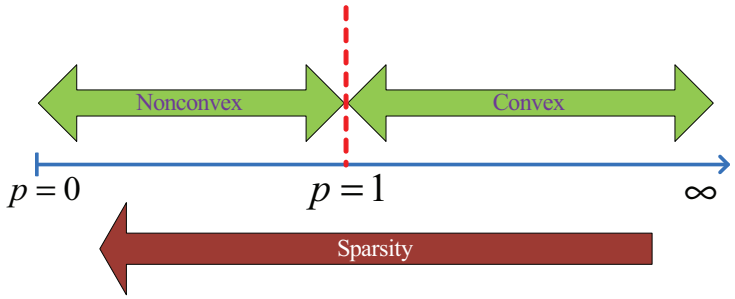

Figure 2.1: p-norm minimization methods.

When $p \geq 1$, (ℓ_p-norm), the three ℓ_p-based optimization problems mentioned above are convex, and can be exchangeable, i.e., the solution of one can be achieved by the other by choosing the suitable regularization parameters or constraints [36]. This is not correct when $0 < p < 1$ (ℓ_p quasi-norm) as these problems become nonconvex. The

trade-off here is that, while the convex problems ($p > 1$) have efficient algorithms to solve and it is guaranteed that the local optimal is also the global one, it does not yield the sparsest solution as the nonconvex ones ($0 < p < 1$). This motivates us to usually choose $p = 1$ as ℓ_1-based optimization problems give the sparsest solution in the convex class. Furthermore, the ℓ_1-penalty version of Basic Pursuit Denoising (also called BPDN or LASSO) in (2.9) when $p = 1$,

$$\min_{\boldsymbol{x}} \frac{1}{2} \|\boldsymbol{y} - \boldsymbol{\Phi}\boldsymbol{x}\|_2^2 + \gamma \|\boldsymbol{x}\|_1 , \tag{2.10}$$

is often more efficient to solve algorithmically [37]- [38]. Also, the BPDN does not need the error and sparsity constraints, and only need the sparsity condition of the signal. When γ in (2.10) is typically chosen as

$$\gamma = \sqrt{8\sigma^2(1+\alpha)\log(N-S)}, \tag{2.11}$$

the BPDN has the performance guarantee (Theorem 3 of [35])

$$\mathrm{MSE}_{\mathrm{BPDN}} \leq \left(\sqrt{3} + 3\sqrt{2(1+\alpha)\log(N-S)}\right)^2 S\sigma^2, \tag{2.12}$$

with probability exceeding

$$\left(1 - \frac{1}{(N-S)^{\alpha}}\right)\left(1 - \exp\left(-\frac{S}{7}\right)\right) \tag{2.13}$$

for some $\alpha > 0$, under the condition that $S \leq 1/(3\mu)$.

2.2 Compressive Sensing based Low-rank Matrix Approximation

Recall that in "classical" CS [1], [29], one takes the sparsity of the sparse signal vector into account and solves the relaxation version of cardinality minimization problem, which is the ℓ_1-norm minimization, subjected to a linear constraint. When we consider low-rank matrix approximation problems, we apply duality concepts between vector cardinality minimization and matrix rank minimization in Table 2.1 [39]. The CS-based low-rank approximation technique leverages the idea from "classical" CS by taking the low-rank feature of a matrix variable into account. It solves the relaxation version of the rank minimization problem, which is the minimization of the nuclear norm (i.e., the sum of the matrix singular values), subject to a linear or affine transformation of the matrix variable [39], [40] (recall that the nuclear norm is the tightest convex hull of the set of the matrix rank).

Table 2.1: Duality concepts of vector cardinality and matrix rank minimization.

Parsimony concept	vector cardinality	matrix rank
Hilbert space norm	Euclidean	Frobenius
Sparsity inducing norm	ℓ_1-norm	nuclear norm
Dual norm	ℓ_∞-norm	opertor norm
Convex relaxation	linear programming	semi-definite programming

For a matrix variable $\boldsymbol{X} \in \mathbb{C}^{m\times n}$ with a linear transformation $\mathcal{A}(\boldsymbol{X}) = \boldsymbol{b}$, where $\mathcal{A} : \mathbb{C}^{m\times n} \to \mathbb{C}^d$ is a linear operator, $\boldsymbol{b} \in \mathbb{C}^d$, $d = mn$ is the sample size, the NNM problem reads

$$\begin{aligned} \underset{\boldsymbol{X}}{\text{minimize}} \quad & \|\boldsymbol{X}\|_* \\ \text{subject to} \quad & \mathcal{A}(\boldsymbol{X}) = \boldsymbol{b}, \end{aligned}$$

where $\|\boldsymbol{X}\|_*$ denotes the nuclear norm of $\boldsymbol{X}$. Its noisy version is the nuclear norm regularization problem

$$\underset{\boldsymbol{X}}{\text{minimize}} \quad \frac{1}{2}\|\boldsymbol{b} - \mathcal{A}(\boldsymbol{X})\|_2^2 + \gamma\|\boldsymbol{X}\|_* \tag{2.14}$$

where γ is a regularization parameter.

For the noiseless setting, it is derived in [39] that the dual problem can be represented in a linear SDP as

$$\begin{aligned} \underset{\boldsymbol{z}}{\text{minimize}} \quad & \boldsymbol{b}^* \boldsymbol{z} \\ \text{subject to} \quad & \begin{bmatrix} \boldsymbol{I}_m & \mathcal{A}^*(\boldsymbol{z}) \\ [\mathcal{A}^*(\boldsymbol{z})]^H & \boldsymbol{I}_n \end{bmatrix} \succeq 0, \end{aligned}$$

where $\mathcal{A}^*$ is the adjoint of $\mathcal{A}$, $\succeq$ denotes the generalized matrix inequality with respect to the Hermitian positive-semidefinite cone [41].

Similar to the RIP of measurement matrix for sparse vector recovery, there are RIP [39] and its milder version named Restricted Strong Convexity (RSC) [40] for low-rank matrix approximation. Those conditions establish error bounds for the low-rank matrix recovery guarantees (2.14) is strictly convex over a restricted set $\mathcal{C}$.

2.3 Joint Channel Estimation and Data Detection

2.3.1 Channel Estimation

In the communication between terminals in either point-to-point or multi-user scenarios, channel estimation is a crucial task since the reliable detection of data is based on the knowledge of channel state information (CSI). In practice, this task is accomplished by sending from the transmitters a training sequence (pilot) before the actual data to probe the channel, and then estimating the channel parameters at the receivers.

Consider the problem of estimation of a frequency-selective time-invariant channel of length N between a transmitter X and a receiver Y, in a single-carrier system. Assuming that the channel has the impulse response denoted by $\boldsymbol{h} = [h_1 \; h_2 \; \ldots \; h_N]^T$. The transmitter needs to send a random but known pilot sequence of length $\mathcal{T} = K_0 + N - 1$, denoted by $\boldsymbol{a} = [a_1 \; a_2 \; \ldots \; a_{\mathcal{T}}]^T$ prior to its actual data transmission. We further assume that the modulation format of the information symbols sent the transmitter is binary

phase-shift keying (BPSK), and the pilot sequence is i.i.d. equally likely ± 1. Since single-carrier signaling is assumed, ISI occurs, and the received signal at the receiver is the linear convolution of the input and the channel impulse response, plus AWGN. Equivalently, the received signal can be written in a compact form as

$$\boldsymbol{y} = \boldsymbol{A}\boldsymbol{h} + \boldsymbol{n}, \tag{2.15}$$

where $\boldsymbol{A}$ is the $K_0 \times N$ partial Toeplitz matrix formed from $\boldsymbol{a}$,

$$\boldsymbol{A} = \begin{bmatrix} a_N & a_{N-1} & \cdots & a_2 & a_1 \\ a_{N+1} & a_N & \cdots & a_3 & a_2 \\ \vdots & \vdots & \ddots & \vdots & \vdots \\ a_{N+K_0-1} & a_{N+K_0-2} & \cdots & a_{K_0+1} & a_{K_0} \end{bmatrix}, \tag{2.16}$$

$\boldsymbol{y}$ is a $K_0 \times 1$ vector of the received symbols; $\boldsymbol{n}$ is a $K_0 \times 1$ vector of AWGN samples, with variance $\sigma^2/2$ per dimension. Writing (2.15) using (2.16), we assume in our scheme that there is no guard interval between the training and data blocks in one frame, neither between consecutive frames, and only take the K_0 interference-free received symbols at the destination as useful observations for channel estimation purposes.

Assuming that the receiver does not have any knowledge about the sparsity or the statistical distribution of the channels, then its *sparsity-ignorant* receiver simply employs the conventional PA channel estimation using the LS method. To have a meaningful estimation, we need to transmit a training symbol vector of length $\mathcal{T} \geq 2N - 1$, which provides us with at least as many interference-free observations as there are unknowns in (2.15). The LS solution for (2.15) is then given by [42]

$$\boldsymbol{h}_{\mathrm{LS}} = (\boldsymbol{A})^{\dagger}\, \boldsymbol{y} = (\boldsymbol{A}'\boldsymbol{A})^{-1}\, \boldsymbol{A}'\boldsymbol{y}.$$

The MSE of the LS method is

$$\mathrm{MSE}_{\mathrm{LS}} = \sigma^2 \mathrm{Tr}\left\{(\boldsymbol{A}'\boldsymbol{A})^{-1}\right\}, \tag{2.17}$$

which results in the lower bound of $\sigma^2(N)/K_0$.

2.3.2 Iterative Channel Estimation and Data Detection

Consider signal and channel models for coded systems as shown in Fig. 2.2. Let $\boldsymbol{b} = [b_0\ b_1\ \ldots\ b_{K_b-1}]^T$ denote the K_b-length binary information vector transmitted. After encoded by a convolutional encoder with rate $R = K_b/N_c$, the corresponding N_c-length coded vector, denoted by $\boldsymbol{c} = [c_0\ c_1\ \ldots\ c_{N_c-1}]^T$ is randomly interleaved and BPSK modulated. The corresponding symbol vector to be transmitted over the ISI channel is denoted by $\boldsymbol{x} = [x_0\ x_1\ \ldots\ x_{N_c-1}]^T$. To prevent the inter-block interference (IBI), consecutive symbol blocks are separated by a guard interval of length $(N-1)$ before transmitted.

Figure 2.2: Signal and channel models for coded systems.

Denote the channel impulse response vector between the transmitter and receiver by $\boldsymbol{h}$. The n-th received signal at the receiver, denoted by y_n, is given by

$$y_n = \sum_{l=0}^{N-1} h_l x_{n-l} + e_n, \tag{2.18}$$

where e_n is the n-th AWGN sample, for $n = 0, 1, \cdots, N_c - 1$.

The optimal receiver requires a jointly optimal design between the channel estimator, equalizer, and channel decoder, which is impractical to be implemented in practice due to its high computational complexity. Below we describe the iterative receiver which

performs channel estimation, turbo equalization and decoding using the a posteriori probability (APP) algorithm, in an iterative fashion, as depicted in Fig. 2.3.

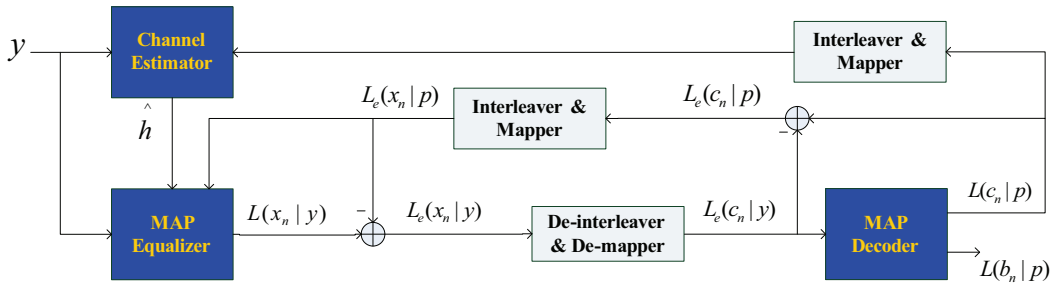

Figure 2.3: Iterative Estimation and Decoding for ISI channel.

After the channel estimation process, the channel estimate vector $\hat{\boldsymbol{h}}$ and the received signal vector $\boldsymbol{y}$ are passed to an equalizer to handle the ISI and then to the decoder to get an estimate of the binary information vector. With the presence of the interleaver, the jointly optimal equalization and decoding is also impractical. Turbo equalization is a suboptimal solution to address this problem by preforming the soft a priori information exchange between the maximum the posteriori (MAP)/APP equalizer and the MAP/APP decoder in an iterative fashion [43]. The log-APP based equalizer computes the *a-posteriori* log-likelihood ratio (LLR) of the coded symbols given the received signal vector

$$
\begin{aligned}
L(x_n|\boldsymbol{y}) &= \ln\frac{P(x_n=1|\boldsymbol{y})}{P(x_n=-1|\boldsymbol{y})} && (2.19)\\
&= \ln\frac{\sum_{\forall \boldsymbol{x}:x_n=1} p(\boldsymbol{y}|\boldsymbol{x})\prod_{i=0}^{N_c-1}P(x_i)}{\sum_{\forall \boldsymbol{x}:x_n=-1} p(\boldsymbol{y}|\boldsymbol{x})\prod_{i=0}^{N_c-1}P(x_i)} && (2.20)\\
&= \underbrace{\ln\frac{\sum_{\forall \boldsymbol{x}:x_n=1}\prod_{i=0}^{N_c-1} p_i(y_i|\boldsymbol{x})\prod_{j=0,j\neq n}^{N_c-1}P_i(x_i)}{\sum_{\forall \boldsymbol{x}:x_n=-1}\prod_{i=0}^{N_c-1} p_i(y_i|\boldsymbol{x})\prod_{j=0,j\neq n}^{N_c-1}P(x_i)}}_{} + L(x_n) && (2.21)\\
&= L_e(x_n|\boldsymbol{y}) + L(x_n), && (2.22)
\end{aligned}
$$

for every $n \in \{0, 1, ..., N_c - 1\}$, where $L_e(x_n|\boldsymbol{y})$ is the extrinsic information of x_n given $\boldsymbol{y}$, and $L(x_n) \triangleq \ln\frac{P_n(x_n=1)}{P_n(x_n=-1)}$ is the prior LLR value of x_n provided from the channel decoder.

With the long channel spread and for large constellation sizes, the above APP-based equalizer again is very complex preventing it from reaching real applications. There is a variety of alternative methods that approximate (2.22) with linear complexity using a soft-input soft-output (SISO) equalizer [43, 44].

These soft values are randomly interleaved and then delivered to the channel decoder. The LLR values of the coded symbols output at the APP decoder are then fed back to the estimator and the equalizer as shown in Fig. 2.3 for the next iteration to refine the results. The APP-decoder also computes the LLR values of $\boldsymbol{b}$ to make hard-decision at the final iteration, when the stopping criterion is satisfied.

2.4 Two-way Relay Communications

TWRC is the combination of two-way channel [45] and the one-way relay channel. Therefore, TWRC takes advantage from both including bandwidth efficiency and spatial diversity, and has attracted many research works recently. Furthermore, it is one of the underlying channels where network coding can be efficiently employed. TWRC consist of two nodes transmit information to each other through a relay node that employs cooperative relay based on network coding [24, 25, 46].

The two most popular protocols for TWRC with network coding are three-phase and two-phase protocols. In the three-phase protocol, as shown in Fig. 2.4, the two source nodes transmit their signal in the broadcast stage (phase I and phase II); and then the relay transmits the network-coded signal in the cooperation stage (phase III). It can be seen that if the relay R is to cooperate with two terminals T_1 and T_2 individually (i.e., without network coding) the relay would then be transmitting the signal from T_1 and T_2 in one phase (or one channel), and vice versa over another phase (another channel). Network coding in this case helps to achieve communication with one time slot less.

If the two-phase relaying protocol is used, as shown in Fig. 2.5, in the broadcast stage,

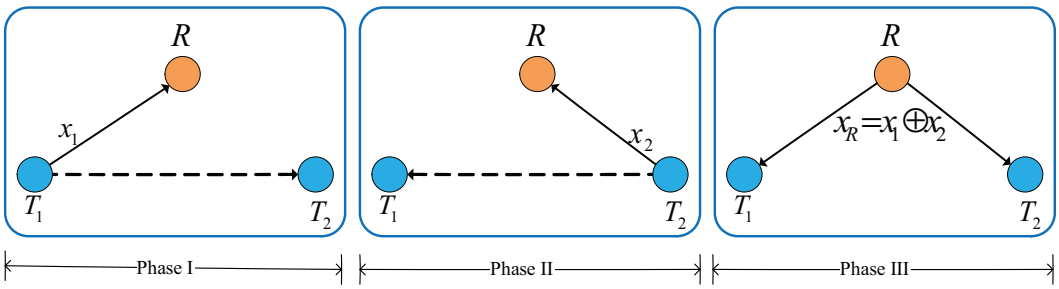

Figure 2.4: Three-phase two-way relaying protocol.

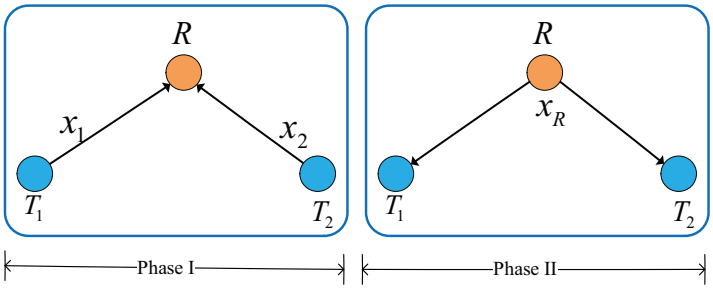

Figure 2.5: Two-phase two-way relaying protocol.

the two source nodes send their data simultaneously to the relay, hence they only need one time slot. Of course, the two-phase protocol can reduce another time slot for the data exchange between two source nodes, but in the broadcast stage, the channel is MAC, making the channel estimation and data detection at the relay more difficult.

Early works on cooperative relaying for TWRC suggested two modes of relaying operation [47]: AF and DF. In the AF mode, the relay does not need to decode the signals sent from the source nodes but just amplifies it (subject to a power constraint) and forwards it to the sources. This mode is also referred to as *analog network coding* in the literature. In DF, the relay needs to detect and demodulate the signals sent from two sources, and then transmitting the exclusive-or (XOR) of the decoded bits to the two sources (after re-modulating it). While DF is prone to error propagation due to decoding errors, AF requires the source nodes to have CSI of the composite channels. A few other relaying protocols have been proposed recently. Those protocols include *estimate-and-forward* [48], [49] (or EF, an estimate of the transmitted symbol is forwarded to the destination), and *compress-and-forward* [50] (or CF, the estimates are source-coded to

exploit possible correlation between channel fades and the source data, then forwarded to the destination). Such protocols were shown to improve the end-to-end performance (in terms of capacity [48], received SNR [51], or bit-error rate (BER)).

Also in terms of the end-to-end performance, it has been demonstrated that the BER performance significantly depends on the detection reliability at the relay nodes [52]. In the ideal situation where detection at the relays is perfect, the diversity of the system is maintained, that is, as if the relay node is collocated with the transmitting source node [47], [53, 54]. However, with imperfect detection, the diversity degrades because of the error propagation. The severity of this degradation depends on the detection reliability level at the relay nodes. Some efforts have been directed towards finding remedies for this problem, especially for DF relaying. The authors in [55–58] (for uncoded networks,i.e., no channel coding used) and [59, 60] (for channel-coded networks) propose to calculate the LLRs of the received bits at the relay , then if the LLR of a bit falls below a predetermined threshold the relay blocks this bit and does not forward it to the destination. Such a technique proved successful in improving the end-to-end BER performance, albeit not achieving full diversity because of blocking correct bits by the threshold.

2.5 Massive MU-MIMO

MIMO is a technology that employs multiple antennas at both transmitter and receiver [61]. Thank to the spatial diversity, MIMO systems can send multiple independent data streams simultaneously, without the need of increasing the bandwidth. This brings many advantages of MIMO links over conventional point-to-point ones such as higher data rates, better reliability, higher bandwidth efficiency, and robustness to interferences. The challenges of MIMO communications come from hardware implementation, i.e., the cost of expensive high power transceivers, the number of radio frequency (RF) chains, or the size of the transmitter and receiver, where multiple antennas are employed.

MIMO wireless communication technology has been supported in cellular networks including the third generation partnership program (3GPP) long term evolution (LTE), ultra-mobile broadband (UMB), high speed downlink packet access (HSDPA) and IEEE 802.16e (WiMAX).

To scale up the data rate ranges to meet the increasing demands for future networks, i.e., beyond 4G networks, massive (or large-scale) MIMO has been proposed [27, 28] as a promising technology. Such technology is based on the same concepts of conventional MIMO but extended to a much larger scale in terms of the number of antennas at both the transmitter and receiver sides. Massive MIMO systems consist of large arrays of tiny active antenna units, each operating at an extremely low power. As a result, not only the data rate can be increased, but also the expensive high power transceivers can be replaced by many low-cost low-power ones. Compared to the classical MIMO, massive MIMO provides many advantages such as higher data rates, better link reliability, and better spectral-energy efficiency tradeoff. One current proposed system for massive MIMO technology is the massive MU-MIMO [28] a shown in Fig. 2.6, where a BS with a very large antenna array serves a multiplicity of distant or well-separated single-(or just a few)-antenna UTs simultaneously.

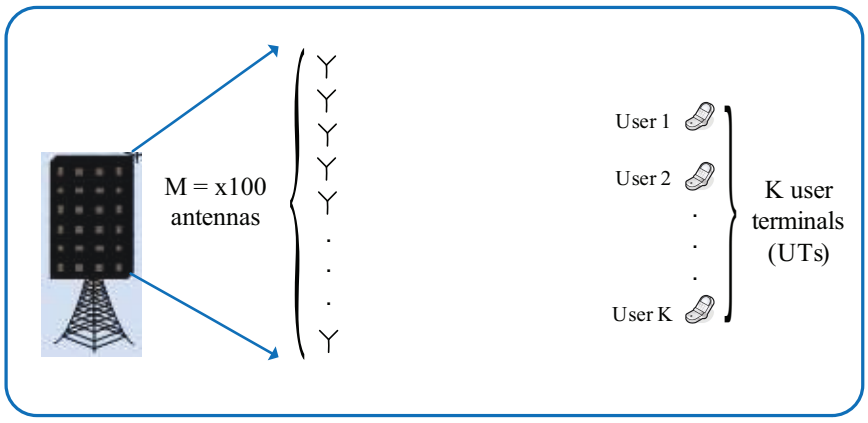

Figure 2.6: Massive MU-MIMO systems of M BS antennas serving K UTs.

Recent studies have shown that massive MIMO brings both opportunities and challenges. On the optimistic side, under some favorable assumptions, as mentioned before,

massive MIMO provides many advantages as compared to conventional MIMO. As an example, theoretical results suggest that adding more antennas at the BS in a massive MU-MIMO system [28] always helps to increase the throughput or reduce the transmit power; and all these promising results can be obtained using some linear-complexity estimation and detection algorithms. The challenging side is that, to obtain those promising results, many optimistic assumptions that do not generally hold in practice are made, including the favorable and rich scattering, the availability of perfect CSI at all UTs and at the BS, and zero inter-cell interference [62]. Particularly, the main limitations of massive MIMO is the uplink channel estimation error and the intercell interference in the downlink, which we present below.

2.5.1 Uplink Channel Estimation in Massive MIMO

In TDD systems, the CSI is estimated in the uplink, and used to perform the precoding/beamforming in the downlink. The conventional and standard way of estimating the CSI is to send from each user a training sequence of length $\mathcal{T} \geq K$ in the training phase of each coherence interval. The channel estimate is then computed by correlating the received signal with the known training sequence using LS or minimum mean-squared error (MMSE) (if the distribution of the channel is available for the latter method). This approach has the advantage that the length of the training sequence scales linearly with the number of users, not with the number of BS antennas [27].

However, when we consider the massive MIMO in the multicell interference-limited scenarios, there exits the crucial limitation of the so-called pilot contamination effect. That is, the quality of the channel information estimated by a cell is affected by the interference from the pilots sent by the users in other cells [62]. If we assume a multicell massive MIMO with L cells, each cell has a BS employed with M antennas serving K users. Then the local CSI estimate in cell l, $1 \leq l \leq L$, is contaminated by the pilots sent from UTs in the other $(L-1)$ cells, due to the non-orthogonality of the LK $\mathcal{T}$-

length pilot sequences ($\mathcal{T} < LK$). This fundamental issue exists due to the small $\mathcal{T}$ in a limited coherence time interval and the large dimension LK, making the training sequences across all the cells not long enough to achieve the orthogonality. This effect results in a significant reduction in the achievable rates of UTs. The problem becomes more critical when the number of users in each cell grows large, and/or the intercell gains between users in a cell to the BS in another cell are relatively strong as compared to the direct link gains.

2.5.2 Precoding in Massive MIMO

In the downlink data transmission, each BS l ($1 \leq l \leq L$) at first precodes the signal vector $\boldsymbol{x}_l$ including the data sent to K users in cell l, by multiplying it with a precoding matrix $\boldsymbol{W}_l = [\boldsymbol{w}_{l1}\ \boldsymbol{w}_{l2}\ \ldots\ \boldsymbol{w}_{lK}]$. Then the broadcast signal vector is $\boldsymbol{s}_l = \sqrt{\lambda_l}\boldsymbol{W}_l\boldsymbol{x}_l = \sqrt{\lambda_l}\sum_{n=1}^{K}\boldsymbol{w}_{ln}x_{ln}$, where λ_l is a normalization parameter. Using ZF precoding, the precoding vector at BS j satisfies

$$\begin{aligned}\boldsymbol{W}_j^{\mathrm{ZF}} &= (\hat{\boldsymbol{H}}_{jj}^{T})^{\dagger} \\ &= \hat{\boldsymbol{H}}_{jj}^{*}(\hat{\boldsymbol{H}}_{jj}^{T}\hat{\boldsymbol{H}}_{jj}^{*})^{-1},\end{aligned}$$

where $\hat{\boldsymbol{H}}_{jj}$ is the estimate of the channel from K users in cell j to BS j. When K grows large, the computational complexity of $(\hat{\boldsymbol{H}}_{jj}^{T})^{\dagger}$ is high, on the order $\mathcal{O}(K^3)$ due to the inversion of the $K \times K$ matrix. By observing that with large M, $\frac{1}{M}\hat{\boldsymbol{H}}_{jj}^{T}\hat{\boldsymbol{H}}_{jj}^{*}$ tends to the identity matrix [28], hence the simpler MF precoding method can be used, $\boldsymbol{W}_j^{\mathrm{MF}} = \hat{\boldsymbol{H}}_{jj}^{*}$. More discussion on precoding methods is given details in [63]. It is proven that when the number of BS antennas grows large, the intracell interference vanishes, but the system performances including the achievable rates are still affected by the intercell interference from the other cells [64]. When the effect of the channel estimation error and the pilot contamination are combined, the achievable rates using this method is affected by both the

intracell and intercell interferences, and hence the overall achievable sum-rate is degraded. In particular, the individual achievable rates of the cell-edge UTs are degraded the most, due to their larger cross-gains as compared to the other UTs [65].

2.6 Concluding Remarks

This chapter has presented the background of CS and various topics that will be further studied in this thesis. We have presented two models of sparse vector and low-rank matrix, where CS can be applied and make important improvements, as well as popular CS algorithms for reconstructing sparse or low-rank channels. We have also covered the backgrounds of joint channel estimation and data decoding methods for point-to-point channels, as well as discussed about TWRC and massive MU-MIMO channels. They are the underlying systems where we will develop CS methods to improve system performances or address the existing challenges, in the next chapters.

Chapter 3

Compressive Multi-channel Estimation

3.1 Introduction

This chapter is concerned with the problem of CMCE. In particular, we develop the theory of CS-based estimation to be able to estimate multiple sparse channels simultaneously instead of performing the estimation of the channels individually. The advantage of doing so is a reduction in the required overhead and/or an improvement in the estimation accuracy. The CMCE problem has been considered in [11], [12] and some references therein, where the common theme there is to reconstruct multiple signals having the same sparsity support. The authors in [11] propose a compressive estimator to simultaneously reconstruct several *jointly* sparse doubly selective channels in multi-carrier MIMO-OFDM systems. In [12], a finite rate of innovation (FRI) sampling and reconstruction scheme is proposed to reconstruct a set of signals in the sparse common-support scenario (SCS-FRI), where its performance achieves the Cramér-Rao bound (CRB) starting from lower signal-to-noise ratio compared to that of the classical single-channel SCS-FRI reconstruction techniques. In this chapter, however, we consider the CMCE problem when the sparse channels do not

necessary have the same support, where the channel observations are the superposition of the outputs of the ISI channels. That is the case when one generally needs to perform channel estimation in multipath MIMO channels, multipath interference channels, or MAC in single-carrier systems. Therefore, our results are useful for multiuser single-carrier transmission techniques, which have regained interest recently in scenarios where low peak-to-average power ratio is expected. In addition, while single-carrier schemes usually require more complex equalization compared to the OFDM-based ones [10], [11], the scheme considered in this chapter does not use any guard interval between data and training blocks in one frame, or between consecutive frames (which is necessary for the OFDM-based ones in terms of cyclic prefixes). This is an advantage of the single-carrier scheme in terms of training sequence length, especially when the sparse channels have very long impulse responses. However, we do not make any claim here that the scheme considered in this chapter outperforms the OFDM-based one.

As another application, we then apply the CMCE concept to a network-coded two-way relay channel, which comprises two sources and one relay node. In the first time slot, the two sources transmit their training sequences that are known a prior to the relay node. In the second time slot, the relay applies analog network coding to the sum of the received signals and broadcasts the result to the two sources. Each source then uses the CMCE method described above to estimate the composite channel (i.e., two hops). This estimate is needed for coherent data detection (channel equalization and decoding) of the two-way relay channel. The underlying channels are assumed to be sparse multipath fading channels. For the rest of the chapter, we refer to this channel as a ISI-TWRC.

The contributions of this chapter are summarized as follows.

- We extend the CS-based channel estimation technique from single-channel to multi-channel scenarios (MAC). We first form the CMCE sensing matrix by cascading partial Toeplitz matrices whose entries are independent and identical distributed (i.i.d), and equally likely ± 1 Bernoulli random variables (r.v.s). We then show that the resulting CMCE sensing matrix satisfies the RIP and low-coherent condition, making the extension from CSCE to CMCE possible.

- We then apply the above result to the problem of estimating the sparse ISI-TWRC, where the estimation of the composite channels can be formulated as a CMCE problem. We prove that for i.i.d. equally likely ± 1 Bernoulli pilots, the two above conditions for the sensing matrix hold for a CMCE method.

- From both theoretical and empirical results, we conclude that CMCE outperforms its CSCE counterpart in term of MSE, for both the MAC and TWRC estimation problems.

3.2 System Model

Consider the problem of simultaneous communications from J sources, denoted by $\{T_j\}_{j=1}^{J}$, to a destination denoted by D in a single-carrier system as shown in Fig. 3.1. The underlying channel is MAC because the communications among all pairs $T_j - D$ share the same time, bandwidth and code. We further assume that each channel between T_j and D, denoted by $\boldsymbol{h}_j = [h_{j,1}\ h_{j,2}\ \ldots\ h_{j,N}]^T$, is a time-invariant frequency-selective channel having S_j-sparse N-length impulse response. This means that out of the channel length N (for the $T_j - D$ link) only S_j coefficients are non-zero, which are further assumed to be i.i.d. Rayleigh distributed. We note here that if each channel has a different length N_j, then we can assume that all the coefficients of $\boldsymbol{h}_j$ from $N_j + 1$ to N are zero, where

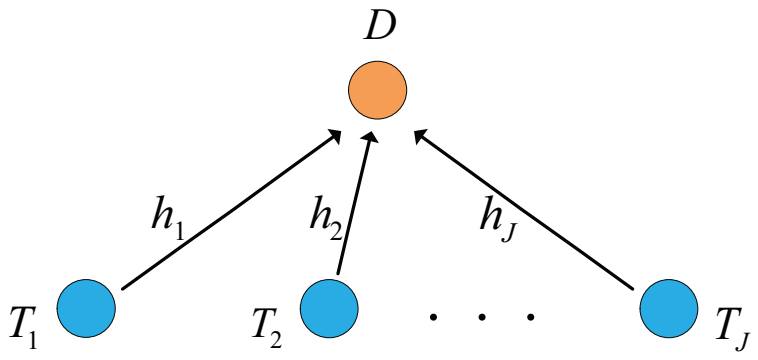

Figure 3.1: J-user MAC channel

$N = \max(N_1, N_2, ..., N_J)$. To simultaneously sense/estimate all channel impulse responses $\{\boldsymbol{h}_j\}_{j=1}^{J}$ at the destination, we need to send from each T_j a random, but known, pilot sequence of length $\mathcal{T} = K_0 + N - 1$, denoted by $\boldsymbol{a}_j = [a_{j,1}\ a_{j,2}\ \ldots\ a_{j,\mathcal{T}}]^T$ prior to its actual information data transmission. The modulation format of the information symbols sent by all sources is assumed to be BPSK, and the pilots are random sequences of i.i.d equally likely ± 1. Since single-carrier is employed, ISI occurs, and the received signal at D is the superposition of all individual outputs of the channels, plus AWGN. Consequently, the signal received at D can be written in matrix form as

$$\boldsymbol{y} = \sum_{j=1}^{J} \boldsymbol{A}_j \boldsymbol{h}_j + \boldsymbol{n}, \tag{3.1}$$

where $\boldsymbol{A}_j$ is the $K_0 \times N$ partial Toeplitz matrix formed from $\boldsymbol{a}_j$,

$$\boldsymbol{A}_j = \begin{bmatrix} a_{j,N} & a_{j,N-1} & \cdots & a_{j,2} & a_{j,1} \\ a_{j,N+1} & a_{j,N} & \cdots & a_{j,3} & a_{j,2} \\ \vdots & \vdots & \ddots & \vdots & \vdots \\ a_{j,N+K_0-1} & a_{j,N+K_0-2} & \cdots & a_{j,K_0+1} & a_{j,K_0} \end{bmatrix}; \tag{3.2}$$

$\boldsymbol{y}$ is a $K_0 \times 1$ vector of the received symbols; $\boldsymbol{n}$ is a $K_0 \times 1$ vector of AWGN samples, with variance $\sigma^2/2$ per dimension. We assume in our scheme that there is no guard interval between the training and data blocks in one frame, neither between consecutive frames,

and only the K_0 interference-free received symbols are considered at the destination as useful observations for channel estimation purposes. Here we use the term "interference" to indicate the *unknown* data symbols contained in the observations. Comparing to the scheme where guard intervals are used, this scheme needs shorter training sequences and resembles more closely the CS problem, where the number of observations is far fewer than the number of unknowns [66].

To cast the problem of channel estimation using the PA method, we stack all vectors $\{\boldsymbol{h}_j\}_{j=1}^{J}$ in (3.1) into a single $JN \times 1$ vector, denoted by $\boldsymbol{h} = \begin{bmatrix}\boldsymbol{h}_1^T & \boldsymbol{h}_2^T & \dots & \boldsymbol{h}_J^T\end{bmatrix}^T$. Then (3.1) can be re-written as

$$\boldsymbol{y} = \boldsymbol{A}\boldsymbol{h} + \boldsymbol{n}, \tag{3.3}$$

where $\boldsymbol{A} = \left[\begin{array}{c:c:c:c} \boldsymbol{A}_1 & \boldsymbol{A}_2 & \cdots & \boldsymbol{A}_J \end{array}\right]$. The problem now is how to estimate the S_Σ-*sparse* ($S_\Sigma = \sum_{j=1}^{J} S_j$) JN-length unknown vector $\boldsymbol{h}$ given the observation vector $\boldsymbol{y}$ and $K_0 \times JN$ sensing matrix $\boldsymbol{A}$, which is a cascade of partial Toeplitz matrices $\boldsymbol{A}_j$, under the presence of random noise vector $\boldsymbol{n}$.

3.3 Sparsity-Ignorant Estimator

Assuming that D does not have any knowledge about the sparsity or the statistical distribution of the channels, then its *sparsity-ignorant* receiver simply employs the conventional PA channel estimation using the LS method. To have a meaningful estimation, we need to transmit a training symbol vector of length $\mathcal{T} \geq (J+1)N - 1$, which provides us with at least as many interference-free observations as there are unknowns in (3.3). The LS solution for (3.3) is then given by [42]

$$\begin{aligned}\boldsymbol{h}_{\text{LS}} &= (\boldsymbol{A})^{\dagger}\,\boldsymbol{y} \\ &= (\boldsymbol{A}'\boldsymbol{A})^{-1}\,\boldsymbol{A}'\boldsymbol{y}.\end{aligned}$$

The MSE of the LS method is

$$\mathrm{MSE}_{\mathrm{LS}} = \sigma^2 \mathrm{Tr}\left\{(\boldsymbol{A}'\boldsymbol{A})^{-1}\right\},$$

which results in the lower bound $\sigma^2(JN)/K_0$.

3.4 Sparsity-Aware Estimator

In CS-based channel estimation, by taking the sparsity feature of the channels into account, we can significantly shorten $\mathcal{T}$ while maintaining sufficient accuracy, or achieving better accuracy compared to the LS method using the same pilot length (or probing time needed), as long as the two following conditions hold. First, the channel has to have S_Σ-*sparsity*, meaning that only S_Σ out of JN coefficients are non-zero ($S_\Sigma \leq JN$) (the remaining ones are zero or approximately zero). Second, the sensing matrix $\boldsymbol{A}$ must satisfy the RIP condition, or has a small mutual coherence, i.e., small correlation between its columns, which is also closely related to the RIP [2]. Next, we show that matrix $\boldsymbol{A}$ in (3.3) satisfies the RIP and has a small mutual coherence under reasonable conditions.

3.4.1 Compressive Sensing Dictionary

From the RIP definition, the sensing matrix $\boldsymbol{A}$ is said to satisfy the $RIP(S_\Sigma, \delta_{S_\Sigma})$ if for any vector $\boldsymbol{v}$ having S_Σ non-zero entries as $\boldsymbol{h}$, the two following inequalities hold for some $\delta_{S_\Sigma} > 0$

$$1 - \delta_{S_\Sigma} \leq \frac{\|\boldsymbol{A}\boldsymbol{v}\|_2}{\|\boldsymbol{v}\|_2} \leq 1 + \delta_{S_\Sigma}.$$

If $\boldsymbol{A}$ is chosen as in the discussion in the previous section, then we have the following result.

Theorem 3.1. *(RIP for the J-user MAC)*
Let $\{a_{j,l}\}_{l=1}^{N+K_0-1}$ *in (3.2) be a sequence of equally likely* $\pm 1/\sqrt{K_0}$ *i.i.d Bernoulli r.v.s.*

Then, $\boldsymbol{A}$ *satisfies the RIP*$(S_\Sigma, \delta_{S_\Sigma})$ *with probability exceeding* $1 - exp\left(-c_1 K_0 / S_\Sigma^2\right)$ *for any* $c_1 \leq \delta_{S_\Sigma}^2/32$ *when* $K_0 \geq c_2 S_\Sigma^2 \log(JN)$*, assuming that* $JN \geq 3$*, where it suffices to choose* $c_2 \geq 96/\left(\delta_{S_\Sigma}^2 - 32c_1\right)$.

Proof. For this proof, we follow the same approach used in [66], where we use the *Hoeffding's standard concentration inequalities* [Appendix B] and *Geršgorin's Disc Theorem* [67] as follows. Consider the $JN \times JN$ Gram matrix of $\boldsymbol{A}$, i.e.,

$$\boldsymbol{G} \triangleq \boldsymbol{A}'\boldsymbol{A} = \begin{bmatrix} \boldsymbol{G}_{1,1} & \boldsymbol{G}_{1,2} & \cdots & \boldsymbol{G}_{1,J} \\ \boldsymbol{G}_{2,1} & \boldsymbol{G}_{2,2} & \cdots & \boldsymbol{G}_{2,J} \\ \vdots & \vdots & \ddots & \vdots \\ \boldsymbol{G}_{J,1} & \boldsymbol{G}_{J,2} & \cdots & \boldsymbol{G}_{J,J} \end{bmatrix}, \tag{3.4}$$

where $\boldsymbol{G}_{j,j}$ is the $N \times N$ Gram matrix of $\boldsymbol{A}_j$, and $\boldsymbol{G}_{j,l} = \boldsymbol{A}_j'\boldsymbol{A}_l$, for $j, l = 1, 2, ..., J$ and $l \neq j$. As in [66], using the Hoeffding's standard concentration inequalities, each diagonal entry of $\boldsymbol{G}_{j,j}$ satisfies

$$\Pr\left(|\boldsymbol{G}_{j,j}(m,m) - 1| \geq \delta_d\right) \leq 2\exp\left(-2K_0\delta_d^2\right),$$

for $m = 1, ..., N$ and $j = 1, ..., J$; and each off-diagonal entry of $\boldsymbol{G}_{j,j}$ satisfies

$$\Pr\left(|\boldsymbol{G}_{j,j}(m,n)| \geq \frac{\delta_o}{S_\Sigma}\right) \leq 4\exp\left(-\frac{K_0\delta_o^2}{8S_\Sigma^2}\right),$$

for $m, n = 1, 2, ..., N$ and $n \neq m$.

Each entry (either diagonal or off-diagonal) of $\boldsymbol{G}_{j,l}$, given by $\boldsymbol{G}_{j,l}(m,n) = \boldsymbol{a}_{j,m}'\boldsymbol{a}_{l,n}$, is the inner product of the l-th column of $\boldsymbol{A}_j$ and n-th column of $\boldsymbol{A}_l$. Since the entries of these vectors are i.i.d, $\boldsymbol{G}_{j,l}(m,n)$ has zero mean and satisfies

$$\Pr\left(|\boldsymbol{G}_{j,l}(m,n)| \geq \frac{\delta_o}{S_\Sigma}\right) \leq 2\exp\left(-\frac{K_0\delta_o^2}{2S_\Sigma^2}\right).$$

The diagonal entries of $\boldsymbol{G}$ include the diagonal entries of each $\boldsymbol{G}_{j,j}$, which satisfy (3.5). Applying the union bound, we have

$$\begin{aligned}\Pr\left(\bigcup_{m=1}^{JN}\{|\boldsymbol{G}(m,m)-1|\geq\delta_d\}\right) &= \Pr\left(\bigcup_{j=1}^{J}\bigcup_{m=1}^{N}\{|\boldsymbol{G}_{j,j}(m,m)-1|\geq\delta_d\}\right)\\ &\leq 2JN\exp\left(-2K_0\delta_d^2\right). \end{aligned} \tag{3.5}$$

The off-diagonal entries of $\boldsymbol{G}$ include the off-diagonal entries of each $\boldsymbol{G}_{j,j}$, and all entries of each $\boldsymbol{G}_{j,l}$. Since $\boldsymbol{G}$ is *symmetric* and $\boldsymbol{G}_{j,l}=\boldsymbol{G}'_{l,j}$ (note that $\boldsymbol{G}_{j,l}$ is not symmetric itself), the number of *unique* off-diagonal entries of $\boldsymbol{G}$ is equal to the number of entries of all $\boldsymbol{G}_{j,l}$, $j>l$, which is $J(J-1)N^2/2$, plus the number of unique off-diagonal entries of all $\boldsymbol{G}_{j,j}$, which is $J(N^2-N)/2$. Applying the union bound, and assume $J\geq 2$, we obtain

$$\begin{aligned}\Pr\left(\bigcup_{m=1}^{J}\bigcup_{n=1,n\neq m}^{J}\left\{|\boldsymbol{G}(m,n)|\geq\frac{\delta_o}{S}\right\}\right) &\leq 2\frac{J(J-1)N^2}{2}\exp\left(-\frac{K_0\delta_o^2}{2S_\Sigma^2}\right)\\ &+ 4\frac{J(N^2-N)}{2}\exp\left(-\frac{K_0\delta_o^2}{8S_\Sigma^2}\right)\\ &\leq 2J^2N^2\exp\left(-\frac{K_0\delta_o^2}{8S_\Sigma^2}\right). \end{aligned} \tag{3.6}$$

From (3.5) and (3.6) and applying the Geršgorin's theorem [66], [67], we obtain

$$\Pr\left(\boldsymbol{X}\text{ does not satisfy RIP}(S_\Sigma,\delta_{S_\Sigma})\right)\leq 2JN\exp\left(-2K_0\delta_d^2\right)+2J^2N^2\exp\left(-\frac{K_0\delta_o^2}{8S_\Sigma^2}\right).$$

If we choose $\delta_d=\delta_o=\delta_{S_\Sigma}/2$, and assuming $N\geq 2$, we have

$$\begin{aligned}\Pr\left(\boldsymbol{X}\text{ satisfies RIP}(S_\Sigma,\delta_{S_\Sigma})\right) &\geq 1-\left(2J^2+J\right)N^2\exp\left(-\frac{K_0\delta_{S_\Sigma}^2}{32S_\Sigma^2}\right)\\ &\geq 1-3J^2N^2\exp\left(-\frac{K_0\delta_{S_\Sigma}^2}{32S_\Sigma^2}\right).\end{aligned}$$

For any $c_1 \leq \delta_{S_\Sigma}^2/32$, we obtain the following lower bound of the RIP satisfying probability

$$\Pr\left(\boldsymbol{X} \text{ satisfies RIP}(S_\Sigma, \delta_{S_\Sigma})\right) \geq 1 - \exp\left(-\frac{c_1 K_0}{S_\Sigma^2}\right) \tag{3.7}$$

for any K_0 satisfies

$$K_0 \geq \frac{32}{\delta_{S_\Sigma}^2 - 32c_1} S_\Sigma^2 \log\left(3J^2N^2\right). \tag{3.8}$$

Assuming that $JN \geq 3$, then (3.7) occurs for any $K_0 \geq c_2 S_\Sigma^2 \log(JN)$, where it suffices to choose

$$c_2 \geq 96/\left(\delta_{S_\Sigma}^2 - 32c_1\right). \tag{3.9}$$

□

Next, we prove that $\boldsymbol{A}$ has small mutual coherence, making it suitable for a CS dictionary. As the definition, the mutual coherence of $\boldsymbol{A}$ is computed as

$$\mu \triangleq \max_{l \neq j} |\langle \boldsymbol{a}_j, \ \boldsymbol{a}_l \rangle|, \tag{3.10}$$

we have the following lemma.

Theorem 3.2. *(Mutual Coherence of $\boldsymbol{A}$)*
The mutual coherence of $\boldsymbol{A}$ is statistically upper bounded by

$$\mu \leq 4\sqrt{K_0^{-1} \log(J^2N^2/\delta)}, \tag{3.11}$$

with probability exceeding $1 - \delta^2$, for some $\delta > 0$.

Proof. As defined in (3.10), the mutual coherence of $\boldsymbol{A}$ is the largest off-diagonal entry

(in the absolute value sense) of $\boldsymbol{G}$. Using the union bound, we obtain the upper bound

$$\begin{aligned}\Pr(\mu \geq \epsilon) &= \Pr\left(\max_{m \neq n} |\boldsymbol{G}(m,n)| \geq \epsilon\right) \\ &< \Pr\left(\bigcup_{m=1}^{J} \bigcup_{n=1, n\neq m}^{J} \{|\boldsymbol{G}(m,n)| \geq \epsilon\}\right).\end{aligned}$$

Using the result from (3.6), we have

$$\Pr(\mu \geq \epsilon) < 2J^2N^2 \ \exp\left(-\frac{K_0\epsilon^2}{8}\right). \tag{3.12}$$

If we choose $\epsilon = 4\sqrt{K_0^{-1}\log\left(J^2N^2/\delta\right)}$, then (3.12) becomes

$$\Pr\left(\mu \geq 4\sqrt{K_0^{-1}\log\left(J^2N^2/\delta\right)}\right) < \delta^2,$$

which completes the proof. □

It is interesting to observe that when $J = 1$, (3.11) becomes an upper bound on the mutual coherence for the single-user case, which is identical to the bound obtained in [42], even though we use a different (and much simpler) proof.

By proving the RIP and the small mutual coherence constant of the measurement matrix $\boldsymbol{A}$ for estimating the total channel vector $\boldsymbol{h}$ in (3.3), we show the suitability of $\boldsymbol{A}$ as a sensing operator[1], and that there exist a CS technique to efficiently estimate the sparse vector $\boldsymbol{h}$. The small mutual coherence constant also quantifies the RIP order of the measurement matrix, as the smaller μ allows to establish a smaller RIP constant and a recovery guarantee for a sparse vector with larger sparse ratio [35, 71].

Remark 3.1. *We only consider the case of random i.i.d. Bernoulli pilot sequences, where the pilot symbols are BPSK (or 2-QAM) modulated, for simplicity. The RIP and*

[1]It should be noticed that RIP is only a necessary condition for a recovery guarantee, and there are other cases where RIP-less guarantees also support a special type of measurement matrices [68–70].

incoherence of the measurement matrix using QAM or other modulation formats can be verified using a similar approach.

Taking the 4-QAM as an example, the normalized sensing matrix $\boldsymbol{A}$ has i.i.d. random elements obeying

$$a_{i,j} \sim \begin{cases} \frac{1}{\sqrt{2K_0}}(1+j) & \text{with probability } 1/4 \\ -\frac{1}{\sqrt{2K_0}}(1+j) & \text{with probability } 1/4 \\ \frac{1}{\sqrt{2K_0}}(1-j) & \text{with probability } 1/4 \\ -\frac{1}{\sqrt{2K_0}}(1-j) & \text{with probability } 1/4 \end{cases}.$$

Since the entries of $\boldsymbol{A}$ also have zero mean and are bounded (in absolute value), the above derivation for BPSK pilot symbols using *Hoeffding's standard concentration inequalities* and *Geršgorin's Disc Theorem* can also applied for QAM. Indeed, the RIP and incoherence conditions can be verified for partial Toeplitz measurement matrices whose entries belong to a more general class of i.i.d. zero-mean sub-Gaussian random variables. In term of the estimation performance, however, we do not make any claim that m-QAM ($m > 2$) outperforms BPSK or the other way around. It is true that dense QAM constellations provide higher spectral efficiency as compared to BPSK. However, the channel estimation task would be more difficult since it requires estimating the amplitude variations in the channel in addition to having knowledge of the phase variations. Extending CMCE to other modulation formats would be an interesting topic to tackle.

3.4.2 CS Reconstruction Technique

Given that the measurement matrix $\boldsymbol{A}$ satisfies the RIP and has low mutual coherence, there are a variety of CS reconstruction techniques that can efficiently solve the problem given in (3.3). They include greedy-based methods such as the IHT [32], (OMP) [33];

and convex optimization-based methods such as the BPDN and Danzig selector [17], as described in Chapter 2. The major weakness of the greedy-based techniques is that their performance guarantee holds only if the magnitudes of all S_Σ non-zero coefficients of $\boldsymbol{h}$ are somewhat above the noise level [35]. If some of them are smaller than the noise level, then the solver may incorrectly define the support set of $\boldsymbol{h}$, making its performance very poor. This can happen in our case especially since the channels are random. The three ℓ_1-based convex optimization methods mentioned above are exchangeable under suitable regularization parameters or constraints [36], and they all require only the sparsity condition. Throughout this chapter, we use the ℓ_1-penalty version of the BPDN method for the CS reconstruction technique, which is defined for (3.3) as

$$\min_{\boldsymbol{h}} \frac{1}{2} \|\boldsymbol{y} - \boldsymbol{A}\boldsymbol{h}\|_2^2 + \gamma \|\boldsymbol{h}\|_1 ,$$

where γ is the turning parameter. When γ is typically chosen as

$$\gamma = \sqrt{8\sigma^2(1+\alpha)\log(JN - S_\Sigma)},$$

the BPDN has the following performance guarantee (Theorem 3 of [35]).

$$\mathrm{MSE}_{\mathrm{BPDN}} \leq \left(\sqrt{3} + 3\sqrt{2(1+\alpha)\log(JN - S_\Sigma)}\right)^2 S_\Sigma \sigma^2,$$

with probability exceeding $(1 - (JN - S_\Sigma)^{-\alpha})\,(1 - \exp(-S_\Sigma/7))$, for some $\alpha > 0$, under the condition that $S_\Sigma \leq 1/(3\mu)$.

We will demonstrate in Section 3.6 via simulations the efficacy of using this CMCE over its CSCE counterpart.

3.5 Channel Estimation for Two-way Relay Sparse ISI Channel

In this section, we show that the estimation of composite channels in the sparse ISI-TWRC case employing analog network coding can be formulated as a CMCE problem, and can be performed efficiently using the CS approach introduced above.

3.5.1 System Model

We consider the system model in Fig. 3.2a, where two sources T_1 and T_2 exchange their information via relay R, in a single-carrier based system. Denote the two uplink channels between T_j and R (for $j = 1, 2$) by $\boldsymbol{h}_j = \{h_{j,l}\}_{l=1}^{L_u}$. Each channel is assumed to be S_j-sparse L_u-length frequency-selective channel. This means that out of L_u there are only S_j dominant coefficients, and the rest are (nearly) zero. We note here that if each channel has a different length L_j, then we can assume that the coefficients of the shorter channel from its end to L_u are zero, where $L_u = \max(L_1, L_2)$. The similar notations are used for the downlink channels between R and T_j, as denoted by $\boldsymbol{h}_3$ and $\boldsymbol{h}_4$ with length L_d, and the sparsities S_3 and S_4, respectively. The channels' coefficients are i.i.d. Rayleigh distributed, and vary from one block to another.

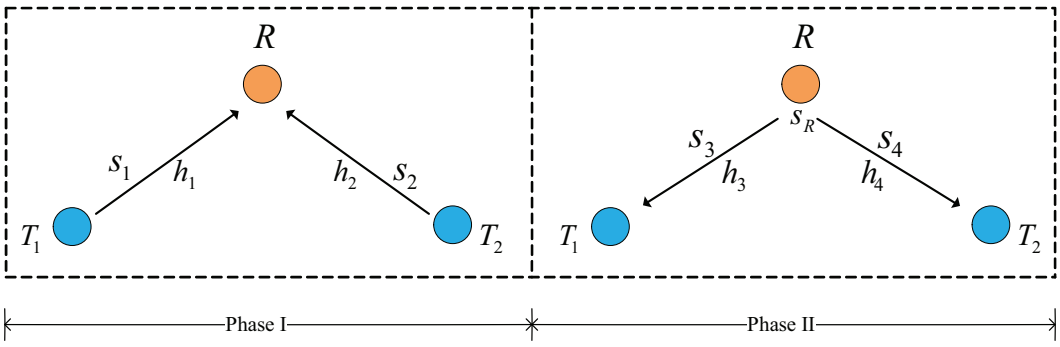

Figure 3.2: Two-phase two-way relaying protocol.

Let $\boldsymbol{p}_j = [p_{j,1}\ p_{j,2}\ \ldots\ p_{j,\mathcal{T}}]^T$ denote the random symmetric Bernoulli ± 1 pilot sequence

of length $\mathcal{T}$ at T_j, known by both sources, where $\mathcal{T} = K_0 + L_h - 1$ ($L_h = L_u + L_d - 1$).

In Phase I, two sources send their pilots simultaneously to the relay. Since ISI occurs, the received signal at R, is

$$\boldsymbol{y}_R = \boldsymbol{H}_1\boldsymbol{p}_1 + \boldsymbol{H}_2\boldsymbol{p}_2 + \boldsymbol{n}_R,$$

where $\boldsymbol{H}_j$ is the $K_0 \times K_0$ Toeplitz matrix,

$$\boldsymbol{H}_j = \begin{bmatrix} h_{j,L_u} & \cdots & h_{j,1} & 0 & \cdots & 0 \\ 0 & \cdots & h_{j,2} & h_{j,1} & \cdots & 0 \\ \vdots & \ddots & \vdots & \vdots & \ddots & \vdots \\ 0 & \cdots & h_{j,L_u} & h_{j,L_u-1} & \cdots & h_{j,1} \end{bmatrix}; \tag{3.13}$$

$\boldsymbol{n}_R$ is a $K_0 \times 1$ vector of complex AWGN samples at R, with variance σ^2. As in the previous section, here we only take the interference-free and collision-free received symbols as useful observations for the channel estimation purpose. Since our protocol applies analog network coding at the relay, the relay does not need to estimate the channels but amplifies $\boldsymbol{y}_R$ by factor [72]

$$\beta = \sqrt{\frac{E_R}{E_1\mathbb{E}\{|\boldsymbol{h}_1|^2\} + E_2\mathbb{E}\{|\boldsymbol{h}_2|^2\} + \sigma^2}},$$

where E_1, E_2, E_R are the transmit power constraints at T_1 and T_2 and R, respectively. The transmitted signal by the relay to the two sources in Phase II is $\boldsymbol{p}_R = \beta\boldsymbol{y}_R$. In Phase II, the received signal at T_1 is (an analogous process is performed at T_2)

$$\begin{aligned} \boldsymbol{y}_1 &= \boldsymbol{H}_3\boldsymbol{p}_R + \boldsymbol{n}_1 \\ &= \beta\boldsymbol{H}_3\left(\boldsymbol{H}_1\boldsymbol{p}_1 + \boldsymbol{H}_2\boldsymbol{p}_2 + \boldsymbol{n}_R\right) + \boldsymbol{n}_1, \end{aligned} \tag{3.14}$$

where $\boldsymbol{n}_1$ is a $K \times 1$ AWGN vector at T_1 with variance σ^2. Denote $\tilde{\boldsymbol{H}}_1 = \beta\boldsymbol{H}_3\boldsymbol{H}_1$,

$\tilde{\boldsymbol{H}}_2 = \beta \boldsymbol{H}_3 \boldsymbol{H}_2$, $\tilde{\boldsymbol{n}}_1 = \beta \boldsymbol{H}_3 \boldsymbol{n}_R + \boldsymbol{n}_1$, then (3.14) is re-written as

$$\boldsymbol{y}_1 = \tilde{\boldsymbol{H}}_1 \boldsymbol{p}_1 + \tilde{\boldsymbol{H}}_2 \boldsymbol{p}_2 + \tilde{\boldsymbol{n}}_1 \tag{3.15a}$$

$$= \boldsymbol{P}_1 \tilde{\boldsymbol{h}}_1 + \boldsymbol{P}_2 \tilde{\boldsymbol{h}}_2 + \tilde{\boldsymbol{n}}_1 \tag{3.15b}$$

$$= \left[\begin{array}{c:c} \boldsymbol{P}_1 & \boldsymbol{P}_2 \end{array} \right] \left[\begin{array}{c} \tilde{\boldsymbol{h}}_1 \\ \hdashline \tilde{\boldsymbol{h}}_2 \end{array} \right] + \tilde{\boldsymbol{n}}_1$$

$$= \boldsymbol{P}_R \tilde{\boldsymbol{h}} + \tilde{\boldsymbol{n}}_1, \tag{3.15c}$$

where $\boldsymbol{P}_R = \left[\begin{array}{c:c} \boldsymbol{P}_1 & \boldsymbol{P}_2 \end{array} \right]$ in which $\boldsymbol{P}_j$ is $K_0 \times L_h$ partial Toeplitz matrix formed by column $\boldsymbol{p}_j$ as

$$\boldsymbol{P}_j = \begin{bmatrix} p_{j,L_h} & p_{j,L_h-1} & \cdots & p_{j,1} \\ p_{j,L_h+1} & p_{j,L_h} & \cdots & p_{j,2} \\ \vdots & \vdots & \ddots & \vdots \\ p_{j,L_h+K_0-1} & p_{j,L_h+K_0-2} & \cdots & p_{j,K_0} \end{bmatrix},$$

$\tilde{\boldsymbol{h}} = \left[\tilde{\boldsymbol{h}}_1; \tilde{\boldsymbol{h}}_2 \right]$ is the effective channel to be estimated at T_1 with total length $L_{\text{eff}} = 2L_h$: $\tilde{\boldsymbol{h}}_1$ is the composite $T_1 - R - T_1$ channel, $\tilde{\boldsymbol{h}}_2$ is the composite $T_2 - R - T_1$ channel; and in (3.15b) we apply the commutative property of the convolution operator. Note that the proposed protocol has the advantage that the channel estimation is performed at the sources not at the relay, and only the composite channels are needed for data detection [72]. We can easily prove that the convolution of S_1-sparse L_u-length channel and S_3-sparse L_d-length channel results in the L_h-length channel with a sparsity of at most $S_1 S_3$. Therefore, the number of dominant taps of $\tilde{\boldsymbol{h}}$, denoted by S_Σ, is at most $S_1 S_3 + S_2 S_3$, and $\tilde{\boldsymbol{h}}$ needed to be estimated at T_1 is sparse if we have $S_\Sigma \ll L_{\text{eff}} = 2(L_u + L_d - 1)$, which is usually the case when $S_1, S_2 \ll L_u$ and $S_3 \ll L_d$.

3.5.2 Sparsity-Ignorant Receiver: Least Square Based

The sparsity-ignorant receiver at T_j simply employs the conventional PA channel estimation using the LS method given that a training symbol vector of length $\mathcal{T} \geq L_{\text{eff}} + L_d - 1 = 2L_u + 3L_d - 3$ is used. The channel estimate of $\tilde{\boldsymbol{h}}$, denoted by $\tilde{\boldsymbol{h}}_{\text{LS}}$, is given by

$$\begin{aligned}\tilde{\boldsymbol{h}} &= (\boldsymbol{P}_R)^{\dagger} \boldsymbol{y}_1 \\ &= (\boldsymbol{P}_R' \boldsymbol{P}_R)^{-1} \boldsymbol{P}_R' \boldsymbol{y}_1.\end{aligned}$$

The MSE for the LS receiver is given by,

$$\text{MSE}_{\text{LS}} = \sigma^2 \text{Tr}\left\{ (\boldsymbol{P}_R' \boldsymbol{P}_R)^{-1} \right\},$$

which results in the lower bound $\sigma^2 L_{\text{eff}}/K_0$.

3.5.3 Sparsity-Aware Receivers: Compressive-Sensing Based

The sparsity-aware receivers perform a CS-based estimation technique such as BPDN, as described in the previous chapter. The implication here is that the sensing matrix for TWRC estimation also satisfies RIP and has low mutual coherence, which can be proven in the following results.

Corollary 3.1. *The sensing matrix for estimating $\tilde{\boldsymbol{h}}$ in (3.15c) satisfies the RIP($S_\Sigma, \delta_{S_\Sigma}$) with probability exceeding $1 - exp\left(-c_1 K_0 / S_\Sigma^2\right)$ for any $c_1 \leq \delta_{S_\Sigma}^2/32$ when $K_0 \geq c_2 S_\Sigma^2 \log L_{eff}$, given that $L_{eff} \geq 3$, where it suffices to choose $c_2 \geq 96/\left(\delta_{S_\Sigma}^2 - 32c_1\right)$.*

Proof. By scaling the sensing matrix $\boldsymbol{P}_R$ so that its column has unit norm, then it exactly has the form of $\boldsymbol{A}$ in Theorem 3.1. Therefore, the result is directly obtained. □

Corollary 3.2. *The mutual coherence of the sensing matrix $\boldsymbol{P}_R$ for estimating $\tilde{\boldsymbol{h}}$ is upper bounded by $4\sqrt{(K_0)^{-1} \log\left(L_{eff}/\delta\right)}$ with probability exceeding $1 - \delta^2$, for some $\delta > 0$.*

Proof. Using the result from Theorem 3.2 and the same argument used in the proof of Corollary 3.1, we can prove Corollary 3.2. □

For comparison purposes, we also consider a channel estimation scheme based on an *Oracle* (ORC), which provides us the support set of the indices of the non-zero coefficients of the channel impulse response, which is denoted by $\text{supp}(\tilde{\boldsymbol{h}}) = \{i : \tilde{h}_i \neq 0\}$. This performance serves as the CRB for all the unbiased estimators considered. The solution of the ORC-based channel estimation is

$$\begin{aligned}\tilde{\boldsymbol{h}}_{\text{ORC}} &= \boldsymbol{P}_{\text{ORC}}^{\dagger}\boldsymbol{y}_1 \\ &= \left(\boldsymbol{P}_{\text{ORC}}'\boldsymbol{P}_{\text{ORC}}\right)^{-1}\boldsymbol{P}_{\text{ORC}}'\boldsymbol{y}_1,\end{aligned}$$

where $\boldsymbol{P}_{\text{ORC}}$ is formed by retaining all the columns of $\boldsymbol{P}_R$ with indices in $\text{supp}(\tilde{\boldsymbol{h}})$.

The bound of the MSE performance for the ORC-based receiver is given by

$$\text{MSE}_{\text{ORC}} = \sigma^2 \text{Tr}\left\{\left(\boldsymbol{P}_{\text{ORC}}'\boldsymbol{P}_{\text{ORC}}\right)^{-1}\right\},$$

which results in the lower bound of $S_\Sigma\sigma^2/K_0$.

3.6 Simulation Results

3.6.1 Compressive Multi-channel Estimation

In this section, we present numerical results to show the performance improvement of using CMCE methods described above. We first examine the improvement in terms of the MSE that the CMCE method provides over its CSCE counterpart, when both use the same CS-based BPDN technique to estimate multiple sparse channels. Here we define the single-channel estimation method as the one estimating each channel of each user-destination pair individually (by sending J training sequences at J orthogonal time slots

for the J-user case). Assume that we need to estimate three sparse channels $\{\boldsymbol{h}_j\}_{j=1}^{3}$, with the same length $N = 16$, and same sparsity $S = 4$ (this assumption does not affect the generality of the results). We further assume that the support set of the channels are: $\text{supp}(\boldsymbol{h}_1) = \{1, 4, 9, 16\}$, $\text{supp}(\boldsymbol{h}_2) = \{1, 3, 10, 16\}$, $\text{supp}(\boldsymbol{h}_3) = \{1, 5, 8, 16\}$. All non-zero coefficients of each channel are assumed to be independent r.v.s and follow Rayleigh distribution. The total power of each channel is normalized to unity. We run the simulation for 5000 random channel realizations.

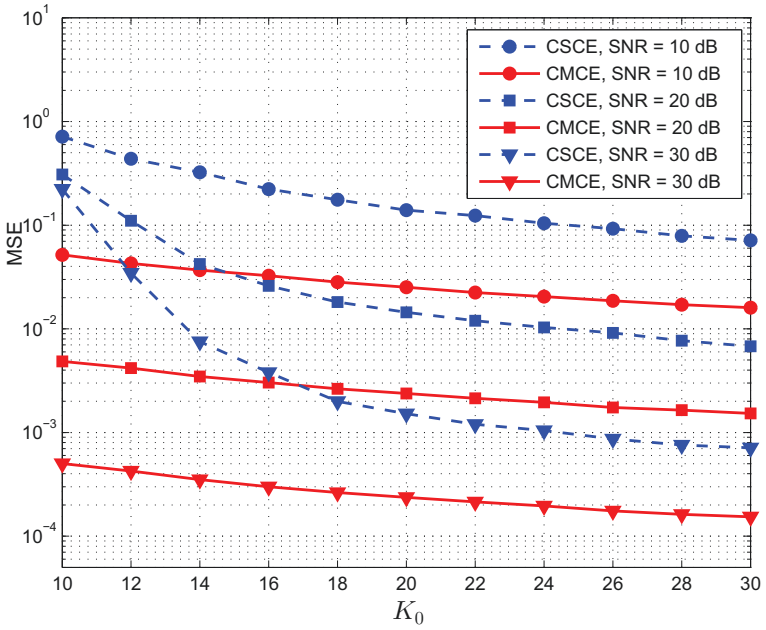

Figure 3.3: MSE comparison between BPDN-based CMCE and CSCE methods with different training lengths, at different SNR, $N = 16, S = 4$.

In the CSCE method, if estimating each channel needs a training of $K_0 + N - 1$ known i.i.d equally likely Bernoulli ± 1, where K_0 is the interference-free observations, then the total training length for estimating all three channels is $3(K_0 + N - 1)$. Fig. 3.3 shows that by using the same total training length, the CMCE method provide significant improvements in term of MSE between the total channel $\boldsymbol{h}$ and its estimates, at different SNR $= E_s/N_0$ of 10, 20 and 30 dB, where SNR is defined as the ratio between symbol power and noise power. It is equivalent to saying that we can shorten the total training length (or probing time) needed by using the CMCE method to achieve the same performance

target. Obviously the CMCE scheme provides a better bandwidth efficiency/performance trade-off as compared to the CSCE scheme.

In the second experiment, we repeat the experiment for the case when SNR = 10 dB, and this time the locations of the non-zero channel coefficients are randomly generated. The final results are averaged over 1000 random support sets. We also present the MSE results when the channel length N of each link is increased to 32, but the ratio S/N is kept at 1/4. The results in Fig. 3.4 also show that CMCE outperforms CSCE for both cases $N = 16$ and $N = 32$ in term of MSE. Furthermore, comparing Figs. 3.3 and 3.4 for the case $N = 16$, $S = 4$, we see that the results do not depend on the locations of non-zero coefficients. The performance for the randomly generated support sets in Fig. 3.4 is the same as that of the fixed one used in Fig. 3.3.

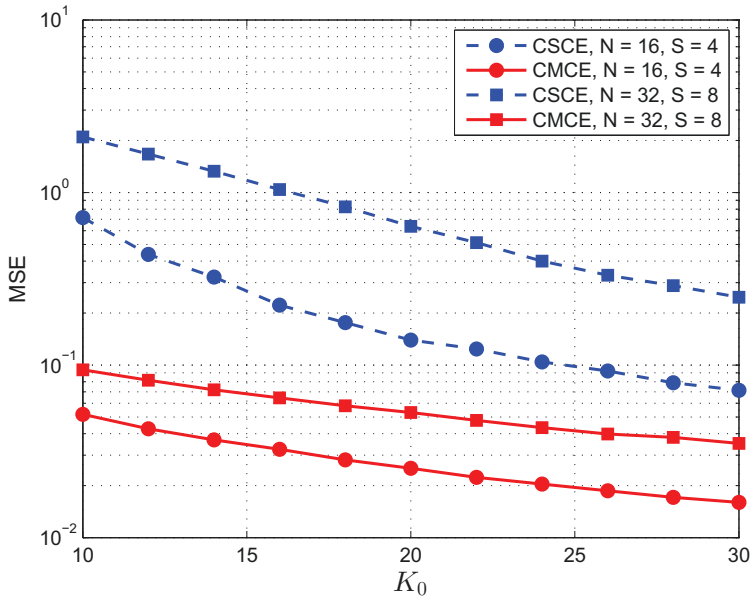

Figure 3.4: MSE comparison between BPDN-based CMCE and CSCE methods with different training lengths, at SNR = 10 dB.

Finally, we present the MSE results using the CMCE approach for different sparsity levels (i.e. S/N ratios) for the case $N = 32$: $S = 4, 8, 12$. Fig. 3.5 shows that we can estimate the total channel $\tilde{\boldsymbol{h}}$ more accurately for smaller values of S (i.e., more sparsity).

Since the LS method does not consider the sparsity of channels, its performance is almost the same at different S, and is much less accurate as compared to the CS method.

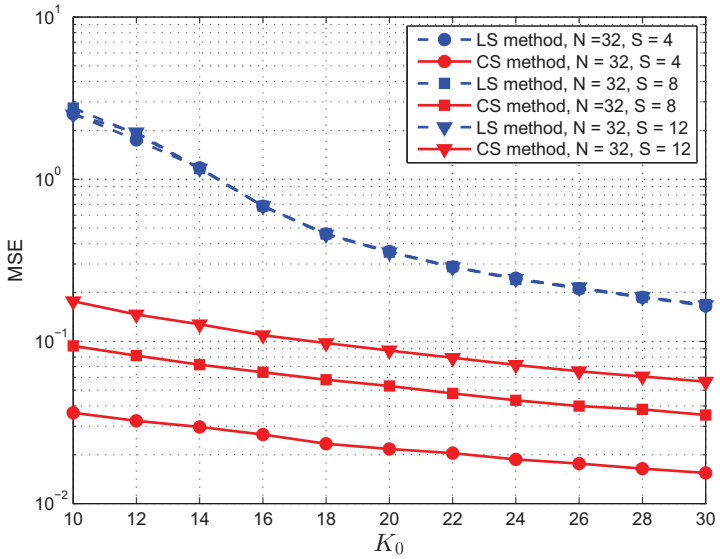

Figure 3.5: MSE comparison between the LS-based and BPDN-based methods using the CMCE approach with different training lengths, at SNR = 10 dB.

3.6.2 Channel Estimation for Sparse ISI-TWRC

Given that the CMCE method outperforms its CSCE counterpart, we next present the performance improvements achieved by using the CMCE method over the traditional LS-based method (also in a multi-channel estimation framework) for the estimation of the sparse ISI-TWRC with analog network coding, as described in Section 3.5. In the simulation, we assume that the sparse ISI-TWRC is symmetric, i.e., the two reciprocical source-relay channels $\boldsymbol{h}_1$ and $\boldsymbol{h}_2$ in Fig. 3.2 have the same sparse impulse response with the support sets $\{1, 4, 9, 16\}$. Again, this assumption is just for simplicity, and does not affect the generality of the simulation, since the results does not depend on the locations of the non-zero coefficients, as seen in the previous section. A known i.i.d. equally likely ± 1 Bernoulli training sequence of length $\mathcal{T} = K_0 + L_d - 1$ is embedded prior to each coded symbol block, with K_0 being the interference-free and collision-free observations. By operating the two-phase transmission scheme as described in Fig. 3.5, at the end of

the second phase, each terminal's receiver performs the multi-channel estimation using CMCE. The number of random channel realizations is also set to 5000. Since this is a symmetric TWRC, only the MSE results at one terminal are presented.

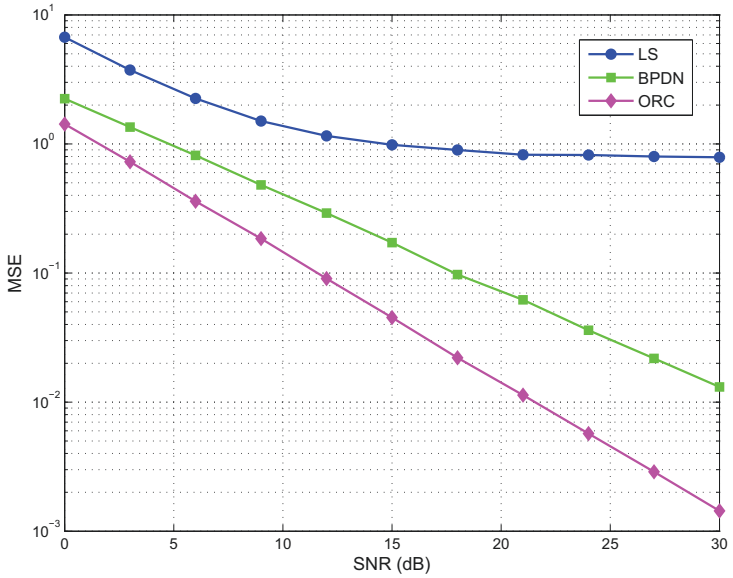

Figure 3.6: MSE comparison of different multi-channel estimation methods for sparse ISI-TWRC with $\mathcal{T} = 60$ (under-determined setting).

The two *composite* source-relay-destination channels that need to be estimated in the multi-channel estimation framework has a total length of $L_{\text{eff}} = 2L_h = 2(L_u + L_d - 1) = 62$, meaning that the length of the training sequence $\mathcal{T}$ has to be at least $62 + L_d - 1 = 77$ for the LS method to work. We show below two simulation results for two settings: one is under-determined where $\mathcal{T} = 60 < 77$, and another is over-determined where $\mathcal{T} = 90 > 77$. Figs. 3.6 and Fig. 3.7, we show the MSEs between the effective channel $\tilde{\boldsymbol{h}}$ and its estimates versus SNR at one terminal for different methods when $\mathcal{T} = 60$ and $\mathcal{T} = 90$, respectively. For comparison purposes, we also show the MSE of the ORC method, and the case when perfect CSI is assumed at the terminal. As expected for the under-determined case ($\mathcal{T} = 60$), we can see a huge improvement of using CS-based BPDN method over the LS one. In this under-determined case, while the LS method has very

poor performances both in MSE, the CS method has the MSE performance approaching that of the ORC-based method at high SNR.

When we increase the length of $\mathcal{T}$ to 90, the MSE performance of the BPDN method closely approaches that of the ORC-based and perfect CSI based methods. In this case, these error performances of the LS method are still far way from the CS-based method and the lower bounds based on ORC and perfect CSI ones.

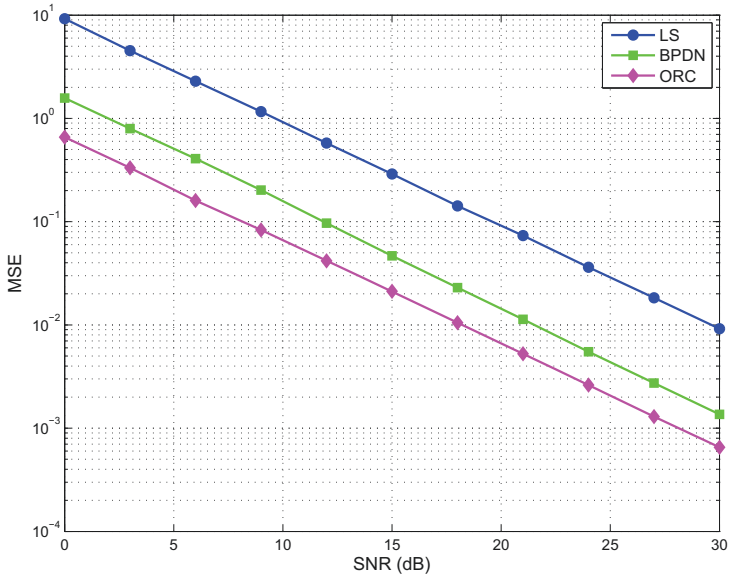

Figure 3.7: MSE comparison of different multi-channel estimation methods for sparse ISI-TWRC with $\mathcal{T} = 90$ (over-determined setting).

3.7 Concluding Remarks

This chapter has addressed the problem of simultaneous estimation of multiple sparse ISI channels that do not necessarily have a common sparsity support, and applied it to the compressive estimation of sparse ISI-TWRC employing analog network coding. Both theoretical and empirical results suggested that the CS-based CMCE method significantly outperforms the traditional LS-based one, which ignores the sparsity feature of the underlying channels.

Chapter 4

Joint Compressive Estimation and Decoding for Sparse ISI-TWRC

4.1 Introduction

In Chapter 3, we have shown that the estimation of the sparse ISI-TWRC can be formulated and efficiently estimated using the CMCE method. In this chapter, we further study the problem of joint channel estimation and data decoding for the sparse ISI-TWRC, operating in both AF and DF modes. This is different from most of the previous works in the literature on compressive channel sensing that only consider the performance of channel estimation [66, 73].

For AF, we first apply the method of multiple-channel estimation developed in the previous chapter for sparse ISI-TWRC and propose an iterative receiver that performs channel estimation and data decoding jointly. We prove that the condition required for CS holds with stronger convergence, and the method provides the better MSE and BER performance as compared to the ones that do not take the sparsity of the channel into account. In DF, we utilize the prior information of the sparsity of the channel into both the estimation and channel equalization processes to improve these end-to-end performances.

Finally, we develop a thresholding technique which mitigate the error propagation of TWRC operating in DF to further improve the end-to-end system performances.

4.2 Amplify-and-Forward TWRC

4.2.1 Signal and Channel Models

The system model is the same as the one in Chapter 3, where two sources T_1 and T_2 exchange their information via relay R, in a single-carrier based system. Since we consider both channel estimation and the data decoding, we describe the signal model as follows (Fig. 4.1).

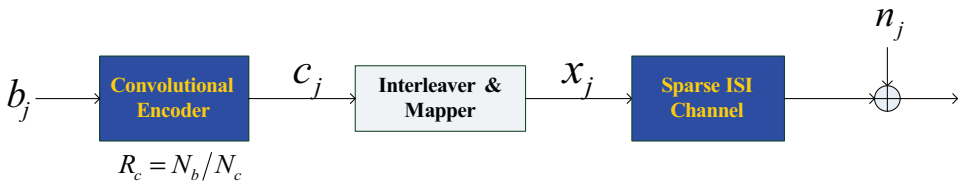

Figure 4.1: Signal and channel models for each T_j-R link.

Let $\boldsymbol{b}_j = \{b_{j,n_b}\}_{n_b=1}^{N_b}$ denote the N_b-length binary information vector transmitted by T_j in one period of data exchange. After having been encoded by each convolutional encoder with rate $R_c = N_b/N_c$, each corresponding M-length coded vector, denoted by $\boldsymbol{c}_j = \{c_{j,n}\}_{n=1}^{N_c}$ is randomly interleaved and BPSK modulated, resulting in the coded symbol vector $\boldsymbol{x}_j = \{x_{j,m}\}_{m=1}^{N_c}$. The transmitted symbol vector at T_j in Phase I is denoted by $\boldsymbol{s}_j = [\boldsymbol{p}_j^T \ \boldsymbol{x}_j^T]^T$, where $\boldsymbol{p}_j = \{p_{j,n}\}_{n=1}^{\mathcal{T}}$ is a random symmetric Bernoulli ± 1 pilot sequence of length $\mathcal{T}$ at T_j, known by both sources, where $\mathcal{T} = K_0 + L_d - 1$.

Each channel $\boldsymbol{h}_j$ is assumed to be S_j-sparse N-length as in Chapter 3. In Phase I, the two sources send their data simultaneously to the relay. Since ISI occurs, the received signal at R, is

$$\boldsymbol{y}_R = \sum_{j=1}^{2} \boldsymbol{H}_j \boldsymbol{s}_j + \boldsymbol{n}_R, \tag{4.1}$$

where $\boldsymbol{H}_j$ is the $(K_0 + N_c) \times (K_0 + N_c)$ Toeplitz matrix,

$$\boldsymbol{H}_j = \begin{bmatrix} h_{j,L_u} & \cdots & h_{j,1} & 0 & \cdots & 0 \\ 0 & \cdots & h_{j,2} & h_{j,1} & \cdots & 0 \\ \vdots & \ddots & \vdots & \vdots & \ddots & \vdots \\ 0 & \cdots & h_{j,L_u} & h_{j,L_u-1} & \cdots & h_{j,1} \end{bmatrix}; \tag{4.2}$$

$\boldsymbol{n}_R$ is a $(K_0 + N_c) \times 1$ vector of complex AWGN samples at R, with variance σ^2. By (4.2), we also discard the observations at R in the collision interval between the uplink in Phase I and the downlink in Phase II. Since our protocol applies analog network coding at the relay, the relay does not need to estimate the channels or decode $\boldsymbol{x}_1$ and $\boldsymbol{x}_2$, but it amplifies its $\boldsymbol{y}_R$ by a factor β [72]. The transmitted signal by the relay to the two sources in phase II is $\boldsymbol{s}_R = \beta \boldsymbol{y}_R$.

In Phase II, the received signal at T_1 is (an analogous process is performed at T_2)

$$\begin{aligned} \boldsymbol{y}_1 &= \boldsymbol{H}_3 \boldsymbol{s}_R + \boldsymbol{n}_1 \\ &= \beta \boldsymbol{H}_3 \left(\boldsymbol{H}_1 \boldsymbol{s}_1 + \boldsymbol{H}_2 \boldsymbol{s}_2 + \boldsymbol{n}_R \right) + \boldsymbol{n}_1, \end{aligned} \tag{4.3}$$

where $\boldsymbol{n}_1$ is a $(K_0 + N_c) \times 1$ AWGN vector at T_1 with variance σ^2. Denote $\tilde{\boldsymbol{H}}_1 = \beta \boldsymbol{H}_3 \boldsymbol{H}_1$, $\tilde{\boldsymbol{H}}_2 = \beta \boldsymbol{H}_3 \boldsymbol{H}_2$, $\tilde{\boldsymbol{n}}_1 = \beta \boldsymbol{H}_3 \boldsymbol{n}_R + \boldsymbol{n}_1$, then (4.3) is re-written as

$$\boldsymbol{y}_1 = \tilde{\boldsymbol{H}}_1 \boldsymbol{s}_1 + \tilde{\boldsymbol{H}}_2 \boldsymbol{s}_2 + \tilde{\boldsymbol{n}}_1 \tag{4.4a}$$

$$= \boldsymbol{S}_1 \tilde{\boldsymbol{h}}_1 + \boldsymbol{S}_2 \tilde{\boldsymbol{h}}_2 + \tilde{\boldsymbol{n}}_1 \tag{4.4b}$$

$$= \boldsymbol{S}_R \tilde{\boldsymbol{h}} + \tilde{\boldsymbol{n}}_1, \tag{4.4c}$$

where $\boldsymbol{S}_R = \left[\begin{array}{c:c} \boldsymbol{S}_1 & \boldsymbol{S}_2 \end{array} \right]$ in which $\boldsymbol{S}_j$ is $(K_0 + N_c) \times L_h$ ($L_h = L_u + L_d$ as defined in

Chapter 3) partial Toeplitz matrix formed by column $\boldsymbol{s}_j$ as

$$\boldsymbol{S}_j = \begin{bmatrix} s_{j,L_h} & s_{j,L_h-1} & \cdots & s_{j,1} \\ s_{j,L_h+1} & s_{j,L_h} & \cdots & s_{j,2} \\ \vdots & \vdots & \ddots & \vdots \\ s_{j,L_h+K_0+N_c-1} & s_{j,L_h+K_0+N_c-2} & \cdots & s_{j,K_0+N_c}. \end{bmatrix}$$

4.2.2 Proposed Iterative Scheme

We first describe our proposed joint iterative estimation and decoding scheme at T_1 as depicted in Fig. 4.2 (an analogous process is performed at T_2). At the initial stage, an estimate of $\tilde{\boldsymbol{h}}$ is obtained from the first K_0 observations in (4.4c) with the known measurement matrix $\boldsymbol{A}^{(1)} = (\boldsymbol{S}_R)_{K_0}$, by using some estimation technique. This estimate will then be used to perform ISI cancellation by a SISO equalizer and then decoding by a SISO decoder to get the first estimates $\tilde{\boldsymbol{x}}_2^{(1)}$ of $\boldsymbol{x}_2$, after we subtract the self-interference $\tilde{\boldsymbol{H}}_1\boldsymbol{s}_1$ (see (4.4a)). Here we adopt a SISO receiver based on the Soft-Cancellation Minimum Mean Square Error (SC/MMSE) method [74]. We denote $L(x_{2,m})$, $L_e(x_{2,m})$ in Fig. 4.2 as the *a-posteriori* LLR and the *extrinsic* LLR of the m-th coded symbol of $\boldsymbol{x}_2$, respectively [74]; and $L_e(x_{2,m}|p) = L(x_{2,m}) - L_e(x_{2,m})$. Similar definitions are used for $L(c_{2,m})$, $L_e(c_{2,m})$, $L_e(c_{2,m}|p)$, and $L(b_{2,m})$.

After the initial stage, the hard decision of $\tilde{\boldsymbol{x}}_2$ will be fed back to the channel estimator to improve the system performance in the next iteration. Here and in the sequel, the number of iterations refers to the number of times we feed back the symbol estimates from the decoder to the estimator, not the number of "inner" iterations between the equalizer and the decoder, which is set to one in this chapter. At the i-th iteration ($i \geq 2$), the updated measurement matrix is $\boldsymbol{A}^{(i)} = \tilde{\boldsymbol{S}}_R^{(i)}$, which is formed by the pilots, $\boldsymbol{x}_1$, and the i-th estimates $\tilde{\boldsymbol{x}}_2^{(i)}$.

If the sources do not have any knowledge about the sparsity or the statistical distri-

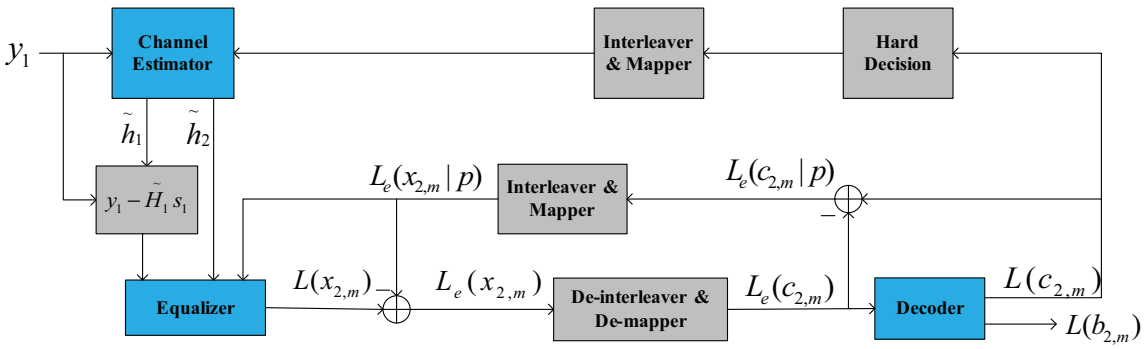

Figure 4.2: Join iterative estimation and decoding for ISI-TWRC at T_1.

bution of the channels, their receivers simply employ the conventional LS-based channel estimation method (the decoding process is the same as above), which provides the estimate of $\tilde{\boldsymbol{h}}$ at the i-th iteration, $\tilde{\boldsymbol{h}}_{\mathrm{LS}}^{(i)}$, as

$$\begin{aligned}\tilde{\boldsymbol{h}}_{\mathrm{LS}}^{(i)} &= \left(\boldsymbol{A}_{\mathrm{LS}}^{(i)}\right)^{\dagger} \boldsymbol{y}_1^{(i)} \\ &= \left\{\left(\boldsymbol{A}_{\mathrm{LS}}^{(i)}\right)' \boldsymbol{A}_{\mathrm{LS}}^{(i)}\right\}^{-1} \left(\boldsymbol{A}_{\mathrm{LS}}^{(i)}\right)' \boldsymbol{y}_1^{(i)},\end{aligned}$$

where $\boldsymbol{y}_1^{(i)} = (\boldsymbol{y}_1)_{K_0}$, and $\boldsymbol{y}_1^{(i)} = \boldsymbol{y}_1$ for $i \geq 2$.

The MSE for the LS receiver at the i-th iteration is given as

$$\mathrm{MSE}_{\mathrm{LS}}^{(i)} = \sigma^2 \mathrm{Tr}\left\{\left\{\left(\boldsymbol{A}_{\mathrm{LS}}^{(i)}\right)' \boldsymbol{A}_{\mathrm{LS}}^{(i)}\right\}^{-1}\right\},$$

which results in the lower bound $\sigma^2 L_{\mathrm{eff}}/K_0$ at the first iteration and (asymptotically) $\sigma^2 L_{\mathrm{eff}}/(K_0 + N_c)$ at the final iteration, with the assumption that the coded symbols fed back to the channel estimator at the final iteration are all correct.

Estimating and decoding sparse ISI-TWRC under the condition $S_\Sigma \ll L_{\mathrm{eff}}$ can be more efficiently solved by a CS-based technique, provided that the measurement matrix satisfies the RIP [1, 29]; and the performance is further improved if it is done in an iterative fashion as shown below. The implication here is that, after each iteration, the measurement matrix satisfies the RIP with higher accuracy, and more observations are

available which lead to further performance improvements. In this chapter, we also use the convex optimization-based ℓ_1-penalty version of BPDN method as it is claimed to be stable under noisy setting, and requires only the sparsity condition. The estimate of $\tilde{\boldsymbol{h}}$ in the i-th iteration using BDPN is

$$\tilde{\boldsymbol{h}}^{(i)}_{\text{BPDN}} = \underset{\tilde{\boldsymbol{h}}}{\text{argmin}} \left\{ \frac{1}{2} \left\| \boldsymbol{y}_1^{(i)} - \boldsymbol{A}^{(i)}_{\text{BPDN}} \tilde{\boldsymbol{h}} \right\|_2^2 + \gamma \left\| \tilde{\boldsymbol{h}} \right\|_1 \right\},$$

where γ is the turning parameter, typically chosen as $\gamma = \sqrt{8\sigma^2(1+\alpha)\log(L_{\text{eff}} - S_\Sigma)}$ for a fairly small α [35], $\boldsymbol{A}^{(i)}_{\text{BPDN}}$ is the measurement matrix at the i-th iteration using BDPN.

In light of the above, we have the following result.

Theorem 4.1. *At the final iteration when the iterative scheme converges, the normalized measurement matrix for estimating $\tilde{\boldsymbol{h}}$ in (4.4c) satisfies the RIP($S_\Sigma, \delta_{S_\Sigma}$) with probability exceeding $1 - exp\left(-c_1(K_0+N_c)/S_\Sigma^2\right)$ for any $c_1 \leq \delta^2_{S_\Sigma}/32$ when $K_0 + N_c \geq c_2 S_\Sigma^2 \log L_{eff}$, given that $L_{eff} \geq 3$, where it suffices to choose $c_2 \geq 96/\left(\delta^2_{S_\Sigma} - 32c_1\right)$. Furthermore, upon convergence the MSE performance of the BPDN method is upper bounded by $S_\Sigma \sigma^2 \log(L_{eff})/(K_0+N_c)$ within a constant factor.*

Proof. The RIP of the measurement matrix in (4.4a) for the first iteration is proved in Chapter 3. Here we provide the RIP of the updated measurement matrix in the subsequent iterations; plus the convergence of the scheme.

From the second iteration, the number of *effective observations* used for channel estimation is increased from K_0 to $K_0 + N_c$ thanks to the iterative process. Practically, considering a small number of incorrectly decoded symbols, say $N_E^{(i)} \ll N_c$ at the i-th iteration are fed back to the channel estimator, then the measurement matrix at the i-th iteration is $\boldsymbol{A}^{(i)} = \boldsymbol{S}_R + \boldsymbol{E}^{(i)}$, where $\boldsymbol{E}^{(i)}$ is the error matrix whose most of entries are zero and the non-zero entries $(+1/-1)$ are caused by incorrectly decoded symbols. It is equivalent to saying that the channel estimation algorithm applies for the $(K_0+N_c)\times L_{\text{eff}}$ measurement matrix $\boldsymbol{S}_R$ and for an increasing noise $\tilde{\boldsymbol{n}}^{(i)}_{1,E} = \tilde{\boldsymbol{n}}_1 - \boldsymbol{E}^{(i)}\tilde{\boldsymbol{h}}$ with variance

$\sigma_E^{2\,(i)}$.

Since we feed back the randomly interleaved BPSK estimates of coded symbols, all the unique entries of the measurement matrix $\boldsymbol{S}_R$ are supposed to be symmetric ± 1 Bernoulli distributed (assuming that the information data is i.i.d. binary with equally likely 0's and 1's). As proven above, $\boldsymbol{S}_R$ satisfies the RIP with the size $(K_0 + N_c) \times L_{\text{eff}}$. Given that the MSE of the channel estimation error using an CS-based algorithm is proportional to the noise variance and inversely proportional to the number of observations used, feeding back the decoded symbols for channel estimation purposes provides some iterative gains, as the increase in the number of observations (from K_0 to $K_0 + N_c$) is generally faster than the increase of the variance noise (from σ^2 to $\sigma_E^{2\,(i)}$), at high SNR and when the codeword length is large.

With the assumption that the smaller MSE of the estimation error of the estimator the lower the BER of the decoder, then $N_E^{(i+1)} < N_E^{(i)}$ leading to $\sigma_E^{2\,(i+1)} < \sigma_E^{2\,(i)}$. Over the iterative process, $N_E^{(i)}$ approaches zero, and $\sigma_E^{2\,(i)}$ approach σ^2. The algorithm converges, an the results of Theorem 4.1 follows if in the result of Corollary 3.1 in Chapter 3 we replace K_0 by $K_0 + N_c$. □

Given that the better the MSE performance of the estimator, better BER performance of the decoder is expected. Furthermore, the above performance guarantee, in fact, is an upper bound, and more practical useful numerical results are given in Section 4.4. Finally, we consider the scheme based on *Oracle* (ORC), which provides us the locations of the non-zero taps of $\tilde{\boldsymbol{h}}$. The ORC estimator performs the LS method with a measurement matrix comprising only the columns corresponding to the non-zero locations of $\tilde{\boldsymbol{h}}$ [34]. Its performance serves as the Cramér-Rao bound for the above estimators.

4.3 Decode-and-Forward TWRC

4.3.1 Transmission and Relaying Protocols

We assume an ISI-TWRC similar to the one used in the previous section, where a three-phase relaying protocol is used, as shown in Fig. 4.3. The difference here is that the relay operates in the DF mode, and there exist the direct links between two sources. All the channels are assumed to be sparse, each has an arbitrary sparsity. In the first two time slots (phases), each source uses one slot to broadcast its respective signal. We express the received signals at both sources and at the relay as

$$\boldsymbol{y}_{T_iR} = \boldsymbol{H}_{T_iR}\boldsymbol{s}_i + \boldsymbol{n}_{T_iR}, \tag{4.5}$$

$$\boldsymbol{y}_{T_iT_j} = \boldsymbol{H}_{T_iT_j}\boldsymbol{s}_i + \boldsymbol{n}_{T_iT_j}, \tag{4.6}$$

where $\boldsymbol{y}_{T_iR}$ is the received signal at the relay from T_i, and $\boldsymbol{y}_{T_iT_j}$ is the signal received at T_j from T_i, for $i, j \in \{1, 2\}, i \neq j$; $\boldsymbol{s}_i = [\boldsymbol{p}_i^T \ \boldsymbol{x}_i^T]^T$ denotes the signal vector transmitted by T_i, including the training sequence (the channel coded vector $\boldsymbol{x}_i$ is obtained from encoding binary vector $\boldsymbol{b}_i$, as in the previous section). All the above channel matrices are in Toeplitz forms, formed from their corresponding channel vector. Finally, $\boldsymbol{n}_{T_iR}$ and $\boldsymbol{n}_{T_iT_j}$ are complex AWGN samples with variance σ^2, for the source-relay link and the inter-source links, respectively. For the rest of the chapter, we assume BPSK modulation throughout.

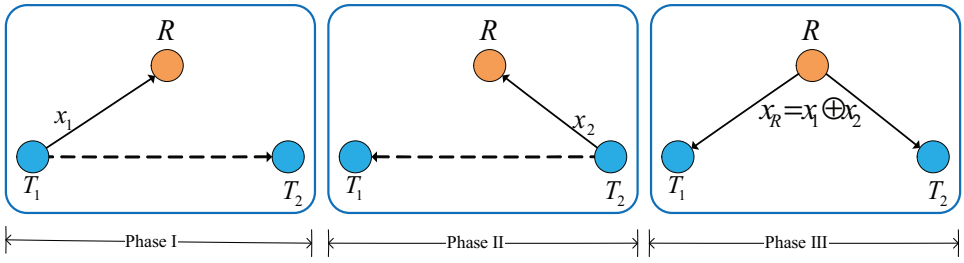

Figure 4.3: Three-phase relaying protocol with network coding, DF mode.

At the end of the broadcast stage (2 phases), the relay performs the single-channel estimation to get the channel estimates, and iterative SISO-type equalization and decoding is performed to get their binary information estimates $\hat{\boldsymbol{b}}_1$ and $\hat{\boldsymbol{b}}_2$. Next, the relay physically network encodes them by using bit-wise exclusive-or (XOR) addition as

$$\boldsymbol{b}_R = \hat{\boldsymbol{b}}_1 \oplus \hat{\boldsymbol{b}}_2.$$

The resulting binary vector, denoted by $\boldsymbol{b}_R$ is then convolutionally channel re-encoded, randomly interleaved, and BPSK modulated to get the transmitted symbol vector in Phase III, denoted by $\boldsymbol{x}_R$. The transmitted signal by the relay to the two sources in Phase III is $\boldsymbol{s}_R = [\boldsymbol{p}_R^T \ \boldsymbol{x}_R^T]^T$, where $\boldsymbol{p}_R$ is the pilot sequence sent by the relay, $\boldsymbol{p}_R = \boldsymbol{p}_1 \oplus \boldsymbol{p}_2$. At the end of phase III, the received signal at the terminal T_i, denoted by $\boldsymbol{y}_i$, is given by

$$\boldsymbol{y}_i = \boldsymbol{H}_{RT_i}\boldsymbol{s}_R + \boldsymbol{n}_{RT_i}. \tag{4.7}$$

4.3.2 Sparsity-Aware Iterative Receiver

Different from the AF model, where the estimation, equalization and decoding processes are performed at each source based on the estimated *composite* channels, in the DF mode, they are performed based on the individual channels, first at the relay and then at each source. The SC/MMSE receiver that performs SISO equalization and decoding like the one in the previous section can be used in each phase of the protocol. However, the SC/MMSE ignores the sparsity feature of the ISI channels in the equalization process. In this section, we present another SISO-type receiver that utilizes the prior information of the sparsity of the channels into the channel estimation phase and the equalization process, iteratively. That is, in every iteration, the equalizer directly approximates the *a-posteriori* LLR value of the coded bits, based on a MP algorithm over a factor graph. We note here that this method is not suitable in general for the AF case, since for the

composite channels, the "*effective*" sparsity may be not small enough for the method below to be feasible.

As explained in Chapter 2, computing the exact *a-posteriori* LLR is impractical for general ISI channels due to the large number of channel taps, and hence the high computational complexity. For the case of sparse channels, however, we show below an alternative solution to directly approximating that value for each coded bit. The similar approach based on factor graph has also been investigated for multiuser detection based on Gaussian approximation [75], joint channel estimation, interference mitigating and decoding [76], joint channel estimation and decoding of bit-interleaved coded OFDM (BICM-OFDM) [77].

Sparse ISI Channel Equalization based on Factor Graph

We present an algorithm for a general S-sparse N-length ISI channel having the impulse response $\boldsymbol{h}$, the N_b-length binary input vector $\boldsymbol{b}$ and the N_c-length coded symbol vector $\boldsymbol{x} = [x_0 \ x_1 \ \cdots x_{N_c-1}]$. An example of ISI channel with the sparse impulse response $\boldsymbol{h} = [h_0 \ 0 \ 0 \ h_3 \ 0 \ 0 \ 0 \ h_7]$ is illustrated in Fig. 4.4.

The n-th received signal at the receiver, denoted by y_n, is given by

$$y_n = \sum_{l=0}^{N-1} h_l x_{n-l} + e_n, \tag{4.8}$$

where e_n is the n-th AWGN sample, for $n = 0, 1, \cdots, N_c - 1$.

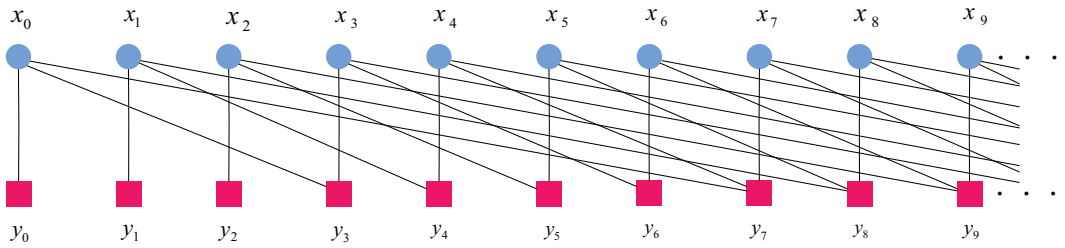

Figure 4.4: Example of factor graph for sparse ISI channel with impulse response $\boldsymbol{h} = [h_0 \ 0 \ 0 \ h_3 \ 0 \ 0 \ 0 \ h_7]$.

The log-APP based equalizer computes the *a-posteriori* LLR of the coded symbols, given the received signal vector as

$$\begin{aligned} L(x_n|\boldsymbol{y}) &= \ln \frac{P(x_n=1|\boldsymbol{y})}{P(x_n=-1|\boldsymbol{y})} \\ &= \underbrace{\ln \frac{\sum_{\forall \boldsymbol{x}:x_n=1} \prod_{i=0}^{N_c-1} p_i(y_i|\boldsymbol{x}) \prod_{j=0,j\neq n}^{N_c-1} P_i(x_i)}{\sum_{\forall \boldsymbol{x}:x_n=-1} \prod_{i=0}^{N_c-1} p_i(y_i|\boldsymbol{x}) \prod_{j=0,j\neq n}^{N_c-1} P(x_i)}}_{} + L(x_n) \\ &= L_e(x_n|\boldsymbol{y}) + L(x_n), \end{aligned}$$

for every $n \in \{0, 1, ..., N_c - 1\}$, where $L_e(x_n|\boldsymbol{y})$ is the extrinsic information of x_n given $\boldsymbol{y}$, and $L(x_n) \triangleq \ln \frac{P_n(x_n=1)}{P_n(x_n=-1)}$ is aprior LLR value of x_n provided from the channel decoder. Below we describe how these soft values can be computed efficiently using factor graph. Consider the joint probability distribution over the symbol variables $\boldsymbol{x} = [x_0, x_2, ..., x_{N_c-1}]^T$, conditioning on the received vector $\boldsymbol{y}$, with the factorization as follows.

$$P(\boldsymbol{x}|\boldsymbol{y}) = Z^{-1} \prod_{i=0}^{N_c-1} P_i(y_i|\boldsymbol{x}) \prod_{j=0}^{N_c-1} P_j(x_j) \prod_{a=0}^{N_c-1} \delta_{\{\boldsymbol{y}_a=(\boldsymbol{H}\boldsymbol{x})_a\}} \tag{4.9}$$

$$\propto \prod_{i=0}^{N_c-1} P_i(y_i|\boldsymbol{x}_i) \prod_{j\in\mathcal{N}(y_i)} P_j(x_j), \tag{4.10}$$

where Z is a distribution normalization, $\delta_{\{\boldsymbol{y}_a=(\boldsymbol{H}\boldsymbol{x})_a\}}$ denotes a Dirac distribution on the hyperplane $\boldsymbol{y}_a = (\boldsymbol{H}\boldsymbol{x})_a$, symbol $\propto$ indicates proportionality to within a normalization constant. $\mathcal{N}(y_i)$ denotes the set of all indices of the symbol nodes connecting to channel node y_i, and $\boldsymbol{x}_i = \{x_i\}_{i\in\mathcal{N}(y_i)}$. This yields a well-defined measure that captures both the probabilistic modeling and "behavioral" modeling [78] of the ISI channel. Applying the sum-product algorithm (as shown in Fig. 4.5), the message sent from symbol node x_n to channel node y_m is given by

$$\lambda_{n\to m}^{(t)}(x_n) \propto P_n(x_n) \prod_{k\in\mathcal{N}(n),k\neq m} \gamma_{k\to n}^{(t)}(x_n), \tag{4.11}$$

where $P_n(x_n)$ is the *aprior* probability of symbol x_n which is fed back from the channel decoder, and acts as the "*local function*" at symbol node x_n. The message sent from channel node y_m to symbol node x_n is given by

$$\gamma_{m\to n}^{(t+1)}(x_n) \propto \sum_{\boldsymbol{x}_m : x_n} P_m\left(y_m|\boldsymbol{x}_m\right) \prod_{j\in\mathcal{M}(m), j\neq n} \lambda_{j\to m}^{(t)}(x_j), \tag{4.12}$$

where $P_m\left(y_m|\boldsymbol{x}_m\right)$ is the "*local function*" at channel node y_m, and is computed by

$$P_m\left(y_m|\boldsymbol{x}_m\right) = \left(\frac{1}{\pi\sigma^2}\right) \exp\left\{ \frac{-\left\| y_m - \sum_{l=0,(m-l)\in\mathcal{M}(m)}^{N-1} h_l x_{m-l} \right\|^2}{\sigma^2} \right\}. \tag{4.13}$$

At the marginalization step, we have

$$\overline{\lambda}_n^{(t)}(x_n) = P_n(x_n) \prod_{k\in\mathcal{N}(n)} \gamma_{k\to n}^{(t)}(x_n). \tag{4.14}$$

Because the factor graph is not cycle-free in general, messages have to be passed multiple times on a given edge iteratively before the marginalization step, as t is the iteration index in (4.11), (4.12) and (4.14). Here the "*flooding schedule*" is used to perform the MP algorithm as described in [78]. Generally, the above method does not provide an exact result like the MAP algorithm but can still achieve a good approximation, for the case of sparse channels, with a complexity of $\mathcal{O}(2^{N_c+S})$. This is much lower than the complexity of the MAP algorithm for general channels, which is in the order of of $\mathcal{O}(2^{N_c+N})$, since we assume that $\boldsymbol{h}$ is sparse, i.e., $S \ll N$.

Since the communication with the channel decoder is done through LLR values, which is simpler to compute and more stable, we need to represent the probabilities $\lambda_{n\to m}^{(t)}(x_n)$ for $x_n \in \{1, -1\}$ in (4.11) by a single LLR value, denoted by $\Lambda_{n\to m}^{(t)}(x_n) \triangleq \ln \frac{\lambda_{n\to m}^{(t)}(x_n=1)}{\lambda_{n\to m}^{(t)}(x_n=-1)}$ as

$$\Lambda_{n\to m}^{(t)}(x_n) = L(x_n) + \sum_{k\in\mathcal{N}(m), k\neq m} \Gamma_{k\to n}^{(t)}(x_n). \tag{4.15}$$

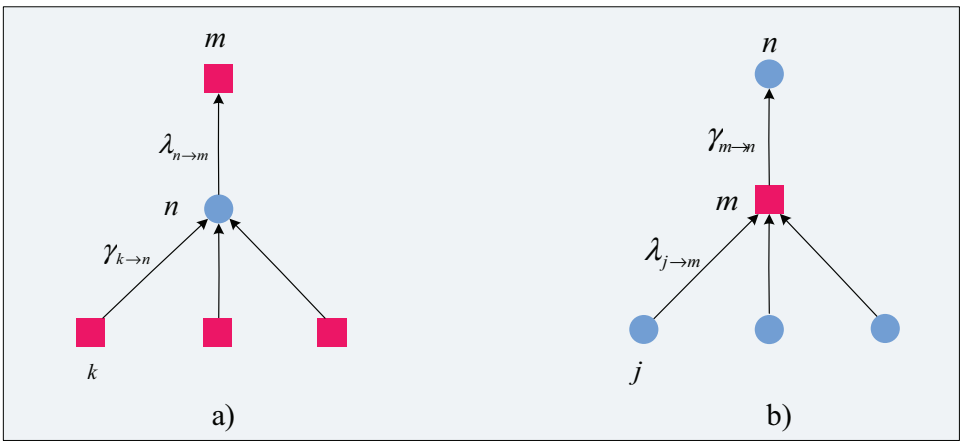

Figure 4.5: Sum-product algorithm: a) message sent from symbol node x_n to channel node y_n and b) message sent from channel node y_n to symbol node x_n.

Similarly, the probabilities $\gamma_{m\to n}^{(t+1)}(x_n)$ for $x_n \in \{1,-1\}$ in (4.12) are represented by $\Gamma_{m\to n}^{(t+1)}(x_n) \triangleq \ln\frac{\gamma_{m\to n}^{(t+1)}(x_n=1)}{\gamma_{m\to n}^{(t+1)}(x_n=-1)}$.

In addition, in (4.12) the probability $\lambda_{j\to m}^{(t)}(x_j)$ is related to the LLR value $\Lambda_{j\to m}^{(t)}(x_j)$ by

$$\lambda_{j\to m}^{(t)}(x_j) = \frac{1+x_j\tanh\left[\frac{1}{2}\Lambda_{j\to m}^{(t)}(x_j)\right]}{2}, \tag{4.16}$$

where (4.16) comes from the fact that $x_j \in \{1,-1\}$. As a result, from (4.12) we have

$$\Gamma_{m\to n}^{(t+1)}(x_n) = \ln\frac{\sum_{\boldsymbol{x}_m:x_n=1} P_m\left(y_m|\boldsymbol{x}_m\right)\prod\limits_{j\in\mathcal{M}(m),j\neq n}\frac{1}{2}\left\{1+x_j\tanh\left[\frac{1}{2}\Lambda_{j\to m}^{(t)}(x_j)\right]\right\}}{\sum_{\boldsymbol{x}_m:x_n=-1} P_m\left(y_m|\boldsymbol{x}_m\right)\prod\limits_{j\in\mathcal{M}(m),j\neq n}\frac{1}{2}\left\{1+x_j\tanh\left[\frac{1}{2}\Lambda_{j\to m}^{(t)}(x_j)\right]\right\}}. \tag{4.17}$$

The process of equalization using MP algorithm over factor graph is described as follow.

Message Passing-based Equalization Algorithm over Factor Graph

procedure MP($\mathcal{N}(n)$, $\mathcal{M}(n)$, $L_e(c_n|p)$ for all n, $i_{\max}$)
  Initialization: $t = 0$, $\Lambda^{(0)}_{n\to m}(x_n)$ = interleaved and mapped value of $L_e(c_n|p)$
    for all n and all $m \in \mathcal{M}(n)$.
    Compute $\Gamma^{(1)}_{m\to n}(x_n)$ via (4.17).
  for $t = 1, t \le t_{\max}$ **do**
    Compute $\Lambda^{(t)}_{n\to m}(x_n)$ via (4.15)
    Compute $\Gamma^{(t+1)}_{m\to n}(x_n)$ via (4.17)
    $t \leftarrow t + 1$
  end for
  return $L^{(t+1)}(x_n|\boldsymbol{y}) = L(x_n) + \sum_{k\in\mathcal{N}(n)} \Gamma^{(t+1)}_{k\to n}(x_n)$
end procedure

In the above MP algorithm, the inputs include the LLR values of the coded symbol provided by the channel decoder, $L_e(c_n|p)$. At stage $t = 0$, we initialize $\Lambda^{(0)}_{n\to m}(x_n)$ as the interleaved and mapped version of $L_e(c_n|p)$ for all n and all $m \in \mathcal{M}(n)$. The maximum number of MP is set to be $t_{\max}$. At the final stage, we output the LLR value $L^{(t)}(x_n|\boldsymbol{y}) \triangleq \ln\frac{\overline{\lambda}^{(t)}_n(x_n=1)}{\overline{\lambda}^{(t)}_n(x_n=-1)}$ which is then delivered to the log-APP decoder (computed from (4.14)).

These soft values are randomly interleaved and then delivered to the channel decoder. The LLR values of the coded symbols output at the APP decoder are then fed back to the estimator and the equalizer for the next iteration to refine the results. The APP-decoder also computes the LLR values of $\boldsymbol{b}$ to make hard-decisions at the final iteration, when the stopping criterion is satisfied.

Decoding at the two sources

At T_1, we detect the symbols sent from T_2 from two received signals, from the direct link and the relay link. In each decoding process, in the first iteration, we first estimate the sparse channel from the first $\mathcal{T}$ symbols of $\boldsymbol{y}_1$ in (4.7) given the known training vector $\boldsymbol{p}_R$, using the ℓ_1-based (or BPDN) sparse channel estimation algorithm. Then the receiver at T_1 runs the sparse ISI channel equalization based on the factor graph described above to

get an estimated binary vectors $\hat{\boldsymbol{b}}_2$ (from the direct link) and $\hat{\boldsymbol{b}}_R$ (from the relaying link). Next, the bit-wise XOR operator between $\hat{\boldsymbol{b}}_R$ with $\boldsymbol{b}_1$ is performed to obtain a another estimated copy of binary vector of $\boldsymbol{b}_2$ at T_1. Finally, the final estimated symbols sent from T_2 will be obtained by maximum ratio combining (MRC). A similar process is performed at T_2 to obtain an estimated binary vector of $\boldsymbol{b}_1$.

4.3.3 Error Propagation Mitigation

One of the drawbacks of the DF protocol in TWRC is that the error propagation at the relay degrades the performance of the system. To combat that effect, it has been suggested to implement a reliability threshold at the relay to control error propagation [57–60]. Specifically, the relay calculates LLR values of the received coded bits sent from each source and compares them with some thresholds to decide as to whether to combine and relay these bits or not. In the event that the reliability of one received bit is below the set threshold, the relay stays silent and transmits nothing (for that bit). That is

$$x_{R,n} = \begin{cases} -\left(\hat{x}_{1,n}\hat{x}_{2,n}\right), & \text{if } \ |L(x_{1,n})| > \mathcal{T}_1, \ |L(x_{2,n})| > \mathcal{T}_2 \\ 0, & \text{otherwise,} \end{cases} \tag{4.18}$$

where $\mathcal{T}_i$ is the preset threshold for bits sent from T_i.

For the case of uncoded flat-fading channel without channel coding, the optimal values of $\mathcal{T}_1$ and $\mathcal{T}_2$ are derived in closed forms in [59]. For the case of sparse ISI channels, the optimization problem is no longer well-defined, and there is no closed form for the optimum values of the thresholds. It is suggested in [59] that the thresholds should be linearly proportional to average channel power of the source-channel links, or the approximated BER for a specific channel coding method. The approximation of the BER for each convolutional code with a SISO equalizer/decoder can be performed using prediction mechanisms as in [79], which are based on the LLR values obtained from the SISO decoder.

Assume that at R we can estimate the BER for the channel link $T_j - R$, denoted by $P_j^{(\mathrm{e})}$. Then by sorting the absolute values of LLR of decoded bits $\hat{x}_{j,n}$ $(n = 1, ..., N_c)$ in an increasing order from $\mathcal{T}_{j,1}$ to $\mathcal{T}_{j,N_c}$, we set $\mathcal{T}_j$ in the thresholding formula (4.18) as $\mathcal{T}_{j,P_j^{(\mathrm{e})}N_c}$. The other symbols that have the absolute of the LLR value smaller than $\mathcal{T}_j$ are set to zero before performing the network coding operation (bit-wise XOR) and sending the resulting symbols to the two terminals at the broadcasting phase.

4.4 Numerical Simulations

4.4.1 Amplify-and-Forward TWRC

In the AF mode, we assume that the sparse ISI-TWRC is symmetric, and the four channels $\{\boldsymbol{h}_j\}_{j=1}^4$ are the same, each has length $L_u = L_d = 16$, sparsity $S_j = 4$ with the index set of non-zero taps $\{1, 4, 9, 16\}$. This symmetric assumption is just for simplicity and does not affect the generality of our method. Averaged channel powers and transmission power at all terminals are normalized to unity. The simulation is run for 5000 random channel realizations. In each data exchange period, each source sends an i.i.d. binary block (with equally likely 0's and 1's) of length $N_b = 512$. A convolutional code $(5, 7)_8$ is employed at each source with code rate $R_c = 1/2$. The SISO equalizer based on the SC/MMSE [74] is used to handle the ISI. The log-APP algorithm is applied for the channel decoders. The number of iterations is set to five, at which the performance is well converged.

In this specific setting, $\tilde{\boldsymbol{h}}$ has a total length of $L_{\text{eff}} = 62$ and sparsity $S_\Sigma = 18$. For a meaningful estimation using the LS method, $\mathcal{T}$ has to be at least $L_{\text{eff}} + L_d - 1 = 77$. First we set $\mathcal{T} = 60$ (6% approximately in length of each coded block) so that the setting is under-determined at the first iteration. In Figs. 4.6 and 4.7, we show the MSEs between $\tilde{\boldsymbol{h}}$ and its estimates, and the BERs versus the SNR at T_1, respectively, using different methods (similar results for T_2 due to symmetry). For comparison purposes, we also show the MSE and BER of the ORC method, and the BERs of ORC and of the case when CSI

is assumed at the terminals.

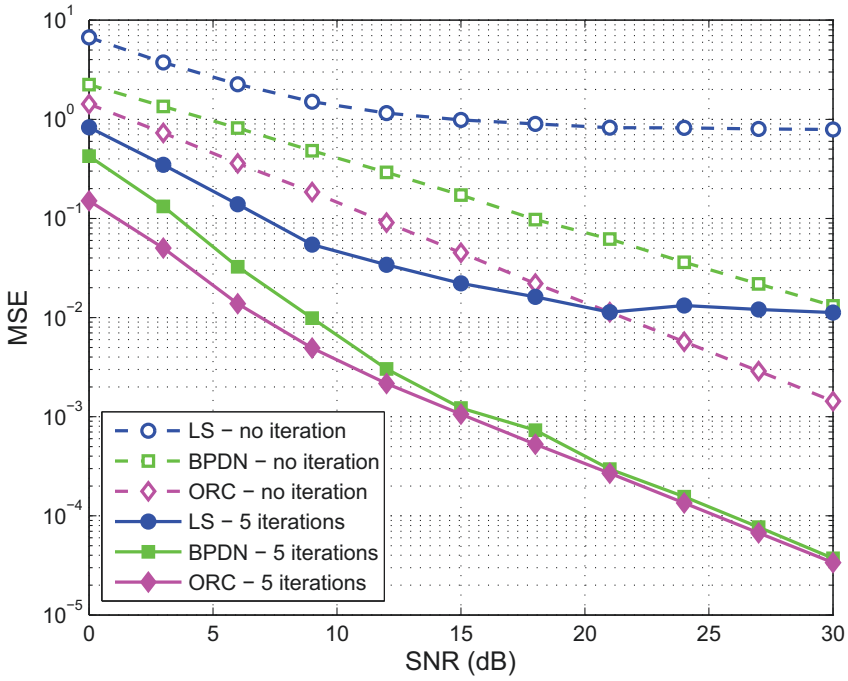

Figure 4.6: MSE comparison of different methods with $\mathcal{T} = 60$.

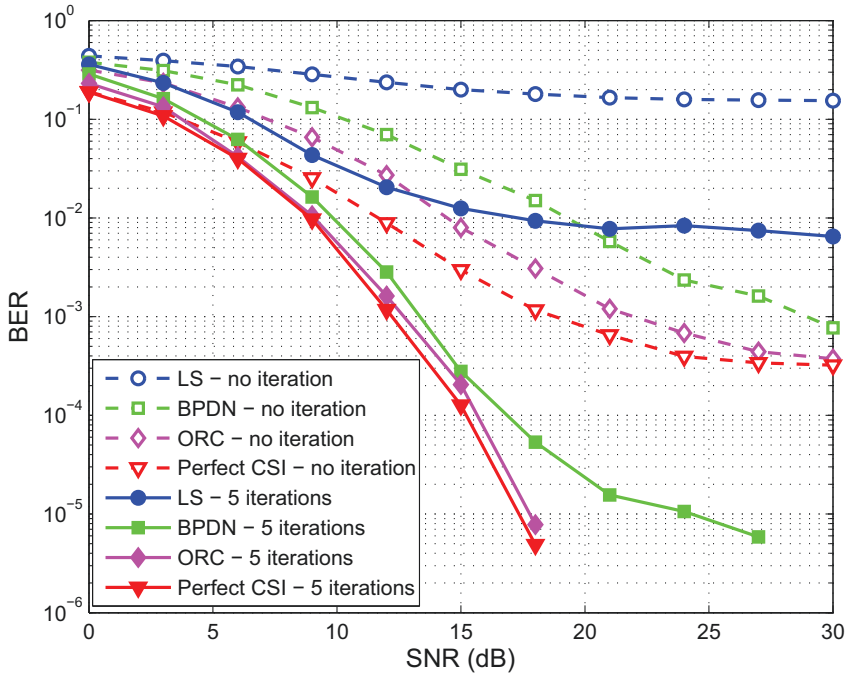

Figure 4.7: BER comparison of different methods with $\mathcal{T} = 60$.

As expected, the CS-based BPDN scheme significantly outperforms the LS scheme at the initial stage (no iteration), and the improvements are bigger at the final iteration. In this stage, while the LS method has very poor performances both in MSE and BER, the BPDN method has the MSE performance approaching that of the ORC method at high SNR, and has far better BER performance than the LS method. It is expected that when $\mathcal{T}$ is increased, the error performances including MSE and BER of the BPDN method to more closely approach that of the ORC-based and perfect CSI based methods.

Next, we we increase the length of $\mathcal{T}$ to 90 (9% approximately in length of each coded block) so that the setting is over-determined at the first iteration. We can see from Figs. 4.8 and 4.9 that the error performances including MSE and BER of the BPDN method closely approaches that of the ORC-based and perfect CSI based methods. In this case, these error performances of the LS method are still far way from CS-based method and the lower bounds based on ORC and perfect CSI ones.

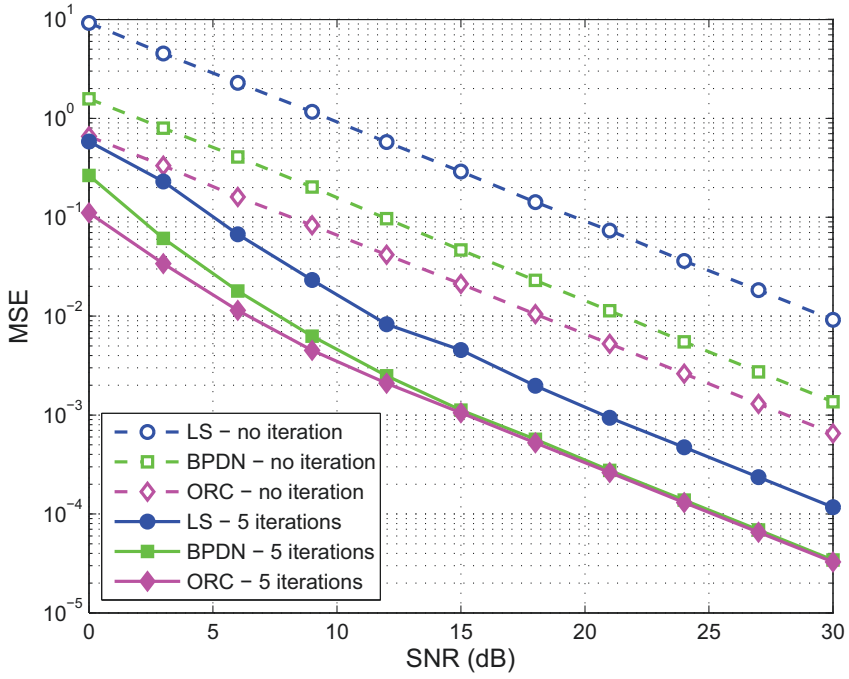

Figure 4.8: MSE comparison of different methods with $\mathcal{T} = 90$.

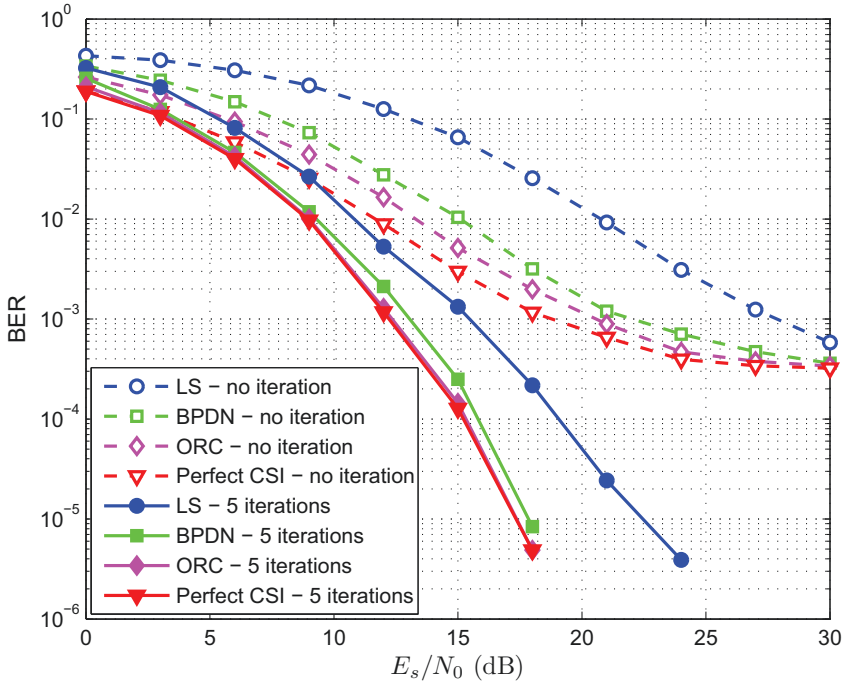

Figure 4.9: MSE comparison of different methods with $\mathcal{T} = 90$.

4.4.2 Decode-and-Forward TWRC

In the TWRC operating DF considered section 4.3, we also assume that all the channels are sparse ISI as in the AF mode. The length of each data block is $N_b = 150$. The convolutional code $(5, 7)_8$ is employed at the transmitter, with code rate $R_c = 1/2$. The number of iterations for MP for the equalizer is five, at which the equalization process is well converged. The log-APP algorithm is employed at the channel decoder. Figs. 4.10 and 4.11 show the MSE and BER performance at T_1 for different receiver types. The results show that the performance in terms of MSE and BER of each receiver is improved over the iterative process (as we set the number of turbo iteration is five). Among the channel estimators, the sparsity-aware channel estimator based on compressive sensing method (BPDN or ℓ_1-norm) outperforms the LS. Among the channel equalizers, the sparsity-aware equalizer based on MP over factor graph outperforms the SC/MMSE. Therefore, the performance of the ℓ_1-message passing (or BPDN-MP) receiver has the best

performance. The MSE and BER are further improved when we apply the thresholding technique at the relay to mitigate the error propagation, as expected.

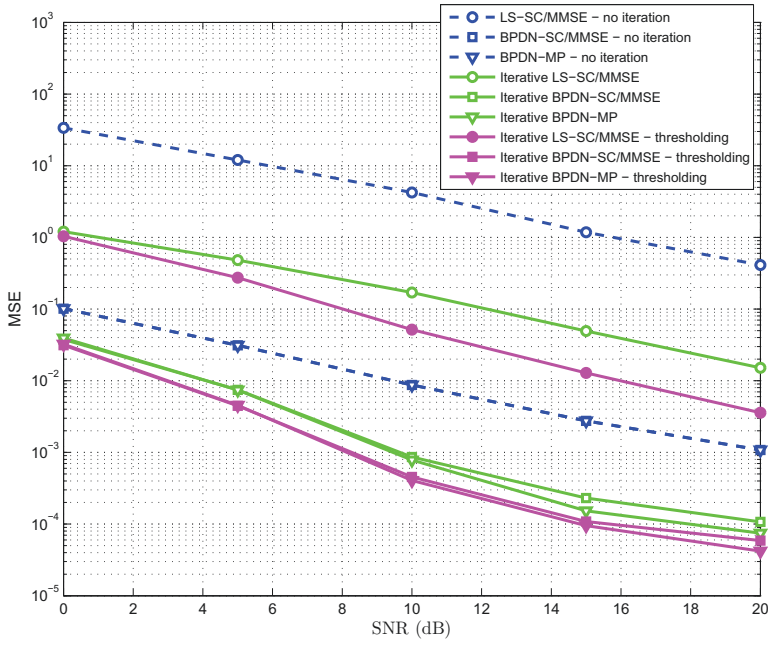

Figure 4.10: MSE comparison of different methods with $\mathcal{T} = 32$.

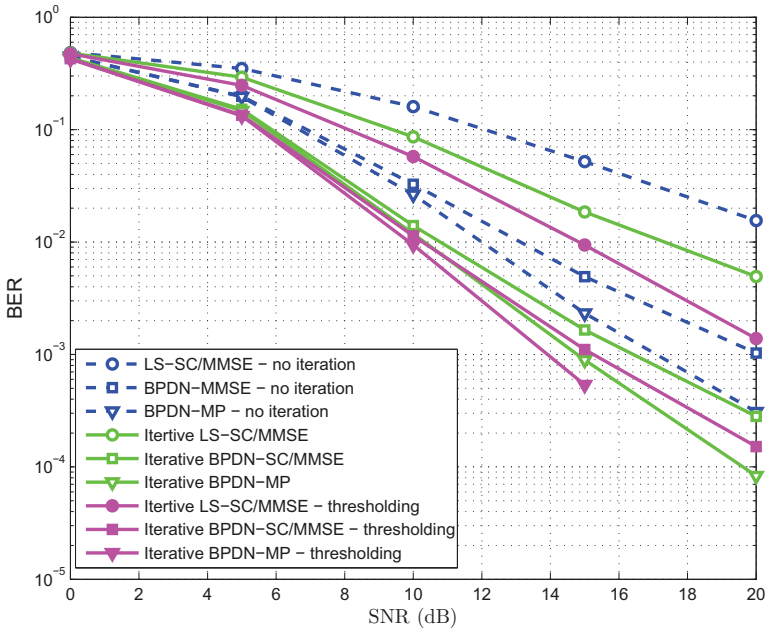

Figure 4.11: BER comparison of different methods with $\mathcal{T} = 32$.

4.5 Conclusions

In this chapter, iterative compressive channel estimation and decoding schemes for network-channel-coded sparse ISI-TWRC have been presented, for both AF and DF relaying. The efficacy of the proposed schemes when taking the sparsity of the channel into account into the channel estimator and/or the equalizer was evaluated and confirmed through numerical examples. It was also suggested that the thresholding technique at the relay helps to improve the system performance as it mitigates the error propagation during the relaying process.

Chapter 5

Compressive Sensing-based Channel Estimation for Massive MIMO Systems via Nuclear Norm Regularization

5.1 Introduction

The tremendous demand for reliable high-speed broadband wireless links is expected to continue growing in the future due to the foreseen rapidly increase in the number of users, amount of data traffic and number of applications. To meet such demands, it is expected that future networks, i.e., beyond 4G networks, will be scaled up to reach the gigabit data rates range over the next 10 years [80]. One of the recent proposed technologies for beyond 4G is *massive* (or *large-scale*) MIMO [63], [28]. Such technology is based on the same concept of conventional MIMO but extended to a much larger scale in terms of the number of antennas at both the transmitter and receiver sides. Compared to classical MIMO, massive MIMO provides many advantages such as higher data rates, better link

reliability, and better spectral-energy efficiency tradeoff.

One current proposed system for massive MIMO technology is the massive multiuser MIMO (MU-MIMO) [28], where a BS with a very large antenna array serves a multiplicity of distant or well-separated single-(or just a few)-antenna UTs simultaneously. Previous results show that for a system in which the number of BS antennas M greatly exceeds the number of UTs K ($M \gg K$) , under the most favorable assumption of the propagation channel, and with the perfect CSI available at all UTs and at the BS, the thermal noise and interference vanish, and the required transmit powers are reduced as M increases [28]. This also means that adding more antennas at the BS always helps to increase the throughput or reduce the transmit powers; and all these results can be obtained using some linear-complexity estimation and detection algorithms.

The above information-theoretic results for massive MU-MIMO, however, are based on optimistic assumptions, and there are still many practical issues that need to be addressed. For example, the most favorable propagation channel assumption requires a very rich scattering environment, which does not generally hold in practice. Furthermore, requiring a very large number of antennas at the BS and zero antenna correlation at the same time is almost impossible. In addition, the perfect CSI assumption at all UTs and the BS is not realistic, because such high dimensional channel matrix needs to be estimated within a coherence time interval.

In this chapter, we propose a CS based approach to address the channel estimation problem of a MU-MIMO system where both dimensions of the channel matrix grow large, while adopting a realistic propagation channel model. The large-dimensional channel estimation problem occurs in massive MIMO systems with a large number of autonomous users in a single-cell case. It also occurs when we estimate not only the channel parameters of desired links in a given cell, but also those of the interference links from adjacent cells for interference coordination purposes in multi-cell scenarios. In this work, we consider the practical physical finite scattering channel model proposed in [28, 81–83]. When both

dimensions of the channel matrix grow large, the channel estimation problem becomes particularly challenging due to the large number of matrix entries to be estimated. Our proposed method is based on CS and aims to improve the system performance by relying on two key ideas. The first is that, with the finite scattering channel having a limited number of (dominant) directions, the degrees of freedom (DoF) of the channel matrix is much smaller than its large number of free parameters, making low-rank matrix approximation based on CS robust. The second comes from the fact that for the large-scale MU-MIMO channel estimation problem, all the favorable results established by CS methods become stable (the accurate reconstruction occurs with an overwhelming probability).

The related works on massive MIMO channel estimation include [28, 62, 63, 82, 83], where LS or MMSE (when the second-order statistics of the channel is available for the latter) is performed within TDD systems. Channel estimation based on CS methods has been considered in [20, 84], and references therein, where the sparse channel vector is reconstructed by a small number of random incoherent projections. Unlike these prior works, our work is based on more recent results in CS, where the idea of the sparsity model of the signal vector is generalized to the low-rank model of the matrix variable [39, 40]. CS-based low-rank approximation has also been applied in diverse contexts in statistics and signal processing, but to the best of our knowledge, it has not been investigated in MIMO channel matrix estimation. Our main results include the formulation of the massive MU-MIMO channel estimation problem as a convex low-rank matrix approximation optimization under noisy setting, whose dual problem can be represented as a quadratic SDP. By doing this, the problem can be conveniently solved by a SDP solver (in polynomial time). We also obtain an explicit choice of the regularization parameter and a useful upper bound of the Frobenius norm of the error for the case of Bernoulli training matrix. Since prior works in this topic have been done for continuous Gaussian ensembles, our results are useful for the MU-MIMO channel matrix estimation due to the discrete nature of the pilot signaling.

The rest of the chapter proceeds as follows. We first describe the system and channel models in Section 5.2, and then review the LS-based MU-MIMO channel estimation method in TDD systems in Section 5.3. In Section 5.4, we propose the CS-based MU-MIMO channel estimation method via nuclear norm regularization problem and discuss the choice of regularization parameter. Numerical experiments are presented in Section 5.5. Section 5.6 concludes the chapter.

5.2 System and Channel Models

5.2.1 Large-scale MU-MIMO System Model

In this section, we shall describe the system model adopted in this chapter. Consider a MU-MIMO system operating in TDD with a BS equipped with an array of a large number of antennas M. In the uplink (i.e. reverse link), the BS receives signals sent from K autonomous single-antenna UTs (assuming that K is large but $K \leq M$). At time t, the received baseband signal at the BS, denoted by $\boldsymbol{y}(t) \in \mathbb{C}^M$, is given by

$$\boldsymbol{y}(t) = \boldsymbol{H}\boldsymbol{x}(t) + \boldsymbol{n}(t), \tag{5.1}$$

where $\boldsymbol{H} \in \mathbb{C}^{M \times K}$ is the flat-fading quasi-static MU-MIMO complex-valued channel matrix, $\boldsymbol{x} = [x_1(t)\ x_2(t)\ \ldots\ x_K(t)]^T \in \mathbb{C}^K$ is the transmit signal vector of K users; and $\boldsymbol{n}(t) \in \mathbb{C}^M$ is complex-valued AWGN vector at the BS, whose entries are i.i.d. $\mathcal{N}(0, \sigma_n^2)_{\mathbb{C}}$, i.e., zero-mean $\sigma_n^2/2$-variance per dimension random variables. The above generic model characterizes both single-cell scenario with K UTs as well as multi-cell interference-limited scenarios where K is the sum of all numbers of desired UTs in the considered cell and the other interference coming from other UTs in adjacent cells. For the latter case, the $M \times K$ channel matrix is $\boldsymbol{H} = [\boldsymbol{H}_1\ \boldsymbol{H}_2\ \ldots\ \boldsymbol{H}_J]$, where $\boldsymbol{H}_1$ denotes the $M \times K_1$ desired channel matrix in the considered cell with K_1 desired UTs and $\boldsymbol{H}_j$ $(j \neq 1)$ denotes the $M \times K_j$

interference channel matrix from j-th adjacent cell with K_j interfering UTs (assuming there are $J-1$ interference cells, and $K = K_1 + K_2 + \cdots + K_J$).

5.2.2 Physical Finite Scattering Channel Model

We are interested in the realistic finite-dimensional channel model recently studied for massive MU-MIMO [28, 82, 83], where the angular domain is partitioned into a finite number of directions (*i.e.* number of active scatterers). Assuming that there are P i.i.d paths originating from each user k to the BS, each has $M \times 1$ steering vector [81], we have

$$\boldsymbol{a}(\phi_p) = \begin{bmatrix} 1 \\ \exp\left(-j2\pi \frac{D_0}{\lambda} \cos(\phi_p)\right) \\ \vdots \\ \exp\left(-j2\pi \frac{(M-1)D_0}{\lambda} \cos(\phi_p)\right) \end{bmatrix}, \tag{5.2}$$

where $\phi_p \in [-\pi/2, \pi/2]$ is a random AoA corresponding to path $p \in \{1, 2, ..., P\}$ with respect to user k direction, D_0 is the antenna spacing at the BS, and λ is the signal wavelength. The number of paths P is independent from the number of BS antennas M or number of UTs K, and is dependent on the physical propagation environment only. The $M \times 1$ channel vector from UT k to the BS is given by

$$\boldsymbol{h}_k = \frac{1}{\sqrt{P}} \sum_{p=1}^{P} g_{kp} \boldsymbol{a}(\phi_p),$$

where g_{kp} is the random propagation gain from user k to the BS associated with path p, including fast fading, path loss and shadowing [28]. The path loss and shadowing coefficient for all users is assumed to be the same and normalized to unity. This is also assumed for the multi-cell case, where cross gains from interference UTs in other cells are as strong as direct gains [82]–the scenario where we need to estimate CSI of all links for coordination interference purposes. At a result, g_{kp} is assumed to have zero-mean and

unit-variance, and independent from the path direction p.

With the above notation, the $M \times K$ MU-MIMO channel matrix $\boldsymbol{H}$ between K UTs and the BS can be collectively written in a compact form as

$$\boldsymbol{H} = \boldsymbol{A}\boldsymbol{G}, \tag{5.3}$$

where $\boldsymbol{A} = [\boldsymbol{a}(\phi_1)\ \boldsymbol{a}(\phi_2)\ \ldots\ \boldsymbol{a}(\phi_P)]$ is a $M \times P$ full-rank matrix containing P steering vectors, and $\boldsymbol{G}$ is the $P \times K$ path gain channel matrix, $[\boldsymbol{G}]_{p,k}$ denotes the path gain from user k to the BS associated with path p.

Remark 5.1. *The physical finite scattering channel model (5.3) has a DoF $r(M+K-r)$, where r is the rank of $\boldsymbol{H}$, $r = \min\{M, K, P\}$.*

For the massive MU-MIMO system considered in this chapter, we are interested in the regime where both M and K are large ($M \geq K$), and P is small relative to M and K. This model characterizes the poor scattering propagation environment, where the number of physical objects is limited. It also describes the propagation channel where the scatterers appear in groups (called clusters) with similar delays, AoAs, angle-of-departures (AoDs), making the effective number of active directions limited, even the number of physical objects is large [28]. As a result, the actual DoF of the channel matrix is $P(M+K-P)$, not its number of free parameters MK.

5.3 LS-based Channel Estimation

In TDD systems, the CSI is estimated in the uplink, and used to perform the precoding/beamforming or multiuser scheduling (with interference coordination in the multi-cell case) in the downlink using the notion of *reciprocity*. The conventional way of estimating $\boldsymbol{H}$ in (5.1) is by sending at each user a training sequence of length $\mathcal{T} \geq K$ in the training phase of each coherence interval. Assume that the modulation format of the

training symbols sent by all UTs is BPSK, and the pilots are sequences of $\pm\sqrt{\rho}$, ρ is the transmit symbol power. Let $\boldsymbol{\phi}(l)$ denote the $K \times 1$ training signal vector sent by K UTs at channel use l, and $\boldsymbol{\Phi} = [\boldsymbol{\phi}(1)\ \boldsymbol{\phi}(2)\ \ldots\ \boldsymbol{\phi}(\mathcal{T})]$ denotes the $K \times \mathcal{T}$ total training matrix comprised of K $\mathcal{T}$-length training sequences, fulfilling the total power constraint $\|\boldsymbol{\Phi}\|_F^2 = \mathrm{Tr}(\boldsymbol{\Phi}^H\boldsymbol{\Phi}) = \mathcal{P} = K\mathcal{T}\rho$. The $M \times \mathcal{T}$ received signal matrix at the BS is given by

$$\boldsymbol{Y} = \boldsymbol{H}\boldsymbol{\Phi} + \boldsymbol{N}, \tag{5.4}$$

where $\boldsymbol{N}$ is the $M \times \mathcal{T}$ noise matrix with i.i.d. $\mathcal{N}(0, \sigma_n^2)_{\mathbb{C}}$ entries.

Since no statistical knowledge or steering matrix $\boldsymbol{A}$ of the propagation channel matrix $\boldsymbol{H}$ is assumed to be available, the realization of $\boldsymbol{H}$ can be estimated from the known pilot matrix $\boldsymbol{\Phi}$ and the received matrix $\boldsymbol{Y}$ using LS as

$$\begin{aligned}\hat{\boldsymbol{H}}_{\mathrm{LS}} &= \boldsymbol{Y}\boldsymbol{\Phi}^{\dagger} \\ &= \boldsymbol{Y}\boldsymbol{\Phi}^H\left(\boldsymbol{\Phi}\boldsymbol{\Phi}^H\right)^{-1}.\end{aligned}$$

Since all users send the training pilots using the same time-frequency resource, they use orthogonal pilots to avoid the interference at the BS. The optimal estimation error in terms of the Frobenius norm is given by [85]

$$\begin{aligned}\min_{\boldsymbol{H}} \mathbb{E}\{\|\boldsymbol{H} - \hat{\boldsymbol{H}}_{\mathrm{LS}}\|_F^2\} &= \frac{K^2 M}{(\mathcal{P}/\sigma_n^2)} \\ &= \frac{KM}{\mathcal{T}(\rho/\sigma_n^2)}.\end{aligned} \tag{5.5}$$

5.4 CS-based Channel Estimation

5.4.1 Nuclear Norm Regularized Least Squares via Quadratic SDP

In this section, we show that estimating the above described large MU-MIMO channel can be more efficiently solved by a new CS-based low-rank approximation technique via a quadratic SDP. Recall that for a matrix variable $\boldsymbol{X} \in \mathbb{C}^{m\times n}$ with a linear transformation $\mathcal{A}(\boldsymbol{X}) = \boldsymbol{b}$, where $\mathcal{A} : \mathbb{C}^{m\times n} \to \mathbb{C}^d$ is a linear operator, $\boldsymbol{b} \in \mathbb{C}^d$, d is the sample size, the NNM problem reads

$$\begin{aligned} \underset{\boldsymbol{X}}{\text{minimize}} \quad & \|\boldsymbol{X}\|_* \\ \text{subject to} \quad & \mathcal{A}(\boldsymbol{X}) = \boldsymbol{b}, \end{aligned}$$

where $\|\boldsymbol{X}\|_*$ denotes the nuclear norm of $\boldsymbol{X}$. Its noisy version is the nuclear norm regularization problem

$$\underset{\boldsymbol{X}}{\text{minimize}} \quad \frac{1}{2}\|\boldsymbol{b} - \mathcal{A}(\boldsymbol{X})\|_2^2 + \gamma\|\boldsymbol{X}\|_*$$

where γ is a regularization parameter.

By expressing the two sides of (5.4) in vector form and applying the fact that $\text{vec}(\boldsymbol{ABC}) = (\boldsymbol{C}^T \otimes \boldsymbol{A})\text{vec}(\boldsymbol{B})$, $\otimes$ denoting Kronecker product, we can rewrite (5.4) as

$$\text{vec}(\boldsymbol{Y}) = \boldsymbol{\Psi}\text{vec}(\boldsymbol{H}) + \text{vec}(\boldsymbol{N}),$$

where $\boldsymbol{\Psi} = \boldsymbol{\Phi}^T \otimes \boldsymbol{I}_M$. Then the nuclear norm regularization for our channel estimation problem is

$$\underset{\boldsymbol{H}}{\text{minimize}} \quad \frac{1}{2}\,\|\text{vec}(\boldsymbol{Y}) - \boldsymbol{\Psi}\text{vec}(\boldsymbol{H})\|_2^2 + \gamma\|\boldsymbol{H}\|_*. \tag{5.6}$$

To construct a dual problem of (5.6), we introduce a new vector variable $\boldsymbol{r} = \text{vec}(\boldsymbol{Y}) - \boldsymbol{\Psi}\text{vec}(\boldsymbol{H})$, and represent (5.6) as a constrained convex optimization problem as

$$\begin{aligned} \underset{\boldsymbol{H},\boldsymbol{r}}{\text{minimize}} \quad & \frac{1}{2}\|\boldsymbol{r}\|_2^2 + \gamma\|\boldsymbol{H}\|_* \\ \text{subject to} \quad & \boldsymbol{r} = \text{vec}(\boldsymbol{Y}) - \boldsymbol{\Psi}\text{vec}(\boldsymbol{H}). \end{aligned} \tag{5.7}$$

For dealing with complex-valued vectors, noticing that those $M\mathcal{T}$ equalities in the complex domain are equivalent to $2M\mathcal{T}$ in the real domain, the Lagrange multiplier vector associated with this equality constraint, denoted by $\boldsymbol{z}$ is also complex. The well-posed (real-valued) Lagrangian function of (5.7) is given by

$$\mathcal{L}(\boldsymbol{H}, \boldsymbol{r}, \boldsymbol{z}) = \frac{1}{2}\|\boldsymbol{r}\|_2^2 + \gamma\|\boldsymbol{H}\|_* + \Re\left\{\boldsymbol{z}^{\boldsymbol{H}}\left[\text{vec}(\boldsymbol{Y}) - \boldsymbol{\Psi}\text{vec}(\boldsymbol{H}) - \boldsymbol{r}\right]\right\},$$

in which we apply $\Re\{\boldsymbol{u}\}^T\Re\{\boldsymbol{v}\} + \Im\{\boldsymbol{u}\}^T\Im\{\boldsymbol{v}\} = \Re\{\boldsymbol{u}^H\boldsymbol{v}\}$, for any two complex vectors $\boldsymbol{u}$ and $\boldsymbol{v}$ having the same dimension; $\Re\{\cdot\}$ and $\Im\{\cdot\}$ denote the real and the imaginary parts of the enclosed, respectively. The dual function is

$$\begin{aligned} g(\boldsymbol{z}) &= \inf_{\boldsymbol{H},\boldsymbol{r}} \mathcal{L}(\boldsymbol{H}, \boldsymbol{r}, \boldsymbol{z}) \\ &= \Re\left\{[\text{vec}(\boldsymbol{Y})]^H\boldsymbol{z}\right\} + \inf_{\boldsymbol{r}}\left\{\frac{1}{2}\|\boldsymbol{r}\|_2^2 - \Re\left\{\boldsymbol{z}^H\boldsymbol{r}\right\}\right\} \\ &\quad + \inf_{\boldsymbol{H}}\left\{-\Re\left\{\boldsymbol{z}^H\boldsymbol{\Psi}\text{vec}(\boldsymbol{H})\right\} + \gamma\|\boldsymbol{H}\|_*\right\} \\ &= \Re\left\{[\text{vec}(\boldsymbol{Y})]^H\boldsymbol{z}\right\} - \frac{1}{2}\boldsymbol{z}^H\boldsymbol{z} - \sup_{\boldsymbol{H}}\left\{\Re\left\{\langle\boldsymbol{z}, \boldsymbol{\Psi}\text{vec}(\boldsymbol{H})\rangle\right\} - \gamma\|\boldsymbol{H}\|_*\right\}, \end{aligned} \tag{5.8}$$

where (5.8) holds when $\boldsymbol{r} = \boldsymbol{z}$.

Using the fact that $\langle\boldsymbol{z}, \boldsymbol{\Psi}\text{vec}(\boldsymbol{H})\rangle = \left\langle\boldsymbol{\Psi}^H\boldsymbol{z}, \text{vec}(\boldsymbol{H})\right\rangle = \left\langle\text{vec}_{M,K}^{-1}\left(\boldsymbol{\Psi}^H\boldsymbol{z}\right), \boldsymbol{H}\right\rangle$, $\text{vec}_{M,K}^{-1}(\cdot)$

converts a vector into a $M \times K$ matrix, we have

$$
\begin{aligned}
-\sup_{\boldsymbol{H}} \left\{ \Re \left\{ \langle \boldsymbol{z}, \boldsymbol{\Psi} \mathrm{vec}(\boldsymbol{H}) \rangle \right\} - \gamma \left\| \boldsymbol{H} \right\|_* \right\} &= -\sup_{\boldsymbol{H}} \left\{ \Re \left\{ \left\langle \mathrm{vec}_{M,K}^{-1} \left(\boldsymbol{\Psi}^H \boldsymbol{z} \right), \boldsymbol{H} \right\rangle \right\} - \gamma \left\| \boldsymbol{H} \right\|_* \right\} \\
&= -\gamma f_0^* \left(\frac{1}{\gamma} \mathrm{vec}_{M,K}^{-1} \left(\boldsymbol{\Psi}^H \boldsymbol{z} \right) \right) \qquad (5.9) \\
&= \begin{cases} 0 & \left\| \mathrm{vec}_{M,K}^{-1} \left(\boldsymbol{\Psi}^H \boldsymbol{z} \right) \right\|_{\mathrm{op}} \leq \gamma \\ -\infty & \text{otherwise,} \end{cases} \qquad (5.10)
\end{aligned}
$$

where we use in (5.9) the definition of the conjugate function $f_0^*(\cdot)$ of $f_0(\boldsymbol{H}) \triangleq \left\| \boldsymbol{H} \right\|_*$ (for complex matrices), and in (5.10) the theorem of the conjugate function of the dual norm [41]

$$
f_0^*(\boldsymbol{V}) = \begin{cases} 0, & \left\| \boldsymbol{V} \right\|_* \leq 1 \\ \infty & \text{otherwise,} \end{cases} \qquad (5.11)
$$

for operator norm function $f_0(\boldsymbol{V}) = \left\| \boldsymbol{V} \right\|_{\mathrm{op}}$; ($\|\cdot\|_*$ is the dual norm of the operator norm, denoted by $\|\cdot\|_{\mathrm{op}}$).

In light of the above, we can write the dual function as

$$
g(\boldsymbol{z}) = -\frac{1}{2} \boldsymbol{z}^H \boldsymbol{z} + \Re \left\{ [\mathrm{vec}(\boldsymbol{Y})]^H \boldsymbol{z} \right\}.
$$

Finally, the dual problem of (5.7) is

$$
\begin{aligned}
\underset{\boldsymbol{z}}{\text{minimize}} \quad & \frac{1}{2} \boldsymbol{z}^H \boldsymbol{z} - \Re \left\{ [\mathrm{vec}(\boldsymbol{Y})]^H \boldsymbol{z} \right\} \\
\text{subject to} \quad & \left\| \mathrm{vec}_{M,K}^{-1} \left(\boldsymbol{\Psi}^H \boldsymbol{z} \right) \right\|_{\mathrm{op}} \leq \gamma,
\end{aligned}
$$

which can be represented as a quadratic SDP as

$$
\begin{aligned}
\underset{\boldsymbol{z}}{\text{minimize}} \quad & \frac{1}{2} \boldsymbol{z}^H \boldsymbol{z} - \Re \left\{ [\mathrm{vec}(\boldsymbol{Y})]^H \boldsymbol{z} \right\} \\
\text{subject to} \quad & \begin{bmatrix} \gamma \boldsymbol{I}_M & \mathrm{vec}_{M,K}^{-1} \left(\boldsymbol{\Psi}^H \boldsymbol{z} \right) \\ \left[\mathrm{vec}_{M,K}^{-1} \left(\boldsymbol{\Psi}^H \boldsymbol{z} \right) \right]^H & \gamma \boldsymbol{I}_K \end{bmatrix} \succeq 0,
\end{aligned} \qquad (5.12)
$$

where $\succeq$ denotes the generalized matrix inequality with respect to the Hermitian positive-semidefinite cone [41]. (For the noiseless setting, it is derived in [39] that the dual problem can be represented in a linear SDP).

Let $\boldsymbol{z}^*$ be the solution to (5.12), then the result of (5.6), that is the estimate of channel matrix using our CS approach, is

$$\hat{\boldsymbol{H}}_{\mathrm{CS}} = \mathrm{vec}_{M,K}^{-1}\left\{\boldsymbol{\Psi}^{\dagger}\left(\mathrm{vec}(\boldsymbol{Y}) - \boldsymbol{z}^*\right)\right\}.$$

5.4.2 On the Choice of γ and the Performance Guarantee

As mentioned in Chapter 2, the two elements required for the above method are that the linear operator $\mathcal{A}$ has to satisfy certain conditions, and the regularization parameter γ has to be chosen carefully to control the error. There are some popular conditions on $\mathcal{A}$, including RIP [39, 86] and RSC [40]. It has been proved in [86] and discussed in [39] that many matrices with i.i.d. random elements including Gaussian, Bernoulli, "zeros in two-thirds", zero-mean and finite fourth moments obey RIP with high probability when the sample size is large enough. The most popular matrix is the one with i.i.d. Gaussian ensemble having the $(i,j)-th$ element satisfying

$$a_{i,j} \sim \mathcal{N}\left(0, \frac{1}{d}\right),$$

where d is the sample size. Matrix with i.i.d. Bernoulli ensemble has the $(i,j)-th$ element obeying

$$a_{i,j} \sim \begin{cases} \frac{1}{\sqrt{d}} & \text{with probability } 1/2 \\ -\frac{1}{\sqrt{d}} & \text{with probability } 1/2 \end{cases}.$$

Matrix with i.i.d. "zeros in two-thirds" ensemble has the $(i,j)-th$ element as

$$a_{i,j} \sim \begin{cases} \frac{3}{\sqrt{d}} & \text{with probability } 1/6 \\ 0 & \text{with probability } 2/3 \\ -\frac{3}{\sqrt{d}} & \text{with probability } 1/6 \end{cases} .$$

In [86], it is proved that for a matrix variable of size $m \times n$ with rank $r \leq \min\{m,n\}$, a linear measurement with i.i.d. Gaussian ensemble with sample $d > C \max\{m,n\}r$ satisfies RIP with overwhelming probability for some constant $C > 0$. The larger the size of the sample, the higher the probability that the measurement matrix satisfies RIP, and the probability approaches one (almost surely occurs) as the sample size tends to infinity [86]. In this chapter we control the error of the proposed method with Bernoulli ensemble via RSC, which is milder than RIP. We present RSC for our channel estimation problem as follows.

Definition 5.1 (Restricted Strong Convexity [40]). *The linear operator $\mathcal{A} : \mathbb{C}^{M\times K} \to \mathbb{C}^N$ is called to satisfy the Restricted Strong Convexity (RSC) over a restricted set $\mathcal{C} \in \mathbb{C}^{M\times K}$ if*

$$\frac{1}{2N}\|\mathcal{A}(\Delta)\|_2^2 \geq \kappa(\mathcal{A})\|\Delta\|_F^2 \quad \textit{for all } \Delta \in \mathcal{C},$$

for some $\kappa(\mathcal{A}) > 0$, $N = M\mathcal{T}$ is the sample size, $\mathcal{C}$ is the cone of matrices in $\mathbb{C}^{M\times K}$ having rank at most r.

This condition to establish error bounds for the low-rank matrix recovery guarantees that the quadratic loss function in (5.6) is strictly convex over a restricted set $\mathcal{C}$. Next, we need to choose the parameter γ carefully in order to obtain a sufficiently accurate result, and that parameter should be dependent on the noise level and the size of the sample. With the above notation, if we choose γ in (5.6) such that $\gamma \geq 2\|\mathcal{A}^*(\mathrm{vec}(\boldsymbol{N}))\|_{\mathrm{op}}$, $\mathcal{A}^*$ is the adjoint of $\mathcal{A}$, then the optimal solution $\hat{\boldsymbol{H}}_{\mathrm{CS}}$ has an estimation error, in Frobenius

norm, upper bounded as (see Theorem 1 of [40] for details)

$$\|\boldsymbol{H} - \hat{\boldsymbol{H}}_{\mathrm{CS}}\|_F \leq \frac{32\gamma\sqrt{P}}{N\kappa(\mathcal{A})}. \tag{5.13}$$

This is a deterministic result that generally guarantees for any linear operator $\mathcal{A}$ with RSC $\kappa(\mathcal{A})$ and $\gamma \geq 2\|\mathcal{A}^*(\mathrm{vec}(\boldsymbol{N}))\|_{\mathrm{op}}$. For our MU-MIMO channel estimation problem where the pilot sequences are symmetric random Bernoulli, we obtain the more useful following result.

Proposition 5.1 (Error bound for random Bernoulli training matrix)**.** *If we choose in (5.6) the regularization parameter* $\gamma = \sqrt{2(M+K)\mathcal{T}\rho\sigma_n^2}$*, then the CS-based channel estimator has an error upper bounded in squared Frobenius norm*

$$\|\boldsymbol{H} - \hat{\boldsymbol{H}}_{CS}\|_F^2 \leq c\frac{(M+K)P}{\mathcal{T}(\rho/\sigma_n^2)}, \tag{5.14}$$

with probability at least $1 - c_1 exp(-c_2(M^2+K^2)^{1/2})$ *when* $\mathcal{T} > K(1 - c_0/\log K)^{-1}$ *for some constants* $c, c_0, c_1, c_2 > 0$.

Proof. Using our notations, we have $\mathcal{A}(\Delta) = \boldsymbol{\Psi}\mathrm{vec}(\Delta) = \boldsymbol{\Delta}\boldsymbol{\Phi}$.

$$\begin{aligned}
\frac{1}{2N}\|\mathcal{A}(\Delta)\|_2^2 &= \frac{1}{2N}\|\boldsymbol{\Delta}\boldsymbol{\Phi}\|_F^2 \\
&= \frac{1}{2N}\sum_{j=1}^{M\mathcal{T}}\left\|\boldsymbol{\Phi}^T\left(\boldsymbol{\Delta}^T\right)_j\right\|_2^2 \\
&\geq \frac{1}{2N}\sum_{j=1}^{M\mathcal{T}} s_{\min}(\boldsymbol{\Phi}\boldsymbol{\Phi}^T)\left\|\left(\boldsymbol{\Delta}^T\right)_j\right\|_2^2 \\
&= \frac{s_{\min}(\boldsymbol{\Phi}\boldsymbol{\Phi}^T)}{2N}\|\boldsymbol{\Delta}\|_F^2 .
\end{aligned}$$

Therefore, the RSC holds for $\kappa(\mathcal{A}) = s_{\min}(\boldsymbol{\Phi}\boldsymbol{\Phi}^T)/(2N)$, where $s_{\min}(\boldsymbol{\Phi}\boldsymbol{\Phi}^T)$ is the minimum eigenvalue of $(\boldsymbol{\Phi}\boldsymbol{\Phi}^T)$.

Let $\boldsymbol{\Phi} = \sqrt{\rho}\boldsymbol{W}$, where $\boldsymbol{W}$ is the $K \times \mathcal{T}$ matrix whose entries are i.i.d. ± 1 symmetric

Bernoulli random variables. It is proved in [87] that for $\mathcal{T} > K(1 - c/\log K)^{-1}$,

$$\mathbb{P}\{s_{\min}(\boldsymbol{W}\boldsymbol{W}^T) \leq c_\lambda \mathcal{T}\} \leq \exp(-c\mathcal{T}), \tag{5.15}$$

for some constants c, c_λ depending on $\lambda = K/\mathcal{T}$. Thus, the RSC holds for $\kappa(\mathcal{A}) = c_\lambda \rho \mathcal{T}/2M$ with high probability when $\mathcal{T}$ is large enough.

Note that (5.13) occurs if we choose $\gamma \geq 2\|\mathcal{A}^*(\mathrm{vec}(\boldsymbol{N}))\|_{\mathrm{op}} = 2\|\boldsymbol{N}\boldsymbol{\Phi}^T\|_{\mathrm{op}} = 2\sqrt{\rho}\|\boldsymbol{N}\boldsymbol{W}^T\|_{\mathrm{op}}$. Let $\boldsymbol{Z} = \boldsymbol{N}\boldsymbol{W}^{\boldsymbol{T}} \in \mathbb{C}^{M\times K}$, we show next that the entries of $\boldsymbol{Z}$ are i.i.d. sub-Gaussian random variables. This is to obtain an upper bound tail for $\|\boldsymbol{Z}\|_{\mathrm{op}}$ later.

Definition 5.2 (Generalized version of real-valued sub-Gaussian random variable [88])**.** *A complex-valued random variable X is called complex sub-Gaussian with a constant c, denoted as $X \sim Sub(c^2)_{\mathbb{C}}$, if $\Re\{X\}$ and $\Im\{X\}$ are independent real-valued sub-Gaussian random variables with the same sub-Gaussian constant c, denoted as $\Re\{X\} \sim Sub(c^2)$, $\Im\{X\} \sim Sub(c^2)$. This means that there exists a constant $c > 0$ such that*

$$\mathbb{E}\left\{exp\left(\Re\{X\}t\right)\right\} \leq exp\left(c^2t^2/2\right), \tag{5.16}$$

$$\mathbb{E}\left\{exp\left(\Im\{X\}t\right)\right\} \leq exp\left(c^2t^2/2\right), \tag{5.17}$$

for all $t \in \mathbb{R}$. Furthermore, we call X strictly complex sub-Gaussian with variance σ^2, denoted $X \sim SSub(\sigma^2)_{\mathbb{C}}$ where $\sigma^2 = \mathbb{E}\left(\Re\{X\}^2\right) = \mathbb{E}\left(\Im\{X\}^2\right)$, if the above inequalities hold with $c^2 = \sigma^2$, which also requires that $\Re\{X\}$ and $\Im\{X\}$ are independent $SSub(\sigma^2)$ random variables.

Corollary 5.1. *A complex-valued random variable X is complex sub-Gaussian if there exists a constant $c > 0$ such that*

$$\mathbb{E}\left\{exp\left(\Re\{X\bar{t}\}\right)\right\} \leq exp\left(c^2|t|^2/2\right), \tag{5.18}$$

for all $t \in \mathbb{C}$.

Proof. Using the fact that $\Re\{X\bar{t}\} = \Re\{X\}\Re\{t\} + \Im\{X\}\Im\{t\}$, we have

$$\begin{aligned}
\mathbb{E}\left\{\exp\left(\Re\{X\bar{t}\}\right)\right\} &= \mathbb{E}\left\{\exp\left(\Re\{X\}\Re\{t\} + \Im\{X\}\Im\{t\}\right)\right\} && \text{(5.19a)}\\
&= \mathbb{E}\left\{\exp(\Re\{X\}\Re\{t\})\right\}\mathbb{E}\left\{\exp(\Im\{X\}\Im\{t\})\right\}\\
&\leq \exp\left(c^2\Re\{t\}^2/2\right)\exp\left(c^2\Im\{t\}^2/2\right) && \text{(5.19b)}\\
&= \exp\left(c^2|t|^2/2\right),
\end{aligned}$$

where in (5.19a) we apply the assumption that $\Re\{X\}$ and $\Im\{X\}$ are independent random variables, and (5.19b) holds as per Definition 5.2. □

Lemma 5.1. *The entries of* $M \times K$ *matrix* $\boldsymbol{Z} = \boldsymbol{N}\boldsymbol{W}^T$ *are i.i.d.* $Sub(\mathcal{T}\sigma_n^2/2)_{\mathbb{C}}$.

Proof. The (m,k)-th entry of $\boldsymbol{Z}$ is $\boldsymbol{Z}_{m,k} = \sum_{l=1}^{\mathcal{T}} \boldsymbol{W}_{k,l}\boldsymbol{N}_{m,l}$, where $\boldsymbol{W}_{k,l}$ is symmetric Bernoulli ± 1 random variable, and $\boldsymbol{N}_{m,l}$ is $\mathrm{SSub}(\sigma_n^2)_{\mathbb{C}}$. We have $\boldsymbol{Z}_{m,k}\bar{t} = \sum_{l=1}^{\mathcal{T}} \boldsymbol{W}_{k,l}\boldsymbol{N}_{m,l}\bar{t}$. Therefore,

$$\begin{aligned}
\mathbb{E}\left\{\exp\left(\Re\left\{\boldsymbol{Z}_{m,k}\bar{t}\right\}\right)\right\} &= \mathbb{E}\left\{\exp\left(\Re\left\{\sum_{l=1}^{\mathcal{T}}\boldsymbol{W}_{k,l}\boldsymbol{N}_{m,l}\right\}\Re\{t\} + \Im\left\{\sum_{l=1}^{\mathcal{T}}\boldsymbol{W}_{k,l}\boldsymbol{N}_{m,l}\right\}\Im\{t\}\right)\right\}\\
&= \prod_{l=1}^{\mathcal{T}}\mathbb{E}\left\{\exp\left(\Re\{\boldsymbol{N}_{m,l}\}\Re\{\boldsymbol{W}_{k,l}t\}\right)\right\}\prod_{l=1}^{\mathcal{T}}\mathbb{E}\left\{\exp\left(\Im\{\boldsymbol{N}_{m,l}\}\Im\{\boldsymbol{W}_{k,l}t\}\right)\right\}\\
&\leq \prod_{l=1}^{\mathcal{T}}\exp\left(\sigma_n^2/2\Re\{\boldsymbol{W}_{k,l}t\}^2/2\right)\prod_{l=1}^{\mathcal{T}}\exp\left(\sigma_n^2/2\Im\{\boldsymbol{W}_{k,l}t\}^2/2\right) && \text{(5.20)}\\
&\leq \exp(\mathcal{T}\sigma_n^2/2|t|^2/2), && \text{(5.21)}
\end{aligned}$$

where (5.20) holds by definition for $\mathrm{SSub}(\sigma_n^2/2)$ of $\Re\{\boldsymbol{N}_{m,l}\}$ and $\Im\{\boldsymbol{N}_{m,l}\}$, and in (5.21) we apply the fact that $|\boldsymbol{W}_{k,l}| = 1$. Therefore, the result of Lemma 5.1 follows by Corollary 5.1. □

Since the entries of $\boldsymbol{Z}$ are independent copies of $\mathrm{Sub}(\mathcal{T}\sigma_n^2/2)_{\mathbb{C}}$, applying Corollary

2.3.5 of [89],[1] we obtain the upper tail bound for the operator norm of the normalized matrix $\frac{1}{\sqrt{\mathcal{T}\sigma_n^2}}\boldsymbol{Z}$, which is given by

$$\mathbb{P}\{\frac{1}{\sqrt{L\sigma_n^2}}\|\boldsymbol{Z}\|_{\text{op}} \geq q\sqrt{M}\} \leq C\text{exp}(-cqM), \tag{5.22}$$

for $q \geq C$, where C, c are some absolute constants. If we choose in (5.22)

$$q = \sqrt{(M+K)/2M} \geq 1/\sqrt{2}, \text{ for } C \leq 1/\sqrt{2},$$

we have

$$\mathbb{P}\{\|\boldsymbol{Z}\|_{\text{op}} \geq \sqrt{(M+K)L\sigma_n^2/2}\} \leq C\text{exp}(-c\sqrt{(M+K)M/2}).$$

With $K \leq M$, $\|\boldsymbol{Z}\|_{\text{op}} \leq \sqrt{(M+K)\mathcal{T}\sigma_n^2/2}$ with probability at least $1 - C\text{exp}(-c(M^2 + K^2)^{1/2})$, for some (slightly different) constant c. Replacing $\gamma = 2\sqrt{\rho}\sqrt{(M+K)\mathcal{T}\sigma_n^2/2}$ and $\kappa(\mathcal{A}) = c_\lambda\rho\mathcal{T}/2N$ into (5.13), the result of Proposition 5.1 follows. □

As M and K grow large, with an overwhelming probability, this error upper bound decreases at a rate within a constant of $(M+K)P/(\mathcal{T}\rho/\sigma_n^2)$, which is faster than the lower bound of the LS's error rate, $MK/(\mathcal{T}\rho/\sigma_n^2)$. This means that the CS method helps to reduce the pilot power or length used by each UT, which is important since the UTs are usually required to operate in a low-power regime. We also note that the above performance guarantee, in fact, is an (asymptotic) upper bound for the estimation error, which almost surely holds in the large-scale problems considered in this chapter. How large the training length required or how much the CS-based method is better than the LS-based in different scales is quite conservative in practice. More useful and practical numerical results are given in Section 5.5 showing that this method outperforms the LS in a variety of settings. The above polynomial-time quadratic SDP has higher complexity

[1]The result of Corollary 2.3.5 in [89] applies for the i.i.d. ensembles of independent, zero-mean and uniformly bounded random variables, and it also holds for the ensemble of i.i.d. complex sub-Gaussian random variables that are "usually bounded" (see the discussions on p. 18 and p. 130 of [89])

compared to LS, as the dual problem has $M\mathcal{T}$ variables and one $(M+K)\times(M+K)$ semidefinite constraint, but this can be justified as this estimation task is done at the BS, which has powerful processing capability. Modern SDP solver can afford the problem with matrix variables having each size up to a hundred [39].

5.5 Numerical Results

In this section, we compare the channel error performance of our proposed CS method with the conventional LS numerically. In the first experiment, we simulate a MU-MIMO system with $M = 60$, $K = 40$ UTs (corresponding the 40-user single-cell scenario or 4-cell scenario with 10 UTs per cell). The number of paths $P = 20$, and the steering vector has $D_0/\lambda = 0.3$, AoA $\phi_p = -\pi/2 + (p-1)\pi/P$, $p = 1, 2, ..., P$ as in [63, 82]. The modulation format for pilot symbols is BPSK. We use the following normalized squared Frobenius norm error to evaluate the performance of each estimator.

$$Err = 10\log_{10}\left(\frac{1}{MK}\|\boldsymbol{H} - \hat{\boldsymbol{H}}\|_F^2\right),$$

where $\hat{\boldsymbol{H}}$ is the channel estimate using LS or CS method. For the CS estimator, we choose $\gamma = \sqrt{2(M+K)\mathcal{T}\rho\sigma_n^2}$ as in Proposition 5.1. Since no additional knowledge about the channel statistics or physical propagation parameters is required for both methods, this is a fair comparison.

In Fig. 5.1, we display the normalized error versus the total training power to noise ratio SNR $= \mathcal{P}/\sigma_n^2$ with different $\mathcal{T} \in \{45, 50, 55\}$, for both the LS and our proposed CS methods. It can be seen from Fig. 5.1 that when $\mathcal{T}$ increases, the normalized error of both methods decreases, but the CS-based method achieves significantly better performance, as expected from the analysis.

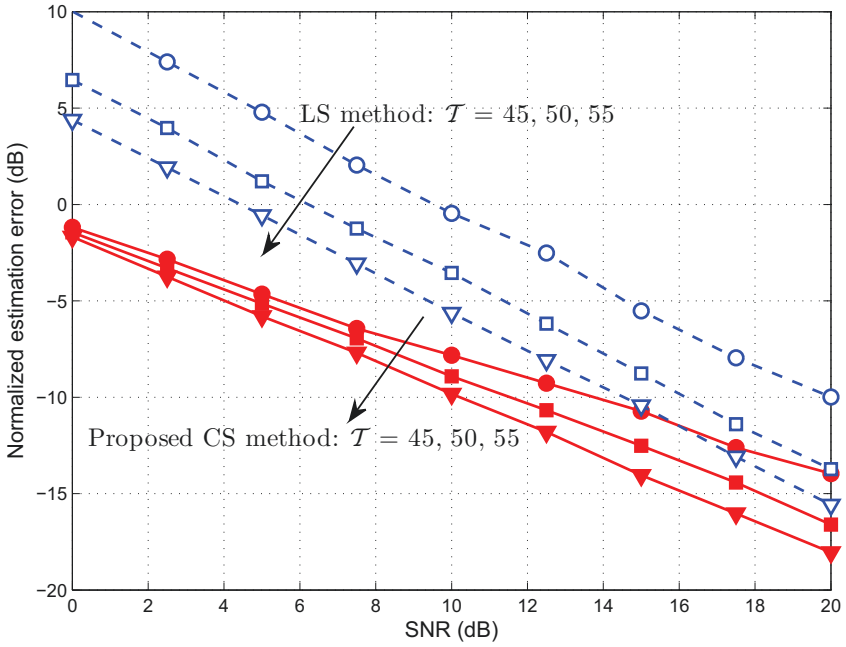

Figure 5.1: Comparison of normalized estimation error versus SNR between LS and CS methods for $M = 60$, $K = 40$, $\mathcal{T} \in \{45, 50, 55\}$.

Next, we fix $M = 60$, and change M to 30 and 50, respectively. The simulation results of both methods using $\mathcal{T} = 55$ displayed in Fig. 5.2 show that the normalized estimation error of both increases when we increase the number of UTs K. Again, the proposed CS method outperforms the LS in terms of error performance, and the performance loss from $K = 30$ to $K = 50$ of CS is less than that of the LS. It is because the error of the CS-based method grows with the DoF of the channel matrix, not its ambient dimensions (sizes).

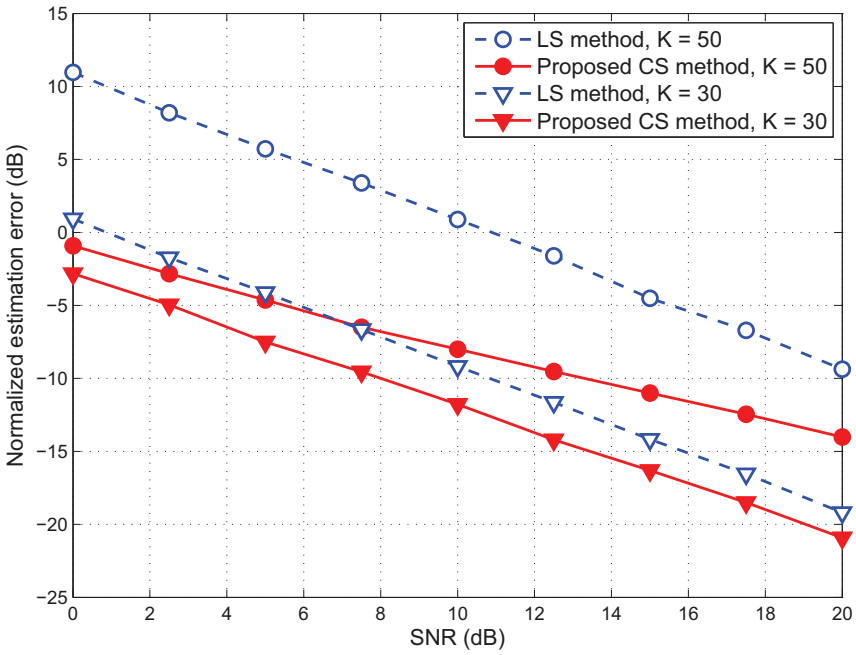

Figure 5.2: Comparison of normalized estimation error versus SNR between LS and CS methods for $M = 60$, $K \in \{30, 50\}$, $\mathcal{T} = 55$.

Finally, we repeat the first experiment with $M = 80$, and the results obtained are shown in Fig. 5.3. Comparing Figs. 1 and 3, the normalized error performances are almost the same for two cases $M = 60$ and $M = 80$. This can be explained for the LS method in a TDD system, as in (5.5) the estimation error after normalized is linearly proportional to the number of UTs K, inversely proportional to the pilot length $\mathcal{T}$, and independent on the number of BS antenna M. The proposed CS-based method also shares these advantageous features, but achieves better performance, thanks to the imposing of the rank (or nuclear norm) constraint on the channel matrix.

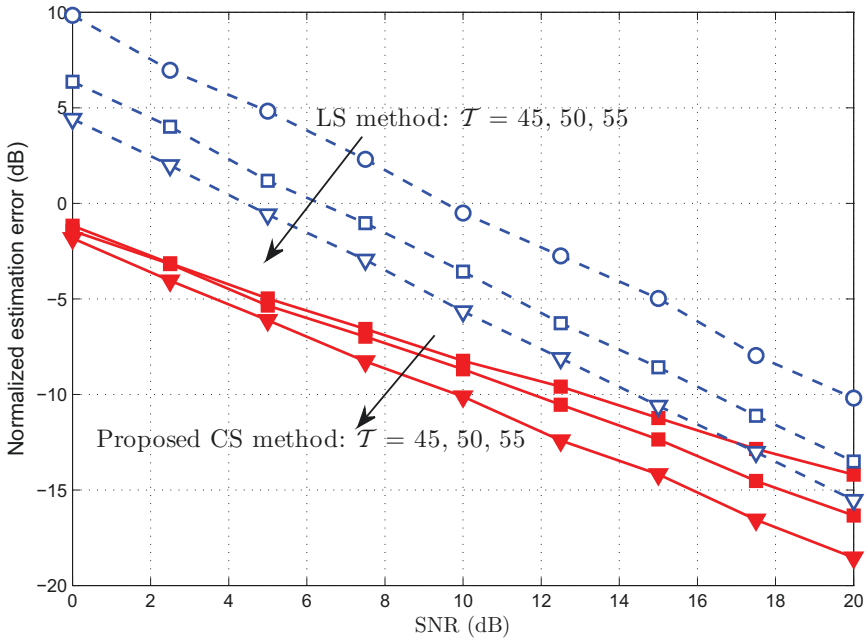

Figure 5.3: Comparison of normalized estimation error versus SNR between LS and CS methods for $M = 80$, $K = 40$, $\mathcal{T} \in \{45, 50, 55\}$.

5.6 Concluding Remarks

We have proposed in this chapter a new approach to estimate the massive MU-MIMO channel matrix based on CS. Analysis and experimental results show that the proposed method has a substantial improvement over the traditional LS for a realistic physical finite scattering channel model, when both dimensions of the MU-MIMO channel matrix to be estimated grow large. Furthermore, the improvement obtained by the proposed method does not require any additional knowledge about the statistical distribution or physical parameters of the propagation channel.

Chapter 6

Compressive rank-q Channel Sensing and Precoding for Multicell Massive MIMO Systems

6.1 Introduction

In Chapter 5, we have shown that estimating the massive MIMO channel with realistic propagation model can be efficiently solved by using CS. This chapter is concerned with both of the problems of uplink channel estimation and downlink precoding in the multicell massive MIMO systems based on CS.

6.1.1 Problem Statement and Objectives

Massive MIMO is expected to play a major role towards achieving the target of gigabit data rates that would be offered by the future cellular networks [80]. Recent studies have shown that massive MIMO brings both opportunities and challenges [28, 65]. On the optimistic side, compared to the classical MIMO, under some favorable assumptions, massive MIMO provides many advantages such as higher data rates, better link reliability,

and better spectral-energy efficiency tradeoff. The challenging side is that, to obtain those promising results, many optimistic assumptions that do not generally hold in practice are made. Indeed, the asymptotically optimal results are derived with the assumptions of favorable and rich scattering channel [28], the availability of perfect CSI at all UTs and at the BS, and zero intercell interference [62]. More recent works on massive MIMO studied more realistic settings including the correlated channel with finite scattering model and imperfect CSI acquisition, and in interference-limited multicell scenarios [63], [82]. It is shown that, when taking all the above practical conditions into account, there exist some fundamental problems, and the overall performance of the massive MIMO system is still far away from the theoretical limits.

One of the main limitations of massive MIMO is the pilot contamination effect in the uplink training under the multicell scenario. In single-cell systems operating in TDD mode, the channel estimation is performed via the uplink (the reverse link) training, and then the estimates are used to design ZF based precoding vectors for the downlink (the forward link) using the notion of *reciprocity*. As a result, the training overhead linearly scales with the number of UTs, not the number of BS antennas, making TDD viable for massive MIMO. In multicell systems, however, pilot contamination occurs, that is, the quality of the channel information estimated by a cell is affected by the interference from the pilots sent by the users in other cells [62]. This is due to the fact that the training sequences across all the cells can not be long enough (due to the short coherence time) to be orthogonal for accurate estimation. The problem becomes more critical when the number of users in each cell grows large, and/or the intercell gains between users in a cell to the BS in another cell are relatively strong as compared to the direct link gains. Since we do not have the estimate of the global channel, the existing methods have focused on nulling out the intracell interference only. Strong intercell gains not only severely degrade the quality of the uplink channel estimation, but also limit the effectiveness of downlink precoding due to the intercell interference. When those effects are added up, the achievable

rate of the overall system performance is significantly reduced. Recent works have showed that the degradation of the achievable rate due to pilot contamination and the downlink intercell interference are also present for realistic correlated finite dimensional massive MIMO channels [82].

In this chapter, we propose a new estimation and precoding method to mitigate both of the above-mentioned effects of pilot contamination and the strong intercell interference in a realistic finite dimensional channel model. Specifically, given a certain length of pilot sequences, we propose in the uplink a CS based rank-q channel matrix approximation approach to estimate as many dominant singular subspaces of the global multicell massive MIMO channel matrix as possible. Then, an intercell-interference-aware (IA) precoding method based on the estimated global channel information is performed in the downlink to mitigate not only the intracell interference but also the intercell interference of the channel. Our proposed scheme aims to help the estimation and precoding processes at each BS, resulting in improvements in the achievable rates of all users in the system.

Prior work on the estimation of correlated massive MIMO channels includes [63], [28], [82]- [83], where LS or MMSE is performed with the assumption that TDD is used. Our proposed framework, however, is based on more recent developments in CS where the sparsity model of the signal vector is generalized to the low-rank model of the matrix variable [39, 40]. The feasibility of invoking CS for the underlying channel model is attributed to the sparsity inherent in the highly correlated massive MIMO channel (i.e., small number of physical direction), or in cases where only a small number of UTs in neighbouring cells are active (i.e., have strong intercell gains), which makes the global CSI matrix rank-deficient. In such cases, for short training sequences, the global channel estimation problem becomes an under-determined problem, rendering classical estimation techniques inapplicable. The importance of using CS for such channels becomes even greater as the channel matrix dimensions grow large. Furthermore, another feature that distinguishes our proposed estimation framework is that it does not require any knowledge

about the statistical distribution or physical parameters of the propagation channel. As for the proposed zero-forcing-based precoding method, it is different from previous works since it considers the multicell system as a "big" channel, and uses the approximation of the most dominant singular subspace of the global channel CSI in hand to design the ZF precoding vectors.

6.1.2 Contributions

The technical contributions of this chapter are as follows.

- We use CS to solve the pilot contamination and intercell interference problems in multicell multiuser massive MIMO systems. The notion here is that, instead of estimating the global channel matrix, only the most dominant q singular subspaces of the global channel matrix are estimated. Hence we refer to this technique as rank-q channel approximation. We show that with modest values of q (compared to the actual rank of the global matrix), only little performance degradation is experienced.

- Given the high computational complexity of the common SDP-based method used in the estimation process, which becomes prohibitively complex, we present two other low-complexity greedy techniques including IHT and Matrix Factorization. We show that the proposed techniques outperform the existing method based on LS, for the same training sequence length.

- We use the estimate of the global channel matrix to design IA-ZF downlink precoding vectors with the objective of mitigating both the intracell interference caused by UTs in a cell and the intercell interference coming from UTs in neighboring cells.

- We derive a lower bound on the downlink achievable rate while assuming knowledge of the exact rank-q global channel matrix approximation assumption. This bound

is used as a benchmark for the proposed techniques. We show that the achievable rate is dependent on q where, as expected, the rate is higher with larger q since the approximation error becomes smaller.

6.1.3 Chapter Organization

The rest of the chapter is organized as follows. We describe the system and channel models in Section 6.2. In Section 6.3, we review single-cell downlink precoding and channel estimation methods in TDD systems, where the two drawbacks of this scheme are pointed out in the multicell scenarios with strong intercell gains. Section 6.4 describes our proposed intercell-interference-aware precoding method based on the uplink best rank-q global channel approximation. In Section 6.5, we analyze the achievable rate with the exact rank-q channel approximation assumption. Section 6.6 presents various CS-based techniques for rank-q channel matrix estimation, including SDP, IHT and Matrix Factorization methods, along with their pros and cons. Numerical results are presented in Section 6.7. Section 6.8 concludes the chapter.

6.2 System and Channel Models

6.2.1 Multicell Massive MU-MIMO System Model

In this section, we describe the system model adopted in this chapter. Consider a MU-MIMO system in a multi-cell interference-limited system as shown in Fig. 6.1, which operates in TDD with L cells [63], [28]. Each cell has one BS equipped with an array of a large number of antennas M, serving K single-antenna UTs simultaneously. In the uplink, at time t, the received signal vector at the BS of cell j, denoted by $\boldsymbol{y}_j \in \mathbb{C}^M$, is given by

$$\boldsymbol{y}_j^{\mathrm{ul}}(t) = \sqrt{\rho_{\mathrm{ul}}} \sum_{l=1}^{L} \boldsymbol{H}_{jl} \boldsymbol{x}_l^{\mathrm{ul}}(t) + \boldsymbol{n}_j^{\mathrm{ul}}(t), \tag{6.1}$$

where ρ_{ul} denotes the uplink signal-to-noise ratio (SNR), $\boldsymbol{H}_{jl} = [\boldsymbol{h}_{jl1}\ \boldsymbol{h}_{jl2}\ \ldots\ \boldsymbol{h}_{jlK}] \in \mathbb{C}^{M\times K}$ is the flat-fading quasi-static MU-MIMO complex-valued channel matrix from cell l to BS j, where $[\boldsymbol{H}_{jl}]_{(m,k)}$ is the channel gain from user k in cell l to antenna m of BS j; $\boldsymbol{x}_j^{\text{ul}}(t) = \left[x_{j1}^{\text{ul}}(t)\ x_{j2}^{\text{ul}}(t)\ \ldots\ x_{jK}^{\text{ul}}(t)\right]^T \in \mathbb{C}^K$ is the transmit signal vector of K users in cell l; and $\boldsymbol{n}_j^{\text{ul}}(t) = \left[n_{j1}^{\text{ul}}(t)\ n_{j2}^{\text{ul}}(t)\ \ldots\ n_{jM}^{\text{ul}}(t)\right]^T \in \mathbb{C}^M$ is the complex-valued additive white Gaussian noise (AWGN) vector at BS j, whose entries are independent and identically distributed (i.i.d.) $\mathcal{N}(0,1)_{\mathbb{C}}$, i.e., zero-mean, 1/2-variance per dimension random variables. With ρ_{ul} being the uplink SNR, the transmit signal vector $\boldsymbol{x}_j^{\text{ul}}(t)$ has the unity power constraint, i.e,

$$\mathbb{E}\{\boldsymbol{x}_j^{\text{ul}}(t)(\boldsymbol{x}_j^{\text{ul}}(t))^H\} = 1.$$

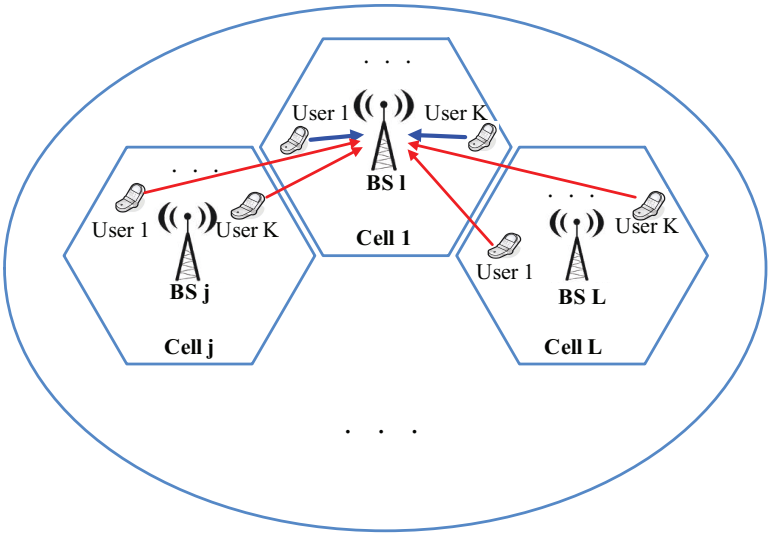

Figure 6.1: Multi-cell MU-MIMO system model.

For the downlink, i.e., the forward link, the channel coefficients are the transpose of the corresponding uplink ones, and the received signal at UT k in cell j at time t is given by

$$y_{jk}^{\text{dl}}(t) = \sqrt{\rho_{\text{dl}}} \sum_{l=1}^{L} \boldsymbol{h}_{ljk}^T \boldsymbol{s}_l(t) + n_{jk}^{\text{dl}}(t), \tag{6.2}$$

where ρ_{dl} denotes the downlink SNR, $\boldsymbol{s}_l(t) \in \mathbb{C}^M$ is the precoded transmit vector from BS l, and $n_k^{\text{dl}}(t) \sim \mathcal{N}(0,1)_{\mathbb{C}}$ is the noise at user k.

6.2.2 Physical Finite Scattering Correlated Channel Model

We are interested in the realistic finite-dimensional channel model, which was recently studied for massive MU-MIMO [28], [82], [83]. In this model, the angular domain is partitioned into a finite number of directions (i.e., number of active scatterers). Assuming that there are in total P i.i.d paths originating from each user k in cell j, each path has an $M \times 1$ steering vector [81]

$$\boldsymbol{a}(\phi_p) = \begin{bmatrix} 1 \\ \exp\left(-j2\pi \frac{D_0}{\lambda} \cos(\phi_p)\right) \\ \vdots \\ \exp\left(-j2\pi \frac{(M-1)D_0}{\lambda} \cos(\phi_p)\right) \end{bmatrix}, \tag{6.3}$$

where $\phi_p \in [-\pi/2, \pi/2]$ is a random angle of arrival (AoA) corresponding to path $p \in \{1, 2, ..., P\}$ with respect to user k direction, D_0 is the antenna spacing at the BS, and λ is the signal wavelength. The channel vector from user k in cell l to BS j is given by

$$\boldsymbol{h}_{jlk} = \frac{1}{\sqrt{P}} \sum_{p=1}^{P} g_{jlkp} \boldsymbol{a}(\phi_p),$$

where $g_{jlkp} \sim \mathcal{N}\left(0, \delta_{jlk}^2\right)_{\mathbb{C}}$ is the random propagation gain from user k in cell l to BS j. The variance δ_{jlk} is the channel's average attenuation including the path loss and shadowing effects [28], [83].

To account for the effect of the user's random location in term of the direct- and cross-gains in a multi-cell setting, our model makes use of three different values of δ_{jlk}^2 as follows. For the direct link, δ_{llk}^2 is normalized to unity for all K UTs in each cell l. For a set of links from users $k \in \mathbb{K}_{jl}$ with a cardinality $K_c < K$ in cell l located near the edge between two adjacent cells l and j, $\delta_{jlk}^2 = \delta_c^2 \leq 1$ $(j \neq l)$, for all $k \in \mathbb{K}_{jl}$. For the other cross-links from each user $k \notin \mathbb{K}_{jl}$ in cell l to BS j $(j \neq l)$, $\delta_{jlk}^2 = \delta_d^2 \leq \delta_c^2$. Those assignments are simple but allow for classifying three different types of user locations

to describe the direct- and cross-links in multi-cell systems. Extension to more general distance-based power-law decaying path-loss distributions is straightforward.

With the above model, the $M \times K$ MU-MIMO channel matrix $\boldsymbol{H}_{jl}$ between K UTs in cell l and BS j can be collectively written in a compact form as

$$\boldsymbol{H}_{jl} = \frac{1}{\sqrt{P}} \boldsymbol{A} \boldsymbol{G}_{jl},$$

where $\boldsymbol{A} = [\boldsymbol{a}(\phi_1)\ \boldsymbol{a}(\phi_2)\ \ldots\ \boldsymbol{a}(\phi_P)]$ is a $M \times P$ full-rank matrix containing P steering vectors, and $\boldsymbol{G}_{jl}$ is the $P \times K$ path gain channel matrix, $[\boldsymbol{G}_{jl}]_{(p,k)}$ denotes the path gain from user k in cell l to BS j associated with path p.

Remark 6.1. *In the correlated MIMO channel with the physical finite scattering model described above, the global channel matrix from all UTs in all cells to the BS j, denoted by $\boldsymbol{H}_j = [\boldsymbol{H}_{j1}\ \boldsymbol{H}_{j2}\ \ldots\ \boldsymbol{H}_{jL}] \in \mathbb{C}^{M \times LK}$, has a DoF $r(M + LK - r)$, where r is the rank of $\boldsymbol{H}_j$, $r \leq \min\{M, LK, P\}$.*

Indeed, the global channel $\boldsymbol{H}_j$ at BS j can be written as

$$\begin{aligned} \boldsymbol{H}_j &= \frac{1}{\sqrt{P}} \boldsymbol{A} \left[\boldsymbol{G}_{j1}\ \boldsymbol{G}_{j2}\ \ldots\ \boldsymbol{G}_{jL}\right] \\ &= \frac{1}{\sqrt{P}} \boldsymbol{A} \boldsymbol{G}_j, \end{aligned} \tag{6.4}$$

where $\boldsymbol{G}_j = [\boldsymbol{G}_{j1}\ \boldsymbol{G}_{j2}\ \ldots\ \boldsymbol{G}_{jL}] \in \mathbb{C}^{P \times LK}$. Since the rank of $\boldsymbol{A}$ is smaller than $\min\{M, P\}$, and the rank of $\boldsymbol{G}_j$ is smaller than $\min\{P, LK\}$, then the rank of $\boldsymbol{H}_j$ is at most $\min\{M, LK, P\}$.

For the massive MU-MIMO system considered in this chapter, we consider the scenario when both M and K are large ($M \gg LK$), and $P = \beta_P M (0 < \beta_P \leq 1)$, i.e, P is proportional to M [63]. If we further assume that $K < P < LK < M$, then the local channel matrix $\boldsymbol{H}_{jj}$ has a full column-rank of K, but the global channel $\boldsymbol{H}_j$ is not full rank (the maximum rank of $\boldsymbol{H}_j$ is P). This highly correlated MU-MIMO model characterizes the poor scattering propagation environment, where the number of physical objects is

limited. It also describes the propagation channel where the scatterers appear in groups (called clusters) with similar delays, AoAs and angle-of-departures (AoDs), making the effective number of active directions limited, even when the number of physical objects is large [28]. In this case, the rank of $\boldsymbol{H}_j$ is P, and the actual DoF of the channel matrix is $P(M + LK - P)$, not its number of free parameters MLK.

For the case $P > LK$, and when the average power of the cross links δ_d^2 is small relative to δ_c^2 (i.e. only K_c users in each neighbouring cell are active), we show later that the global channel matrix $\boldsymbol{H}_j$ can be well approximated by a matrix with rank $K + (L-1)K_c$.

6.3 Single-cell Precoding: Pilot Contamination and Intercell Interference Effects

6.3.1 LS Channel Estimation

In TDD systems, the CSI is estimated in the uplink, and used to perform the precoding/beamforming in the downlink. The conventional and standard way of estimating the CSI is to send from each user a training sequence of length $\mathcal{T} \geq K$ in the training phase of each coherence interval. Denote $\sqrt{\rho_{\text{tr}}}\boldsymbol{\theta}_{jk} = \sqrt{\rho_{\text{tr}}}\,[\boldsymbol{\theta}_{jk}(1)\ \boldsymbol{\theta}_{jk}(2)\ \ldots\ \boldsymbol{\theta}_{jk}(\mathcal{T})]$ as the $1 \times \mathcal{T}$ training signal vector sent by UT k in cell j, which is orthogonal with respect to $\sqrt{\rho_{\text{tr}}}\boldsymbol{\theta}_{jn}$ (that of UT n in cell j), and fulfills the total training power constraint ρ_{tr}. That means, $\boldsymbol{\theta}_{jk}\boldsymbol{\theta}_{jn}^H = 1$ if $n = k$ and 0 otherwise. Let $\boldsymbol{\Theta}_j = \left[\boldsymbol{\theta}_{j1}^T\ \boldsymbol{\theta}_{j2}^T\ \ldots\ \boldsymbol{\theta}_{jK}^T\right]^T$ be the $K \times \mathcal{T}$ total training matrix comprised from K $\mathcal{T}$-length training sequences in cell j. The $\boldsymbol{M} \times \mathcal{T}$ received signal matrix at BS j is given by

$$\begin{aligned}\boldsymbol{Y}_j &= \sqrt{\mathcal{T}\rho_{\text{tr}}}\sum_{l=1}^{L}\boldsymbol{H}_{jl}\boldsymbol{\Theta}_l + \boldsymbol{N}_j \\ &= \sqrt{\mathcal{T}\rho_{\text{tr}}}\boldsymbol{H}_j\boldsymbol{\Theta} + \boldsymbol{N}_j, \end{aligned} \tag{6.5}$$

where $\boldsymbol{\Theta} = \left[\boldsymbol{\Theta}_1^T\ \boldsymbol{\Theta}_2^T\ \ldots\ \boldsymbol{\Theta}_L^T\right]^T \in \mathbb{C}^{LK\times T}$, $\boldsymbol{N}_j$ is the $M \times T$ noise matrix with i.i.d. $\mathcal{N}(0,1)_{\mathbb{C}}$ entries.

Here we assume that there is no statistical knowledge or steering matrix $\boldsymbol{A}$ of the propagation channel matrix $\boldsymbol{H}_{jl}$ available at each BS j[1]. As such, the channel realizations are estimated using the LS method by correlating the received matrix $\boldsymbol{Y}_j$ in (6.5) with the known training matrix. If only the "local" CSI $\boldsymbol{H}_{jj}$ needs to be estimated at BS j, then the LS estimate of $\boldsymbol{h}_{jjk}$ is given by

$$\begin{aligned}\hat{\boldsymbol{h}}_{jjk}^{\mathrm{LS}} &= \frac{1}{\sqrt{\rho_{\mathrm{tr}}}}\boldsymbol{Y}_j\boldsymbol{\theta}_{jk}^H \\ &= \sum_{l=1}^{L}\left[\boldsymbol{h}_{jl1}\ \boldsymbol{h}_{jl2}\ \ldots\ \boldsymbol{h}_{jlK}\right]\left[\boldsymbol{\theta}_{l1}^T\ \boldsymbol{\theta}_{l2}^T\ \ldots\ \boldsymbol{\theta}_{lK}^T\right]^T\boldsymbol{\theta}_{jk}^H + \frac{1}{\sqrt{\rho_{\mathrm{tr}}}}\boldsymbol{N}_j\boldsymbol{\theta}_{jk}^H \\ &= \boldsymbol{h}_{jjk} + \sum_{l\neq j}\boldsymbol{h}_{jlk} + \tilde{\boldsymbol{n}}_{jk}^{\mathrm{tr}},\end{aligned} \tag{6.6}$$

where $\tilde{\boldsymbol{n}}_{jk}^{\mathrm{tr}} = \frac{1}{\sqrt{\rho_{\mathrm{tr}}}}\boldsymbol{N}_j\boldsymbol{\theta}_{jk}^H \sim \mathcal{N}\left(0, \rho_{\mathrm{tr}}^{-1}\sigma_n^2\boldsymbol{I}_M\right)_{\mathbb{C}}$, and in the above we assume that the same set of orthogonal pilot sequences is reused in every cell [62].

From (6.6), we can see that the local CSI estimate in cell j is contaminated by the pilots sent from UTs in the other $(L-1)$ cells, due to the non-orthogonality of the LK $\mathcal{T}$-length pilot sequences ($\mathcal{T} < LK$). This fundamental issue exists in massive multicell MU-MIMO system due to the small $\mathcal{T}$ in a limited coherent time interval and the large dimension LK, resulting in a significant reduction in the achievable rates of UTs, especially the ones in the cell-edge area, as we will show in the next section.

[1]Our approach is different from the MMSE estimators in which either statistical distribution [63], [62] or both statistical distribution and physical steering matrix A [82] of the channels are assumed to be available at all BSs. In fact, this assumption is more reasonable for the intercell-interference-aware methods, because the availability of all those parameters of all channels at each BS is not realistic.

6.3.2 Singe-cell Precoding

In the downlink, the received signal at UT k in cell j in (6.2) can be re-written as

$$y_{jk}^{\mathrm{dl}} = \sqrt{\rho_{\mathrm{dl}}\lambda_j}\boldsymbol{h}_{jjk}^T\boldsymbol{w}_{jk}x_{jk}^{\mathrm{dl}} + \underbrace{\sqrt{\rho_{\mathrm{dl}}\lambda_j}\sum_{n\neq k}\boldsymbol{h}_{jjk}^T\boldsymbol{w}_{jn}x_{jn}^{\mathrm{dl}}}_{\text{intracell interference}} + \underbrace{\sqrt{\rho_{\mathrm{dl}}}\sum_{l\neq j}\sqrt{\lambda_l}\sum_{n=1}^{K}\boldsymbol{h}_{ljk}^T\boldsymbol{w}_{ln}x_{ln}^{\mathrm{ul}}}_{\text{intercell interference}} + n_{jk}^{\mathrm{dl}},$$

where we use $\boldsymbol{s}_l = \sqrt{\lambda_l}\boldsymbol{W}_l\boldsymbol{x}_l = \sqrt{\lambda_l}\sum_{n=1}^{K}\boldsymbol{w}_{ln}x_{ln}$, $\boldsymbol{W}_l = [\boldsymbol{w}_{l1}\ \boldsymbol{w}_{l2}\ \ldots\ \boldsymbol{w}_{lK}]$ is the precoding matrix at BS l, and λ_l is a normalization parameter, given by

$$\lambda_l = \left(\mathbb{E}\left\{\frac{1}{K}\mathrm{tr}\{\boldsymbol{W}_l\boldsymbol{W}_l^H\}\right\}\right)^{-1}. \tag{6.7}$$

Using ZF precoding, the precoding vector at BS j satisfies[2]

$$\begin{cases}\hat{\boldsymbol{h}}_{jjk}^T\boldsymbol{w}_{jk}^{\mathrm{ZF}} = 1\\ \hat{\boldsymbol{h}}_{jjk}^T\boldsymbol{w}_{jn}^{\mathrm{ZF}} = 0,\ n\neq k.\end{cases} \tag{6.8}$$

In matrix form, ZF requires

$$\hat{\boldsymbol{H}}_{jj}^T\boldsymbol{W}_j^{\mathrm{ZF}} = \boldsymbol{I}_K,$$

or (assuming that $\hat{\boldsymbol{H}}_{jj}^T$ has a full rank of K), we have

$$\begin{aligned}\boldsymbol{W}_j^{\mathrm{ZF}} &= (\hat{\boldsymbol{H}}_{jj}^T)^{\dagger}\\ &= \hat{\boldsymbol{H}}_{jj}^*(\hat{\boldsymbol{H}}_{jj}^T\hat{\boldsymbol{H}}_{jj}^*)^{-1}.\end{aligned}$$

Using the worst-case independent Gaussian noise analysis [62, Theorem 1], the ergodic achievable downlink rate of user k in cell j is computed as

$$R_{jk}^{\mathrm{dl}} = \log_2(1+\gamma_{jk}^{\mathrm{dl}}), \tag{6.9}$$

[2]We use $\hat{\boldsymbol{h}}$ for the estimate of $\boldsymbol{h}$ without specifying any estimation method, and will use the superscript LS, CS, and q to differentiate the LS, CS or exact rank-q channel estimators, respectively.

where γ_{jk}^{dl} denotes the associated signal-to-noise-plus-interference ratio (SNIR) with ZF precoding[3]. Assuming that UT k in cell j does not know the instantaneous $\boldsymbol{h}_{jjk}$, but knows its average, then γ_{jk}^{dl} is given by

$$\gamma_{jk}^{\text{dl-ZF}} = \frac{\lambda_j \left|\mathbb{E}\left\{\boldsymbol{h}_{jjk}^T \boldsymbol{w}_{jk}\right\}\right|^2}{\rho_{\text{dl}}^{-1} + \lambda_j \text{var}\left\{\boldsymbol{h}_{jjk}^T \boldsymbol{w}_{jk}\right\} + \sum_{n\neq k} \lambda_j \mathbb{E}\left\{\left|\boldsymbol{h}_{jjk}^T \boldsymbol{w}_{jn}\right|^2\right\} + \sum_{l\neq j} \sum_{n=1}^{K} \lambda_l \mathbb{E}\left\{\left|\boldsymbol{h}_{ljk}^T \boldsymbol{w}_{ln}\right|^2\right\}}, \tag{6.10}$$

where the expectation is taken over all channel realizations [62,63]. In short, the argument in [62] bases on the fact that the information rate of this channel with uncorrelated additive noise (not independent neither Gaussian) is always larger than that of the point-to-point channel with independent Gaussian noise of same variance, which has the information rate given by (6.9). The ergodic achievable downlink sum-rate of all users in cell j (i.e., the lower bound on sum capacity or total system throughput in cell j [62]) is

$$R_j^{\text{dl}} = \sum_{k=1}^{K} R_{jk}^{\text{dl}}. \tag{6.11}$$

If we assume that the local CSI is perfectly known at each BS j, the SNIR of UT k in cell j in this case, denoted by $\gamma_{jk}^{\text{dl-ZF-CSI}}$, is given by

$$\gamma_{jk}^{\text{dl-ZF-CSI}} = \frac{\lambda_j}{\rho_{\text{dl}}^{-1} + \sum_{l\neq j} \sum_{n=1}^{K} \lambda_l \mathbb{E}\left\{\left|\boldsymbol{h}_{ljk}^T \boldsymbol{w}_{ln}\right|^2\right\}}. \tag{6.12}$$

With the above perfect CSI assumption, the intracell interference vanishes, but the SNIR is still affected by the intercell interference from the other cells. When the effect of channel estimation error and the pilot contamination are combined, we see from (6.12) that the SNIR using this method is affected by both intracell and intercell interferences, and hence the overall achievable sum-rate is degraded. In particular, the individual achievable rates of the cell-edge UTs are degraded the most, due to their larger cross-gains as compared

[3]We denote by $\gamma^{\text{dl-IA-ZF}}$, $\gamma^{\text{dl-IA-ZF-CSI}}$ and $\gamma^{\text{dl-IA-ZF-}q}$ the SINR with IA-ZF, IA-ZF-CSI, IA-ZF-q schemes, respectively. Similar notations are used for the precoding vector $\boldsymbol{w}$.

to the other UTs.

6.4 Intercell-interference-aware Precoding with Rank-q Channel Approximation

Single-cell precoding assumes that the BS in each cell has an estimate of its local CSI only. If it has an estimate of the global CSI, i.e., the channel information not only from the users in its cell but also from the users in other cells, then an intercell-interference-aware ZF (IA-ZF) precoding method can be used to improve the system performance. To this end, we propose in the next section a IA-ZF precoding method that aims at mitigating the intercell and intracell interference, with an assumption that we have an estimate of $\boldsymbol{H}_j$ at each BS. We then elaborate on the advantages and disadvantages of the proposed method with this assumption, and propose a way to overcome the challenges facing implementing it.

6.4.1 Intercell-interference-aware ZF Precoding

IA-ZF precoding at BS j aims at suppressing the interference to a user not only from its BS but also from BSs in other cells. The precoding matrix at each BS j is designed to satisfy

$$\begin{cases} \hat{\boldsymbol{H}}_{jj}^T \boldsymbol{W}_j^{\text{IA-ZF}} = \boldsymbol{I}_K, \ j = 1, 2, ..., L \\ \hat{\boldsymbol{H}}_{jl}^T \boldsymbol{W}_j^{\text{IA-ZF}} = \boldsymbol{0}_K, \ l \neq j, \end{cases}$$

where $\hat{\boldsymbol{H}}_{jl}^T$ is an estimate of the $M \times K$ channel matrix from UTs in cell l to BS j. In a collective form, we have

$$\underbrace{\begin{bmatrix} \hat{\boldsymbol{H}}_{j1}^T \\ \vdots \\ \hat{\boldsymbol{H}}_{jj}^T \\ \vdots \\ \hat{\boldsymbol{H}}_{jK}^T \end{bmatrix}}_{LK \times M} \underbrace{\begin{bmatrix} \boldsymbol{w}_{j1}^{\text{IA-ZF}} & \boldsymbol{w}_{j2}^{\text{IA-ZF}} & \dots & \boldsymbol{w}_{jK}^{\text{IA-ZF}} \end{bmatrix}}_{M \times K} = \begin{bmatrix} \boldsymbol{0}_K \\ \vdots \\ \boldsymbol{I}_K \\ \vdots \\ \boldsymbol{0}_K \end{bmatrix}; \tag{6.13}$$

In order for (6.13) with LK^2 equations and MK unknowns to have a solution, we must have $MK > LK^2$ or $M > LK$, which is usually the case in massive MU-MIMO systems.

For each UT k in cell j, the precoding vector $\boldsymbol{w}_{jk}$ satisfies

$$\begin{cases} \hat{\boldsymbol{h}}_{jjk}^T \boldsymbol{w}_{jk} = 1 \\ \tilde{\boldsymbol{H}}_{jjk}^T \boldsymbol{w}_{jk} = \boldsymbol{0} \\ \hat{\boldsymbol{H}}_{jl}^T \boldsymbol{w}_{jk} = \boldsymbol{0}, \ l \neq j. \end{cases} \tag{6.14}$$

where $\tilde{\boldsymbol{H}}_{jjk} = \begin{bmatrix} \hat{\boldsymbol{h}}_{jj1} & \dots \hat{\boldsymbol{h}}_{jj(k-1)} & \hat{\boldsymbol{h}}_{jj(k+1)} & \dots & \hat{\boldsymbol{h}}_{jjK} \end{bmatrix} \in \mathbb{C}^{M \times (K-1)}$. In (6.14), the first condition makes sure that the SNR is the same at each user, the second condition guarantees zero intracell interference, and the third constraint guarantees zero intercell interference. Consequently, (6.14) can be rewritten as

$$\hat{\boldsymbol{H}}_j^T \boldsymbol{w}_{jk} = \boldsymbol{b}_{jk}, \tag{6.15}$$

where $\boldsymbol{b}_{jk} = [\underbrace{0, ...0}_{\text{cell 1}}, ..., \underbrace{0...1...0}_{\text{cell j}}, ..., \underbrace{0, ...0}_{\text{cell L}}]^T$.

Assume that $\hat{\boldsymbol{H}}_j$ has the following singular value decomposition (SVD).

$$\begin{aligned}\hat{\boldsymbol{H}}_j &= \hat{\boldsymbol{U}}_j \hat{\boldsymbol{\Sigma}}_j \hat{\boldsymbol{V}}_j^H \\ &= \begin{bmatrix}\hat{\boldsymbol{U}}_j^q & \hat{\boldsymbol{U}}_j^0\end{bmatrix} \begin{bmatrix}\hat{\boldsymbol{\Sigma}}_j^q & \mathbf{0} \\ \mathbf{0} & \hat{\boldsymbol{\Sigma}}_j^0\end{bmatrix} \begin{bmatrix}\hat{\boldsymbol{V}}_j^q & \hat{\boldsymbol{V}}_j^0\end{bmatrix}^H,\end{aligned}$$

where $\hat{\boldsymbol{U}}_j$ and $\hat{\boldsymbol{V}}_j$ are $M \times Q_j$ and $LK \times Q_j$ unitary matrices, respectively. $\boldsymbol{\Sigma}_j = \text{diag}\{\sigma_{j1}, \sigma_{j2}, ..., \sigma_{jQ_j}\} \in \mathbb{C}^{Q_j \times Q_j}$ is the $Q_j \times Q_j$ diagonal matrix containing Q_j ($Q_j \leq \min\{LK, M\}$) non-zero singular values of $\boldsymbol{H}_j$: $\sigma_{j1} \geq \sigma_{j2} \geq ...\sigma_{jQ_j} > 0$. The "economic" SVD solution of (6.15) is given by

$$\boldsymbol{w}_{jk}^{\text{IA-ZF}} = \hat{\boldsymbol{U}}_j (\hat{\boldsymbol{\Sigma}}_j)^+ (\hat{\boldsymbol{V}}_j)^H \boldsymbol{b}_{jk}, \tag{6.16}$$

where $(\hat{\boldsymbol{\Sigma}}_j)^+$ is the diagonal matrix, $(\hat{\boldsymbol{\Sigma}}_j)_{ii}^+ = \frac{1}{\sigma_{ji}}$ for $1 \leq i \leq Q_j$.

If we assume perfect global CSI knowledge at each BS j, since there is no interference in this case, the SNR at UT k in cell j is

$$\gamma_{jk}^{\text{dl-IA-ZF-CSI}} = \rho_{\text{dl}} \lambda_j, \tag{6.17}$$

which is significantly greater than the SNIR in (6.12) when using the intercell-interference-ignorant precoding method.

6.4.2 Best Rank-q Global Channel Approximation

As analyzed above, to perform IA-ZF, we need the global channel estimate $\hat{\boldsymbol{H}}_j$ of $\boldsymbol{H}_j$. However, obtaining a good estimate of $\boldsymbol{H}_j$ is almost impossible due to the large dimensions of $\boldsymbol{H}_j$ and the limited time dedicated for the training phase. A more feasible assumption is that we can only obtain a rank-q approximation of $\boldsymbol{H}_j$ (we present CS-based methods to obtain this estimate later). Assume that by some low-rank matrix approximation method,

we obtain the best rank-q approximation of $\boldsymbol{H}_j$ (in terms of 2-norm error), denoted by $\boldsymbol{H}_j^q$, $q < Q_j$ [90]. This means that $\boldsymbol{H}_j^q$ is the solution to the following optimization problem

$$\begin{aligned} \underset{\boldsymbol{X}}{\text{minimize}} \quad & \|\mathcal{A}(\boldsymbol{H}_j) - \boldsymbol{z}\|_2^2 \\ \text{subject to} \quad & \text{rank}(\boldsymbol{X}) \leq q, \end{aligned} \tag{6.18}$$

where $\mathcal{A} : \mathbb{C}^{M \times LK} \to \mathbb{C}^{M\mathcal{T}}$ is some linear measurement operator, and $\boldsymbol{z} \in \mathbb{C}^{M\mathcal{T}}$ is the measured data. Expressing both sides of (6.5) in vector form and applying the fact that $\text{vec}(\boldsymbol{ABC}) = (\boldsymbol{C}^T \otimes \boldsymbol{A})\text{vec}(\boldsymbol{B})$, $\otimes$ denoting Kronecker product, we have

$$\text{vec}(\boldsymbol{Y}_j) = \boldsymbol{\Psi}\text{vec}(\boldsymbol{H}_j) + \text{vec}(\boldsymbol{N}_j),$$

where $\boldsymbol{\Psi} = \boldsymbol{\Theta}^T \otimes \boldsymbol{I}_M$. Then we have $\mathcal{A}(\cdot) = \boldsymbol{\Psi}\text{vec}(\cdot)$, and $\boldsymbol{z} = \text{vec}(\boldsymbol{Y}_j)$. It is proved that the solution of (6.18) is $\boldsymbol{H}_j^q = (\boldsymbol{U}_j)_q \text{diag}\{\sigma_{j1}, ..., \sigma_{jq}\}(\boldsymbol{V}_j)_q^H$, where $(\boldsymbol{U}_j)_q$ and $(\boldsymbol{V}_j)_q$ are the matrices formed from the first q columns of $\boldsymbol{U}_j$ and $\boldsymbol{V}_j$, respectively. The approximation error is then given as

$$\|\boldsymbol{H}_j - \boldsymbol{H}_j^q\|_F^2 = \sum_{i=q+1}^{Q_j} \sigma_{ji}^2.$$

If we assume that not all intercell links are as strong as the intracell ones, and the links are highly correlated, this will lead to many singular values of $\boldsymbol{H}_j$ that are small or close to zero. Then the "true" rank of $\boldsymbol{H}_j$ is smaller than Q_j. Since the largest singular values correspond to the most important singular subspaces of $\boldsymbol{H}_j$, nulling the other smaller singular values will make the channel estimation task easier, while not sacrificing the overall system performance by much. If the "true" rank of $\boldsymbol{H}_j$ is q, then the above errors should be small as all the eigenvalues σ_{ji} are small for $i = q+1, ..., Q_j$; and the estimate obtained should be good enough to perform ZF-IA precoding. Assuming that $\boldsymbol{H}_j^q$ has SVD $\boldsymbol{H}_j^q = \boldsymbol{U}_j^q \boldsymbol{\Sigma}_j^q (\boldsymbol{V}_j^q)^H$, then the corresponding precoding vector using IA-ZF

is computed as

$$\boldsymbol{w}_{jk}^{\text{IA-ZF-q}} = \boldsymbol{U}_j^q (\boldsymbol{\Sigma}_j^q)^+ (\boldsymbol{V}_j^q)^H \boldsymbol{b}_{jk}.$$

6.5 Achievable Rate Performance Analysis

In this section, we present the performance analysis of the capacity lower bound of the proposed IA-ZF precoding method, while assuming each BS j has the exact rank-q approximation of the global channel $\boldsymbol{H}_j$. This can be done by firstly analyzing the SINR of each user k in cell j and then applying the relations (6.9) and (6.11).

Looking at the multicell MU-MIMO as a one "big" MIMO channel, the $LK \times 1$ vector of the signals received by all LK users in all L cells, denoted by $\boldsymbol{y}^{\text{dl}}$, is given by

$$\begin{aligned}\boldsymbol{y}^{\text{dl}} &= \sqrt{\rho_{\text{dl}}\lambda_j}\boldsymbol{H}_j^T \boldsymbol{W}_j \boldsymbol{x}_j^{\text{dl}} + \sqrt{\rho_{\text{dl}}} \sum_{l \neq j} \sqrt{\lambda_l} \boldsymbol{H}_l^T \boldsymbol{W}_l \boldsymbol{x}_l^{\text{dl}} + \boldsymbol{n}^{\text{dl}} \\ &= \sqrt{\rho_{\text{dl}}\lambda_j}\boldsymbol{H}_j^T (\hat{\boldsymbol{H}}_j^T)^\dagger \sum_{k=1}^{K} \boldsymbol{b}_{jk} x_{jk}^{\text{dl}} + \sqrt{\rho_{\text{dl}}} \sum_{l \neq j} \sqrt{\lambda_l} \boldsymbol{H}_l^T (\hat{\boldsymbol{H}}_l^T)^\dagger \sum_{k=1}^{K} \boldsymbol{b}_{lk} x_{lk}^{\text{dl}} + \boldsymbol{n}^{\text{dl}}, \end{aligned} \tag{6.19}$$

where $\boldsymbol{n}^{\text{dl}} = \begin{bmatrix} n_1^{\text{dl}} & n_2^{\text{dl}} & \dots & n_{LK}^{\text{dl}} \end{bmatrix}^T$, and $\tilde{\boldsymbol{H}}_j^T = \boldsymbol{H}_j^T - \hat{\boldsymbol{H}}_j^T$ is the channel estimation error for the case of the exact rank-q approximation. Taking the jk-th element of $\boldsymbol{y}^{\text{dl}}$ in (6.19), the received signal of UT k in cell j is computed as

$$\begin{aligned} y_{jk}^{\text{dl}} &= \sqrt{\rho_{\text{dl}}\lambda_j} \left[\overline{\boldsymbol{H}}_j\right]_{((j-1)K+k,(j-1)K+k)} x_{jk}^{\text{dl}} + \sqrt{\rho_{\text{dl}}\lambda_j} \sum_{n \neq k} \left[\overline{\boldsymbol{H}}_j\right]_{((j-1)K+k,(j-1)K+n)} x_{jn}^{\text{dl}} \\ &\quad + \sqrt{\rho_{\text{dl}}} \sum_{l \neq j} \sqrt{\lambda_l} \sum_{n=1}^{K} \left[\overline{\boldsymbol{H}}_l\right]_{((j-1)K+n,(j-1)K+n)} x_{ln}^{\text{dl}} + n_{jk}^{\text{dl}}, \end{aligned} \tag{6.20}$$

where $\overline{\boldsymbol{H}}_j \triangleq \boldsymbol{H}_j^T (\hat{\boldsymbol{H}}_j^T)^\dagger$. Using the same argument as the one in [62], the SNIR for user k in cell j using IA-ZF is given by

$$\gamma_{jk}^{\text{dl-IA-ZF}} = \frac{\text{term 1}}{\rho_{\text{dl}}^{-1} + \text{term 2} + \text{term 3}}, \tag{6.21}$$

where

$$\text{term } 1 = \lambda_j \left| \mathbb{E}\left\{ \left[\overline{\boldsymbol{H}}_j\right]_{((j-1)K+k,(j-1)K+k)} \right\} \right|^2,$$

$$\text{term } 2 = \lambda_j \text{var}\left\{ \left[\overline{\boldsymbol{H}}_j\right]_{((j-1)K+k,(j-1)K+k)} \right\},$$

$$\text{term } 3 = \sum_{(l,k)\neq(j,n)} \lambda_l \mathbb{E}\left\{ \left| \left[\overline{\boldsymbol{H}}_l\right]_{((j-1)K+k,(j-1)K+n)} \right|^2 \right\}.$$

From (6.21) we can see that if the global channel $\boldsymbol{H}_j$ is full column-rank (i.e. $P > LK$ and $\boldsymbol{H}_j$ is invertible), and with perfect global CSI available as the BS j, then $\overline{\boldsymbol{H}}_j = \boldsymbol{I}_{LK}$. Consequently, we can completely null out both the intracell and intercell interference. When $K < P < LK$, since the global channel is rank-deficient and is no longer invertible, the intracell and intercell interference is not completely nulled out. In the following, we present a capacity lower bound for the case in which the exact rank-q approximation of the global channel is available at each BS j.

For exact rank-q ($q < Q$) channel approximation $\hat{\boldsymbol{H}}_j^T = \boldsymbol{H}_j^q$, we have

$$\begin{aligned}
\overline{\boldsymbol{H}}_j &= \boldsymbol{H}_j^T (\boldsymbol{H}_j^q)^\dagger \\
&= \left[\boldsymbol{V}_j^q \ \boldsymbol{V}_j^{Q-q}\right]^* \begin{bmatrix} \hat{\boldsymbol{\Sigma}}_j^q & \boldsymbol{0} \\ \boldsymbol{0} & \hat{\boldsymbol{\Sigma}}_j^{Q-q} \end{bmatrix} \left[\boldsymbol{U}_j^q \ \boldsymbol{U}_j^{Q-q}\right]^T \times \left(\boldsymbol{U}_j^q\right)^* \left(\Sigma_j^q\right)^\dagger \left(\boldsymbol{V}_j^q\right)^T \\
&= \left(\boldsymbol{V}_j^q\right)^* \left(\boldsymbol{V}_j^q\right)^T. \qquad (6.18)
\end{aligned}$$

Therefore,

$$\left[\overline{\boldsymbol{H}}_j\right]_{((j-1)K+k,(j-1)K+k)} = \left\| \underline{\boldsymbol{V}_j^q}_{((j-1)K+k,:)} \right\|_2^2. \qquad (6.19)$$

$$\left[\overline{\boldsymbol{H}}_l\right]_{((j-1)K+k,(j-1)K+n)} = \underline{(\boldsymbol{V}_l^q)^*}_{((j-1)K+k,:)} \underline{(\boldsymbol{V}_l^q)^T}_{((j-1)K+n,:)}. \qquad (6.20)$$

From (6.21) to (20), the SNIR of UT k in cell j for the case of exact rank-q channel

approximation is computed as

$$\gamma_{jk}^{\text{dl-IA-ZF-q}} = \frac{\text{term 4}}{\rho_{\text{dl}}^{-1} + \text{term 5} + \text{term 6}}, \tag{6.21}$$

where

$$\text{term 4} = \lambda_j \left| \mathbb{E}\left\{ \left\| \underline{\boldsymbol{V}_j^q}_{((j-1)K+k,:)} \right\|_2^2 \right\} \right|^2,$$

$$\text{term 5} = \lambda_j \text{var}\left\{ \left\| \underline{\boldsymbol{V}_j^q}_{((j-1)K+k,:)} \right\|_2^2 \right\},$$

$$\text{term 6} = \sum_{(l,k)\neq(j,n)} \lambda_l \mathbb{E}\left\{ \left| \underline{(\boldsymbol{V}_l^q)^*}_{((j-1)K+k,:)} \underline{(\boldsymbol{V}_l^q)^T}_{((j-1)K+n,:)} \right|^2 \right\}.$$

As we can see from (6.21), the SNIR (and hence the capacity lower bound) for the case of exact rank-q channel approximation depends on how much we truncate in the SVD of the global channel at each BS. If the channel is low-rank, or if we can accurately estimate the global channel $\boldsymbol{H}_j$ at each BS j with a high enough q, then both the intracell interference and intercell interference are significantly mitigated. Obviously this method allows us to treat the multi-cell scenario as a "big" single-cell one where each BS j has an estimate of the global channel $\boldsymbol{H}_j$, then with the IA-ZF precoding method, there is almost no difference in the achievable rate performance between the cell-edge users and the other ones in a cell. We remark here that the above analysis is based on the idealistic assumption that we can have an exact rank-q channel approximation of the global channel at each BS and the channel itself has only a small number of dominant singular subspace. We use this result as a benchmark for proposed methods. More practical and useful numerical results with actual rank-q channel approximation based on CS-based low-rank matrix approximation are presented in the next section.

6.6 CS-based Rank-q Channel Approximation

6.6.1 SDP-based Method

The problem in (6.18) is NP-hard, which is due to the non-convex nature of the rank constraint [39]. Some relaxation versions to obtain a convex problem in noiseless settings have been proposed in [39] and solved via semi-definite programming (SDP). SDP has also been applied and proved to work with the low-rank MIMO channel estimation problem (with the presence of additive Gaussian noise) [90]. Below, we summarize how CS can invoke SDP for solving the low-rank channel estimation problem. To this end, we express the nuclear norm regularization for our channel estimation problem as

$$\underset{\boldsymbol{H}_j}{\text{minimize}} \quad \frac{1}{2}\left\|\text{vec}(\boldsymbol{Y}_j) - \boldsymbol{\Psi}\text{vec}(\boldsymbol{H}_j)\right\|_2^2 + \gamma\|\boldsymbol{H}_j\|_*, \tag{6.22}$$

which can be represented as a quadratic SDP as

$$\begin{aligned} \underset{\boldsymbol{z}}{\text{minimize}} \quad & \frac{1}{2}\boldsymbol{z}^H\boldsymbol{z} - \Re\left\{[\text{vec}(\boldsymbol{Y})]^H\boldsymbol{z}\right\} \\ \text{subject to} \quad & \begin{bmatrix} \gamma\boldsymbol{I}_M & \text{vec}_{M,K}^{-1}\left(\boldsymbol{\Psi}^H\boldsymbol{z}\right) \\ \left[\text{vec}_{M,K}^{-1}\left(\boldsymbol{\Psi}^H\boldsymbol{z}\right)\right]^H & \gamma\boldsymbol{I}_K \end{bmatrix} \succeq 0. \end{aligned} \tag{6.23}$$

Let $\boldsymbol{z}^*$ be the solution to (6.23), then the result of (6.22), which is the estimate of channel matrix using our CS approach, is

$$\hat{\boldsymbol{H}}_{\text{CS}} = \text{vec}_{M,K}^{-1}\left\{\boldsymbol{\Psi}^\dagger\left(\text{vec}(\boldsymbol{Y}) - \boldsymbol{z}^*\right)\right\}.$$

It has been shown in [90] that, for the discrete Bernoulli pilot sequence, if we choose in (6.22) the regularization parameter $\gamma = \sqrt{2(M+LK)\mathcal{T}\rho_{\text{tr}}}$, then the CS-based channel

estimator has an error that is upper bounded in squared Frobenius norm as

$$\|\boldsymbol{H}_j - \hat{\boldsymbol{H}}_j\|_F^2 \leq c\frac{(M+LK)q}{\mathcal{T}\rho_{\text{tr}}} + c' \sum_{i=q+1}^{Q_j} \sigma_{ji}^2,$$

with a probability of at least $1-c_1\exp(-c_2(M^2+(LK)^2)^{1/2})$ for some constants $c, c'c_0, c_1, c_2 > 0$.

This result with the proof is similar to the one in [90], but the difference here is that we add another term in the left-hand side of (6.24), which accounts for the SVD truncation error. As M and LK grow large, with an overwhelming probability, this error upper bound decreases at a rate within a constant of $(M+LK)q/(\mathcal{T}K\rho_{\text{tr}})$, which is faster than the lower bound of the LS's error rate, $MLK/(\mathcal{T}\rho_{\text{tr}})$. This means that the proposed CS method helps to reduce the pilot power or length used by each UT, which is important since the UTs are usually required to operate in a low-power regime and the coherence time needs to be short.

The above SDP algorithm provides good results with performance guarantee but has high complexity [39], [90], as the dual problem has ML variables and one $(M+LK)\times(M+LK)$ semidefinite constraint. Particularly, for this specific SDP problem, the theoretical analysis estimates that the complexity is $\mathcal{O}((\#\text{variables})^2 \times (\text{size of SDP constraint})^{2.5})$, which is $\mathcal{O}\left((ML)^2(M+LK)^{2.5}\right)$ [41,91]. If we use some general-purpose SDP solver such as SeDuMi [92,93], the complexity could be higher [94]. Therefore, the modern SDP solver can only accommodate problems with matrix variables having each size up to a hundred, and this SDP approach suits for systems with number of BS antennas and number of UTs lower than a 100.

6.6.2 Iterative Hard Thresholding based Method

As mentioned above, the SDP method is still computationally inefficient and can not be used for the very-large MIMO channel, especially when the dimensions grow larger than

a hundred. To overcome this problem, some greedy methods have been recently developed as solutions with modest computational complexity, including compressive sampling matching pursuit (CoSaMP), singular value projection (SVP) or IHT [95], and Matrix Factorization [96]. Some previous works have shown that the IHT provides performance bound similar to that of SDP with overwhelming probability when the matrix dimensions are large [95]. We describe below the IHT algorithm after being adapted to our channel estimation problem.

IHT-based Low-rank Channel Estimation for $\boldsymbol{H}_j$

1: **procedure** IHT$(M, L, K, q, \mu_0, \boldsymbol{\Theta}, \boldsymbol{Y}_j)$
2: **Initialization:** $\hat{\boldsymbol{H}}_j^q = \boldsymbol{0}, \boldsymbol{\Psi} = \boldsymbol{\Theta}^T \otimes \boldsymbol{I}_M, i = 0$
3: **while** Stopping criterion does not satisfy **do**
4: $\hat{\boldsymbol{H}}_j^q \leftarrow \hat{\boldsymbol{H}}_j^q + \mu_0 \text{vec}_{M,LK}^{-1}\left(\boldsymbol{\Psi}^H \text{vec}(\boldsymbol{Y}_j - \hat{\boldsymbol{H}}_j^q \boldsymbol{\Theta})\right)$
5: $[\hat{\boldsymbol{U}}_j^q, \hat{\boldsymbol{S}}_j^q, \hat{\boldsymbol{V}}_j^q] = \text{svds}(\hat{\boldsymbol{H}}_j^q, q)$
6: $\hat{\boldsymbol{H}}_j^q \leftarrow \hat{\boldsymbol{U}}_j^q \hat{\boldsymbol{S}}_j^q (\hat{\boldsymbol{V}}_j^q)^H$
7: $i \leftarrow i + 1$
8: **end while**
9: **return** $\hat{\boldsymbol{H}}_j^q$
10: **end procedure**

In line 1, q is the desired rank of the estimated global channel $\hat{\boldsymbol{H}}_j$, and μ_0 is the step size (for instance, $\mu_0 = 0.5$). In line 4, we apply the conjugate of the operator $\mathcal{A}$, denoted by $\mathcal{A}^* : \mathbb{C}^{M\mathcal{T}\times 1} \rightarrow \mathbb{C}^{M\times LK}$, $\mathcal{A}^*(\boldsymbol{z}) = \text{vec}_{M,LK}^{-1}(\boldsymbol{\Psi}^H \boldsymbol{z})$, $\text{vec}_{M,LK}^{-1}(\cdot)$ converts a vector into a $M \times LK$ matrix. In line 6, the $svds(X, q)$ function performs the hard thresholding operator that computes the top q singular values of X along with the right and left singular vectors. The stopping criterion for the IHT-based method can be that when the preset maximum number of iterations is achieved, or when the estimation error stops improving.

The IHT method described above facilitates fast computation (low complexity) as at each iteration, only a rank-q SVD computation for a $M \times LK$ matrix is required, which has a complexity of $\mathcal{O}(Mq^2)$ (at each iteration) [97]. The matrix-vector multiplication in line 4 has a complexity of $\mathcal{O}\left(2(MLK)(M\mathcal{T})\right)$. The total complexity of this IHT algorithm is

$\mathcal{O}\left(Mq^2 + (MLK)(M\mathcal{T})\right)$, which is much lower than that of the SDP algorithm described above.

Assuming that the resulting $\hat{\boldsymbol{H}}_j^q$ has the SVD $\hat{\boldsymbol{H}}_j^q = \hat{\boldsymbol{U}}_j^q \hat{\boldsymbol{\Sigma}}_j^q (\hat{\boldsymbol{V}}_j^q)^H$, then the corresponding precoding vector using the IA-ZF method is efficiently computed as

$$\hat{\boldsymbol{w}}_{jk}^{\text{IA-ZF-q}} = \hat{\boldsymbol{U}}_j^q (\hat{\boldsymbol{\Sigma}}_j^q)^+ (\hat{\boldsymbol{V}}_j^q)^H \boldsymbol{b}_{jk}.$$

6.6.3 Matrix Factorization based Method

The performance of the IHT-based method depends on the step size μ, which needs to be chosen carefully [32]. In this subsection, we present an alternative rank-q approximation method based on linear matrix factorization [96] that does not require any additional parameters. Assuming that every $M \times LK$ channel matrix $\boldsymbol{H}_j$ can be factorized as (a similar approach is used for estimating other $\boldsymbol{H}_j$, $l \neq j$)

$$\boldsymbol{H}_j = \boldsymbol{H}_a \boldsymbol{H}_b, \tag{6.24}$$

where $\boldsymbol{H}_{ja} \in \mathbb{C}^{M \times q}$, $\boldsymbol{H}_{jb} \in \mathbb{C}^{q \times LK}$. Our rank-$q$ channel approximation problem is to find $\boldsymbol{H}_a$ and $\boldsymbol{H}_b$ that minimize the 2-norm of the estimation error. That is,

$$\underset{\boldsymbol{H}_{ja} \in \mathbb{C}^{M \times q}, \boldsymbol{H}_{jb} \in \mathbb{C}^{q \times LK}}{\text{minimize}} \quad \|\mathcal{A}(\boldsymbol{H}_a \boldsymbol{H}_b) - \text{vec}(\boldsymbol{Y}_j)\|_2^2. \tag{6.25}$$

From the linear channel measurement $\mathcal{A}(\boldsymbol{H}_j) = (\boldsymbol{\Theta}^T \otimes \boldsymbol{I}_M)\text{vec}(\boldsymbol{H}_j)$, we have

$$\begin{aligned}
\mathcal{A}(\boldsymbol{H}_{ja}\boldsymbol{H}_{jb}) &= (\boldsymbol{\Theta}^T \otimes \boldsymbol{I}_M)\text{vec}(\boldsymbol{H}_{ja}\boldsymbol{H}_{jb}) \\
&= (\boldsymbol{\Theta}^T \otimes \boldsymbol{H}_{ja})\text{vec}(\boldsymbol{H}_{jb}) \\
&= (\boldsymbol{\Theta}^T \boldsymbol{H}_{jb} \otimes \boldsymbol{I}_M)\text{vec}(\boldsymbol{H}_{ja}).
\end{aligned}$$

As a result, we can express the linear operator $\mathcal{A}$ on variable $\boldsymbol{H}_j$ by a linear operator on each variable $\boldsymbol{H}_{ja}$ or $\boldsymbol{H}_{jb}$ as

$$\mathcal{A}(\boldsymbol{H}_{ja}\boldsymbol{H}_{jb}) = \mathcal{A}_{\boldsymbol{H}_{ja}}(\boldsymbol{H}_{jb}) = \mathcal{A}_{\boldsymbol{H}_{jb}}(\boldsymbol{H}_{ja}), \tag{6.26}$$

where

$$\mathcal{A}_{\boldsymbol{H}_{ja}}(\cdot) = (\boldsymbol{\Theta}^T \otimes \boldsymbol{H}_{ja})\text{vec}(\cdot),$$

and

$$\mathcal{A}_{\boldsymbol{H}_{jb}}(\cdot) = (\boldsymbol{\Theta}^T\boldsymbol{H}_{jb} \otimes \boldsymbol{I}_M)\text{vec}(\cdot).$$

The incremental-rank power factorization [96] based low-rank channel estimation method alternatingly optimizes $\boldsymbol{H}_{ja}$ and $\boldsymbol{H}_{jb}$ using (6.25) with one variable at a time while treating the other as a constant. Next, we describe the incremental-rank PF algorithm after being adapted to our channel estimation problem.

IRPF-based Low-rank Channel Estimation for $\boldsymbol{H}_j$

1: **procedure** IRPF$(M, L, K, \boldsymbol{\Theta}, \boldsymbol{Y}_j, i_{\max}, \epsilon)$
2: **Initialization:** $r = 1$
3: **while** Stopping criterion 1 does not satisfy **do**
4: **Initialization:** $\boldsymbol{H}_{ja} = \boldsymbol{H}_{ja}^{(0)} \in \mathbb{C}^{M\times r}$, $\hat{\boldsymbol{H}}_{jb} = \hat{\boldsymbol{H}}_{jb}^{(0)} \in \mathbb{C}^{r\times LK}$, $i = 0$
5: **while** Stopping criterion 2 not satisfy **do**
6: With $\boldsymbol{H}_{jb}^{(i)}$ fixed:

$$\boldsymbol{H}_{ja}^{(i+1)} = \arg\min_{\boldsymbol{H}_{ja}} \|\mathcal{A}_{\boldsymbol{H}_{jb}^{(i)}}(\boldsymbol{H}_{ja}) - \mathrm{vec}(\boldsymbol{Y}_j)\|_2^2$$

7: With $\boldsymbol{H}_{ja}^{(i+1)}$ fixed:

$$\boldsymbol{H}_{jb}^{(i+1)} = \arg\min_{\boldsymbol{H}_{jb}} \|\mathcal{A}_{\boldsymbol{H}_{ja}^{(i+1)}}(\boldsymbol{H}_{jb}) - \mathrm{vec}(\boldsymbol{Y}_j)\|_2^2$$

8: $i \leftarrow i + 1$
9: **end while**
10: $r \leftarrow r + 1$
11: **end while**
12: **return** $\hat{\boldsymbol{H}}_j^q = \boldsymbol{H}_{ja}^{(i+1)}\boldsymbol{H}_{jb}^{(i+1)}$
13: **end procedure**

The stopping criterion 3 in line 2 is either that r reaches the preset desired rank q, or that the relative estimation error $\|\mathcal{A}(\boldsymbol{H}_a\boldsymbol{H}_b) - \mathrm{vec}(\boldsymbol{Y}_j)\|_2^2/\|\mathrm{vec}(\boldsymbol{Y}_j)\|_2^2$ is smaller than a predefined threshold ϵ. The stopping criterion 2 in line 5 is either that i reaches the preset number of iteration $i_{\max}$, or that that the relative estimation error is smaller than ϵ. It is suggested that the algorithm starts with small r ($r = 1$) and then increases r gradually until it converges. At each r, we solve the linear least-squares (LLS) optimization problems in line 6 and 7 using the Conjugate Gradient method. We also need to choose the number of iterations $i_{\max}$ at each r large enough to have an accurate result.

At each iteration, the main computational complexity of the IRPF algorithm is for solving the LLS, and is the order of $\mathcal{O}\left((M\mathcal{T})(Mq)^2 + (M\mathcal{T})(qLK)^2\right)$, which is again much lower than that of SDP algorithm. As compared to IHT, the IRPF generally has a higher complexity, but it has an advantage that no knowledge about the "true" rank of the matrix variable or extra parameter "μ_0" is needed, and the algorithm is guaranteed

to converge [96].

6.6.4 On choosing q

The complexity and estimation error of the above methods depend on the selection of q and the pilot length $\mathcal{T}$. Choosing q too small results in large estimation error, whereas choosing q too large results in very high computational cost. From our system model, we observe that if in the global channel $\boldsymbol{H}_j$, there are only $K + (L-1)K_c$ directions corresponding to the $K + (L-1)K_c$ strongest links that are significant, and the rest are small and can be neglected, then finding the best rank-q ($q = K + (L-1)K_C$) approximation of $\boldsymbol{H}_j$ is good enough to design a precoding method that would null both the intracell interference and intercell interference. Furthermore, since the rank of $\boldsymbol{H}_j < \min\{M, P, LK\}$, than we should choose $q < \min\{P, K + (L-1)K_c\}$.

6.7 Numerical Results

In this section, we compare the achievable rates of our proposed scheme with those of the existing ones numerically. Throughout our experiments, we use the following parameters. The number of cells, $L = 7$; the ratio between the number of BS antennas and the number of UTs (in one cell), $M/K = 10$; and the number of cell-edge UTs, $K_c = \lceil K/5 \rceil$, which linearly scales with K. Furthermore, the steering vector has $D_0/\lambda = 0.3$, AoA $\phi_p = -\pi/2 + (p-1)\pi/P$, $p = 1, 2, ..., P$ as in [63].

In the first experiment, we choose $M = 100$, and the number of paths $P = \lceil M/3 \rceil$. The intercell power gains are $\delta_c^2 = 1/3$, $\delta_d^2 = 1/9$, In Fig. 6.2, we illustrate the robustness of the IA-ZF CS-based rank-q schemes over the traditional ZF schemes based on LS estimation, where we choose $q = \min\{K + (L-1)K_c, P\} = K + (L-1)K_c = 22$. We display the achievable sum-rates versus the SNR for all schemes, with a training length $\mathcal{T} = 40$. It can be seen from Fig. 6.2 that our IA-ZF CS rank-q schemes outperform both ZF-LS and IA-

ZF LS, and the CS IRPF method has a slightly better performance as compared to the CS IHT one (in which we choose $\mu = 1$). We also show the achievable sum-rate for the cases that we assume to obtain an exact rank-q approximation using (6.21) and the perfect CSI of the global channel at each BS, which serve as benchmarks for comparison purposes. We can see that the IA-ZF method with the exact rank-q channel approximation has a better performance even when compared to the case of perfect CSI with single-cell precoding. This is in agreement with our analysis since both intercell and intracell interferences are suppressed when the IA-ZF is used. Finally, since $\mathcal{T} = 40 < LK = 70$, the system is under-determined, and thus the IA-LS fails to estimate the global channel. That explains why in the figure the IA-ZF-LS has a lower sum-rate as compared to ZF-LS (single-channel estimation).

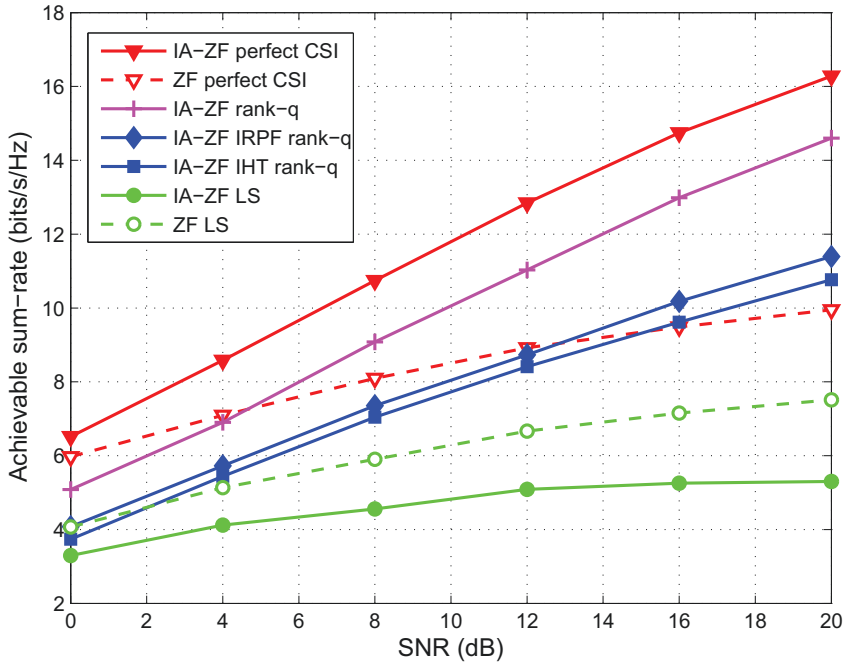

Figure 6.2: Achievable sum-rate versus SNR for different schemes, $M = 100$, $P = \lceil M/3 \rceil$, $\mathcal{T} = 40$, $\delta_c^2 = 1/3$, $\delta_d^2 = 1/9$.

Next, we show in Fig. 6.3 the individual achievable rates of each "normal" UT in cell 1 using different schemes described as above (similar results obtained in other cells). We also observe the robustness of the IA-ZF rank-q schemes as the achievable rate of each

normal UT using these schemes outperforms the conventional ZF LS-based one. There is an interesting observation here is that at low SNR, the ZF scheme slightly outperforms the IA-ZF schemes with perfect or exact rank-q approximation of global CSI at the BS. It is attributed to the fact that, in IA-ZF, we sacrifice some antennas for the intercell interference nulling purpose, leading to a small decrease in the rates of the normal UTs. But in return, as we can see in the next figure, we can significantly suppress the intercell interference and hence increase the achievable rates of the cell-edge UTs.

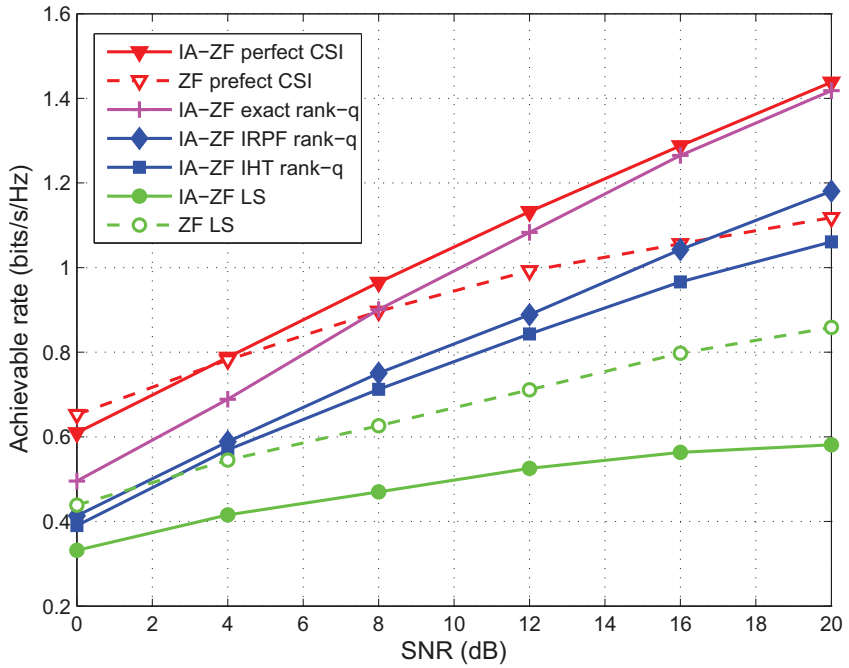

Figure 6.3: Achievable rate of normal UTs versus SNR for different schemes, $M = 100$, $P = \lceil M/3 \rceil$, $\mathcal{T} = 40$, $\delta_c^2 = 1/3$, $\delta_d^2 = 1/9$.

The individual achievable rates of each "cell-edge" UT in cell 1 using different schemes are shown in Fig. 6.4. As expected from the analysis, due to both effects of pilot contamination and intercell interference from the other cells, the achievable rate of each cell-edge UT in a cell is very poor and much lower than that of the normal UT when ZF is used, even when we have perfect local CSI at the BS. By using IA-ZF CS-based rank-q global channel approximation, the achievable rate of each cell-edge UT is greatly improved, almost equal to that of the normal UT.

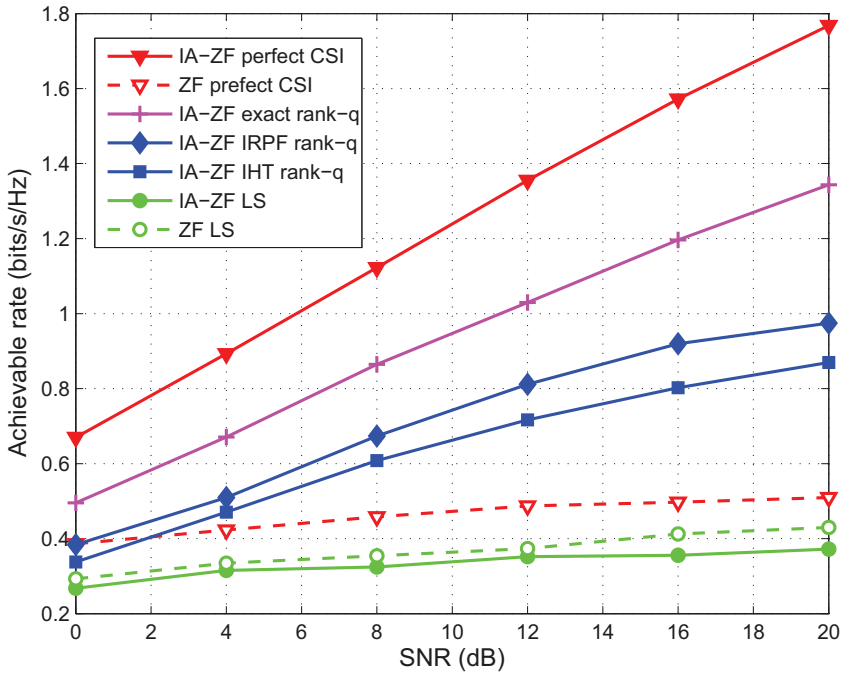

Figure 6.4: Achievable rate of cell-edge UTs versus SNR for different schemes, $M = 100$, $P = \lceil M/3 \rceil$, $\mathcal{T} = 40$, $\delta_c^2 = 1/3$, $\delta_d^2 = 1/9$.

Armed with the above results, we can see that there was a gap between the method using the actual rank-q channel approximation based on IHT and IRPF and the one using the exact rank-q solution, when $\mathcal{T} = 40$. In Fig. 6.5, we display the performance of the described methods with different training lengths $\mathcal{T} \in \{30, 50, 70\}$. (Since the complexity of the IHT is much lower than that of the IRPF with a slightly lower accuracy, we only use IHT from now on). As we increase $\mathcal{T}$ from 30 to 70, the performance gap between the actual CS rank-q and the exact solution becomes smaller, and the gap approaches zero when $\mathcal{T} = 70$. We note here that in all cases, the proposed IA-ZF precoding based on CS rank-q channel approximation outperforms the conventional LS based method, for the same training length.

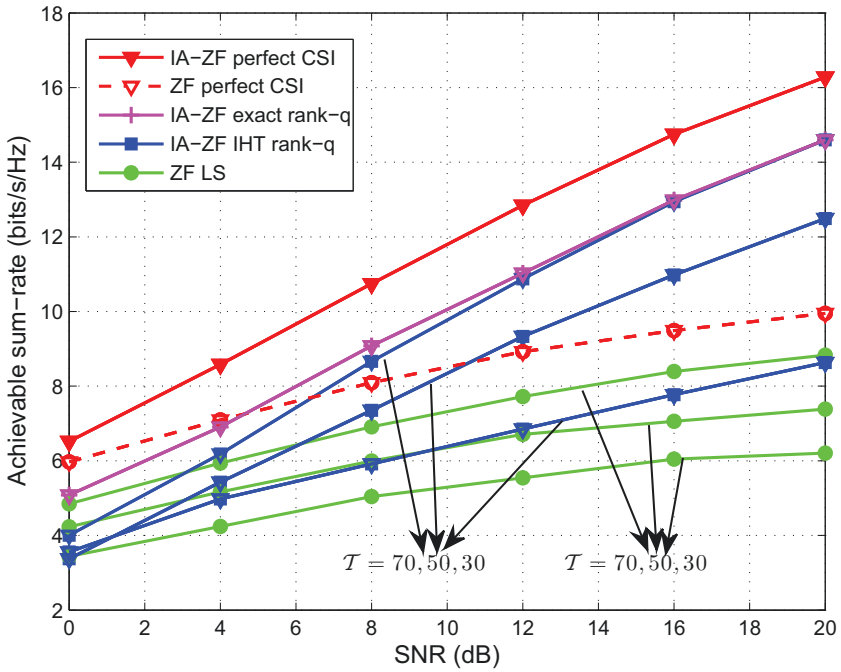

Figure 6.5: Achievable sum-rate versus SNR for different training lengths $\mathcal{T} \in \{30, 50, 70\}$, $M = 100$, $P = \lceil M/3 \rceil$, $\delta_c^2 = 1/3$, $\delta_d^2 = 1/9$.

Next, we change the value of P from $\lceil M/3 \rceil$ to $\lceil M/5 \rceil$, $\delta_c^2 = 1$. The results are plotted in Fig. 6.6. We can see from the figure that since the global channel $\boldsymbol{H}_j$ has rank P, and we choose $q = \min\{K + (L-1)K_c, P\} = P = 20$, the exact rank-$q$ computed using (6.21) has the same performance as the case of perfect CSI. With $\delta_c^2 = 1$, the intercell gains of the cell-edge UTs is as strong as the direct links, resulting in stronger intercell interference as compared to the previous experiments. Therefore, the achievable sum-rate of all schemes decreases. However, the IHT method still outperforms the LS one in this case.

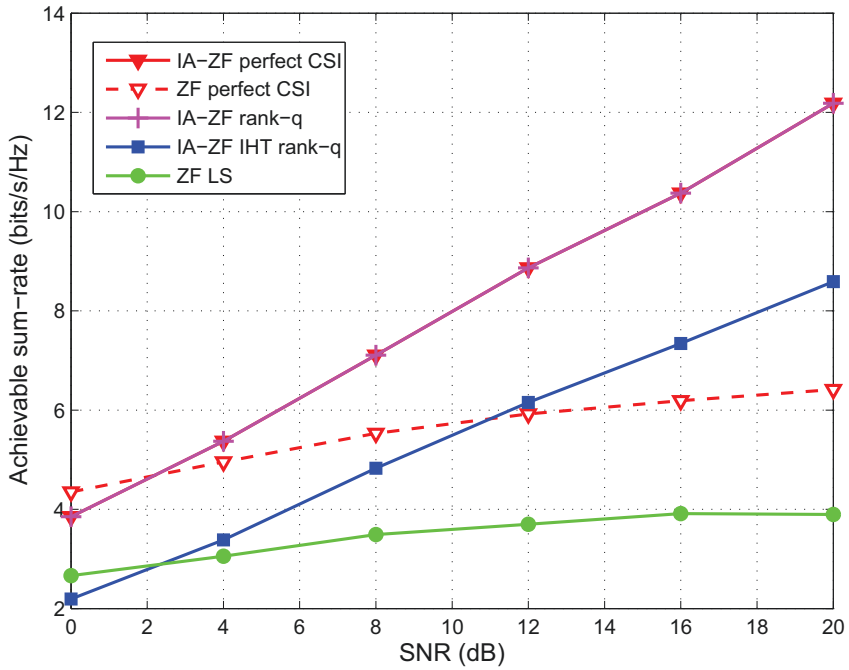

Figure 6.6: Achievable sum-rate versus SNR for different schemes, $M = 100$, $P = \lceil M/5 \rceil$, $\mathcal{T} = 40$, $\delta_c^2 = 1$, $\delta_d^2 = 1/9$.

We now change the value of P to M, $\delta_c^2 = 1$ (rich scattering propagation channel and strong intercell interference), and repeat the same simulations, where $q = \min\{K + (L - 1)K_c, P\} = 22$. The result is shown in Fig. 6.7. Even for this case, the IA-ZF IHT-based rank-q approximation method still outperforms the ZF based on LS. Since P is large, the achievable sum-rate of each scheme in this case is higher as compared to the previous experiments.

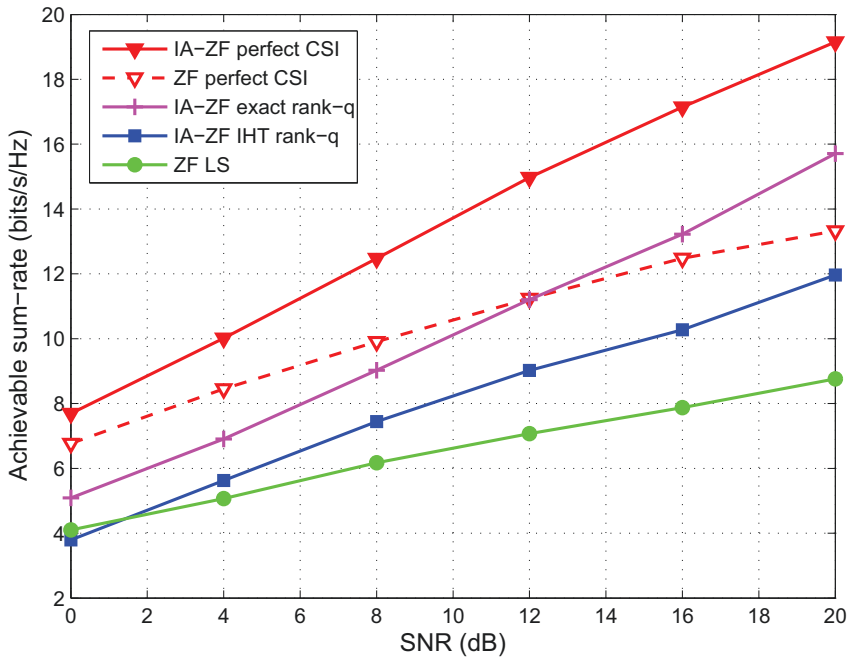

Figure 6.7: Achievable sum-rate versus SNR for different schemes, $M = 100$, $P = M$, $\mathcal{T} = 40$, $\delta_c^2 = 1$, $\delta_d^2 = 1/9$.

Finally, we change the value of M from 100 to 150, and $P = \lceil M/5 \rceil$. In order to see the effect of the intercell interference to the achievable rate of each cell, we repeat the simulations with $\mathcal{T} = 60$, $\delta_d^2 = 0.2$, and vary δ_c^2. It can be shown from Fig. 6.8 that when δ_c^2 is increased (i.e., stronger intercell gains), the achievable sum-rate is decreased. In all cases, the IA-ZF precoding method based on CS-based rank-q channel estimation always provides a better performance as compared to the single-cell ZF precoding method based on the LS channel estimate.

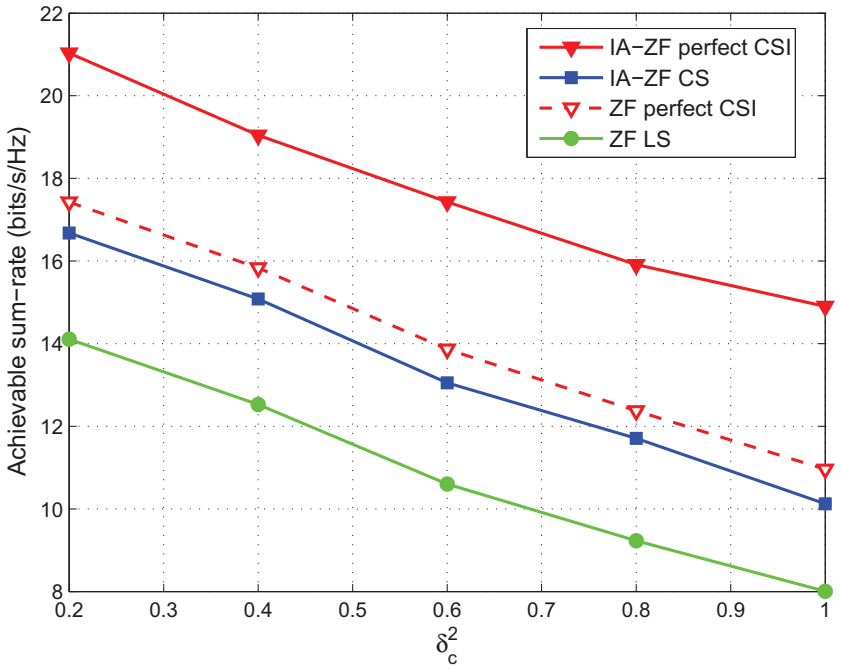

Figure 6.8: Achievable sum-rate versus δ_c^2, $M = 150$, $P = \lceil M/5 \rceil$, $\mathcal{T} = 60$, $\delta_d^2 = 0.2$.

6.8 Concluding Remarks

We have proposed in this chapter a new method based on compressive sensing that aims at rank-q global channel approximations and ZF-based intercell-interference-aware precoding method for multicell massive MIMO systems. The proposed schemes have been shown to be effective in mitigating the effects of the channel training error and the intercell interference, hence improving the achievable rates of the individual users as well as the achievable sum-rate of each cell. In particular, the users that benefit the most from the proposed techniques are the cell-edge users where their achievable rates are comparable to those of the users that do not have strong intercell channel gains with their neighboring BSs. We have also derived a lower bound on the achievable rate with perfect knowledge of the rank-q global channel matrix. Furthermore, we have proposed three CS-based estimation techniques, each with advantages and disadvantages. Through numerical examples, we have shown that the proposed techniques, even with the least

complex estimation algorithm, outperform the conventional scheme based on LS channel estimation and single-cell precoding method, without requiring any knowledge about the statistical distribution or physical parameters of the propagation channel.

Chapter 7

Summary and Future Work

7.1 Summary

CS is a revolutionary theory that has important applications in many areas, including wireless communications. Using CS, signals can be recovered by far fewer samples or measurements much below the Nyquist rate, as long as they are sparse and the measurement is incoherent. In wireless communication problems where the sparsity structure of the signals can be explored, CS helps to reduce significantly the number of transmissions or measurements required bust still can reconstruct them accurately. The impact of CS is even more crucial as the wireless communications often deal with the large-scale problems where many typical signals, channels or events contain sparsity models either implicitly or explicitly.

This thesis has been concerned with the development of new techniques and applications of CS in many complex wireless communication channels and systems including multi-channel multiuser, cooperative relaying, and large MIMO networks. Specifically, we have presented various CS solutions for multiple-channel estimation, iterative estimation and decoding for sparse ISI-TWRC, channel estimation and precoding for large-scale multiuser MIMO systems. We have also provided theoretical results to confirm the ro-

bustness of CS methods, and performance analysis to see the end-to-end performance improvements of the proposed schemes.

In Chapter 3, we have addressed the problem of simultaneous estimation of multiple sparse ISI channels and applied it to the compressive estimation of sparse ISI-TWRC employing analog network coding. Both theoretical and empirical results suggested that the ℓ_1-based CMCE method significantly outperforms the traditional one, which ignores the sparsity feature of the channels. We then apply this concept to iterative channel estimation and data decoding for the sparse ISI-TWRC for both cases of AF and DF relaying protocols in Chapter 4. The proposed iterative schemes have shown significant improvements in terms of end-to-end performances of the systems.

Chapter 5 has extended the theory of CS from sparse channel vector estimation to low-rank channel matrix approximation, and applied it to the problem of channel estimation for massive MU-MIMO channels. A SDP-based method has been proposed, in which the performance guarantee bound of the solution has been provided.

Chapter 6 proposed a communication scheme base on compressive rank-q channel approximation to solve the problems of uplink channel estimation and downlink precoding for multicell massive MIMO. Several reduced-complexity algorithms have been also presented in this chapter to facilitate the implementations of the proposed scheme, and numerous numerical results have confirmed the improvement of it in terms of achievable data rates of users in the interference-limited scenarios.

7.2 Future Work

As far as future work is concerned, we identify a few potential problems, as follows.

1. *Sparse multipath multiple-channel estimation in OFDM-based systems:* Our work only deals with the channel estimation for sparse multipath multiple-channel assuming single-carrier transmission, and for massive MIMO systems, the channel is

assumed to be flat fading. It is natural to consider the same cases in a multi-carrier system, i.e, OFDM-based schemes, and compare the two. We would also consider the problem of channel estimation and precoding for ODFM-based massive MIMO systems over frequency-selective channels.

2. *Deterministic CS dictionaries:* Another issue of random probing for large-scale sparse or low-rank channel estimation not being considered in this thesis is the large memory to store the random pilots at the terminals. Quite recent results addressing the design of the deterministic sensing matrix for sparse approximation [98] could be used to co-design the deterministic or semi-deterministic pilots sent from the terminals. This will save us a lot of memory required otherwise, and particularly useful in the case of large numbers of users in cellular networks, or sensors in wireless sensor networks.

3. *Stochastic CS for communications applications:* The CS-based methods for channel vector estimation and low-rank matrix approximation developed in this thesis assume no knowledge about the statistical distribution of the channel parameters. In many wireless communication scenarios, the statistical distribution of the channel is available at BSs or terminals. By utilizing this information along with the sparsity model of the channels, one can improve the performance of the estimator and detection. Some works have recently considered this problem based on the Bayesian approach for sparse vector [99] or low-rank matrix [100] in machine learning or matrix completion problems. The methods when developed for communications applications where the channels have specific statistical distributions should bring more favorable results.

4. *Reduced-complexity for channel estimation and precoding for massive multiuser MIMO systems:* As the numbers of BS antennas and UTs may continue growing in future massive multiuser MIMO systems, the current estimation and precoding algorithms

may not be simple enough to afford those large dimension problems. Therefore, more lower complexity methods need to be developed to implement massive MIMO systems in reality.

7.3 Publications

1. Sinh L. H. Nguyen and Ali Ghrayeb, "Multicell precoding for downlink massive MIMO based on compressive rank-q channel sensing," *submitted to IEEE Transactions on Communications* (under revision, June 2013).

2. Sinh L. H. Nguyen and Ali Ghrayeb, "Precoding for multicell massive MIMO systems with compressive rank-q channel approximation," in *Proc. IEEE PIMRC'13*, London, September 2013.

3. Sinh L. H. Nguyen and Ali Ghrayeb, "Compressive sensing-based channel estimation for massive multiuser MIMO systems," in *Proc. IEEE WCNC'13*, Shanghai, pp. 3119–3124, April 2013.

4. Sinh L. H. Nguyen, Ali Ghrayeb, and Mazen Hasna, "Iterative compressive estimation and decoding for network-channel-coded two-way relay sparse ISI channels," *IEEE Communications Letters*, vol. 16, no. 12, pp. 1992–1995, December 2012.

5. Sinh L. H. Nguyen, Ali Ghrayeb, Ghaleb Al-Habian, and Mazen Hasna, "Mitigating error propagation in two-way relay channels with network coding," *IEEE Transactions on Wireless Communications*, vol. 9, no. 11, pp. 3380–3390, November 2010.

Appendix A

Vector Norms, Matrix Norms, and Their Dual Norms

A.1 Vector Norms

This appendix presents important vector norms that are frequently used in CS theory: ℓ_0, ℓ_1, and ℓ_∞. In general, the ℓ_p-norm ($p \geq 1$, $p \in \mathbb{R}$) of a vector $x = [x_1, x_2, \cdots, x_n]$, denoted by $\|x\|_p$, is defined as

$$\|\boldsymbol{x}\|_p = \left(\sum_{i=1}^{n} |x_i|^p \right)^{1/p}.$$

Therefore, the $\|x\|_1$, $\|x\|_2$, $\|x\|_\infty$ are formally defined as

$$\begin{aligned} \|\boldsymbol{x}\|_1 &= \sum_{i=1}^{n} |x_i|. \\ \|\boldsymbol{x}\|_2 &= \sqrt{|x_1|^2 + |x_2|^2 + \cdots + |x_n|^2}. \\ \|\boldsymbol{x}\|_\infty &= \max(|x_1|, |x_2|, \cdots, |x_n|). \end{aligned}$$

Definition A.1 (Dual norm of a vector norm [41])**.**

Let $\boldsymbol{u}, \boldsymbol{v} \in \mathbb{R}^n$*. For any given norm* $\|\cdot\|$*, there exists a dual norm, denoted by* $\|\cdot\|_*$*, defined as*

$$\|\boldsymbol{u}\|_* = \sup_{\boldsymbol{v}} \left\{ \langle \boldsymbol{u}, \boldsymbol{v} \rangle = \boldsymbol{u}^T \boldsymbol{v} \middle| \|\boldsymbol{v}\| \leq 1 \right\}.$$

If $\|\cdot\|_p$ is the dual norm of $\|\cdot\|_q$, then ℓ_p is isometrically isomorphic to ℓ_q, i.e., $1/p + 1/q = 1$.

We also have that the dual norm of $\|\cdot\|_1$ is $\|\cdot\|_\infty$. The dual norm of $\|\cdot\|_2$ is itself.

A.2 Matrix norms

Matrix norms are natural generalizations of vector norm, hence inherit many appealing properties from the vector case. For any two matrices $\boldsymbol{X}, \boldsymbol{Y} \in \mathbb{R}^{m \times n}$, the inner product in space $\mathbb{R}^{m \times n}$ is associated with the Frobenius norm, and is define as

$$\begin{aligned} \langle \boldsymbol{X}, \boldsymbol{Y} \rangle &= \mathrm{Tr}(\boldsymbol{X}^T \boldsymbol{Y}) \\ &= \sum_{i=1}^{m} \sum_{j=1}^{n} \boldsymbol{X}_{(i,j)} \boldsymbol{Y}_{(i,j)} \end{aligned}$$

Assume that $\sigma_i(\boldsymbol{X})$ is the i-th largest singular value of matrix $\boldsymbol{X}$,and r is the rank of $\boldsymbol{X}$. The Frobenius norm of $\boldsymbol{X}$ is also equal to the ℓ_2 of the vector of singular values, i.e.

$$\begin{aligned} \|\boldsymbol{X}\|_F &= \sqrt{\mathrm{Tr}(\boldsymbol{X}^T \boldsymbol{X})} \\ &= \sqrt{\sum_{i=1}^{m} \sum_{j=1}^{n} \boldsymbol{X}_{(i,j)}^2} \\ &= \sqrt{\sum_{i=1}^{r} \sum_{j=1}^{n} \sigma_i^2} \end{aligned}$$

The operator norm of matrix $\boldsymbol{X}$ is equal to the largest singular value of it

$$\|\boldsymbol{X}\|_{\text{op}} = \sigma_1(\boldsymbol{X}).$$

The nuclear norm of matrix $\boldsymbol{X}$ is equal to the sum of its singular values (i.e., the ℓ_1-norm of the vector of singular values)

$$\|\boldsymbol{X}\|_* = \sum_{i=1}^{r} \sigma_i(\boldsymbol{X}).$$

Definition A.2 (Dual norm of a matrix norm [39])**.**
Let $\boldsymbol{X}, \boldsymbol{Y} \in \mathbb{R}^{m\times n}$. For any given norm $\|\cdot\|$, there exists a dual norm, denoted by $\|\cdot\|_*$, defined as

$$\|\boldsymbol{X}\|_* = \sup_{\boldsymbol{Y}} \left\{ \langle \boldsymbol{X}, \boldsymbol{Y} \rangle = Tr\left(\boldsymbol{X}^T \boldsymbol{Y}\right) \middle| \|\boldsymbol{Y}\| \leq 1 \right\}.$$

We have a parallel duality structure between vector norm and matrix norm. The operator norm $\|\cdot\|_{\text{op}}$ (i.e., ℓ_∞-norm of the vector of singular values) is the dual norm of the nuclear norm $\|\cdot\|_*$ (i.e., ℓ_1-norm of the vector of the singular values).

Appendix B

Hoeffding's Standard Concentration Inequalities

Theorem B.1 (Hoeffding's Inequality)**.**

Suppose that $X_1, X_2, \cdots, X_n$ are independent real-valued bounded random variables, such that for each i, $a_i \leq X_i \leq b_i$. Let $Y = \sum_i^n X_i$, then the following inequality

$$\mathbb{P}\left\{|Y - \mathbb{E}\{Y\}| \geq t\right) \leq 2\exp\left(-\frac{2t^2}{\sum_i^n R_i^2}\right\}$$

holds for all $t > 0$, where $R_i = b_i - a_i$.

Theorem B.2 (Hoeffding's Inequality for i.d.d. bounded random variables [66])**.**

Suppose that $\{X_i\}_{i=1}^n$ is a sequence of n i.d.d. random variables, such that for each i, $|X_i| \leq a$, with variance $\mathbb{E}\{X_i^2\} = \sigma^2$. Then the following inequality

$$\mathbb{P}\left\{\left|\sum_{i=1}^n X_i^2 - n\sigma^2\right| \geq t\right) \leq 2\exp\left(-\frac{2t^2}{4na^2}\right\}$$

holds for all $t > 0$.

Appendix C

Geršgorin's Disc Theorem

Theorem C.1 (Geršgorin's [67])**.**

Every eigenvalue λ of an $n \times n$ complex-valued matrix $\boldsymbol{A}$ satisfies

$$|\lambda - \boldsymbol{A}_{(i,i)}| \leq \sum_{j \neq i} \boldsymbol{A}_{(i,j)}.$$

Definition C.1 (Geršgorin's Disc)**.**

Suppose $\boldsymbol{A}$ is a $n \times n$ complex-valued matrix whose (i,j)-th element is $\boldsymbol{A}_{(i,j)}$. Let $d_i = \sum_{j \neq i} \boldsymbol{A}_{(i,j)}$. The set

$$D_i = \left\{ z \in \mathbb{C} : |z - \boldsymbol{A}_{(i,i)}| \leq d_i \right\}$$

is called the i-th Geršgorin disc of the matrix $\boldsymbol{A}$. This disc is the interior plus the boundary of a circle, which has a radius d_i and is centered at $\left(\Re\{\boldsymbol{A}_{(i,i)}\}, \Im\{\boldsymbol{A}_{(i,i)}\} \right)$.

Theorem C.2. *The eigenvalues of an $n \times n$ complex-valued matrix $\boldsymbol{A}$ all lie in the union of n Geršgorin discs D_i, $i = 1, 2, \cdots, n$.*

Corollary C.1 (Geršgorin in Respect to Columns)**.**

Every eigenvalue of a matrix $\boldsymbol{A}$ must lie in a Geršgorin disc corresponding to the columns of $\boldsymbol{A}$.

Appendix D

Sub-Gaussian Random Variables

Definition D.1 (Sub-Gaussian random variables)**.**

A real-valued random variable X is said to be Sub-Gaussian if there exists some constant $c > 0$ such that

$$\mathbb{E}\{\exp(tX)\} \leq \exp\left(ct^2/2\right)$$

When this condition is satisfied with a particular value of $c > 0$, we say that X is Sub-Gaussian with parameter c, or $X \sim Sub(c^2)$.

Remark D.1. *If X is zero-mean Gaussian random variable with variance σ^2, then X is Sub-Gaussian with parameter σ.*

Corollary D.1 (Sub-Gaussian zero-mean bounded random variable)**.**

If X is a random variable with $\mathbb{E}\{X\} = 0$, and $|X| \leq B$ (i.e., zero-mean bounded random variable) for some constant B, then X is Sub-Gaussian with parameter B, or $X \sim Sub(B^2)$.

Appendix E

Upper Tail Estimate for I.I.D. Ensembles

Theorem E.1 (Upper tail estimate for i.i.d. ensembles [89])**.**

Suppose that the coefficients $\boldsymbol{X}_{(i,j)}$ *of a* $n \times n$ *matrix* $\boldsymbol{X}$ *are independent, have mean zero, and uniformly bounded in magnitude by 1. Then there exists absolute constants* $C, c > 0$ *such that*

$$\mathbb{P}\{\|\boldsymbol{X}\|_{op} > A\sqrt{n}\} \leq C \exp\left(-cAn\right).$$

for all $A \geq C$*. In particular, we have* $\|\boldsymbol{X}\|_{op} = \mathcal{O}(\sqrt{n})$ *with overwhelming probability.*

Bibliography

[1] E. Candès, J. Romberg, and T. Tao, "Robust uncertainty principles: Exact signal reconstruction from highly incomplete frequency information," *IEEE Trans. Inform. Theory*, vol. 52, no. 2, pp. 489–509, Feb. 2006.

[2] R. G. Baraniuk, "Compressive sensing," *IEEE Signal Process. Mag.*, vol. 24, no. 4, pp. 118–120, Jul. 2007.

[3] D. Takhar, V. Bansal, M. Wakin, M. Duarte, D. Baron, J. Laska, K. Kelly, and R. Baraniuk, "A compressed sensing camera: New theory and an implementation using digital micromirrors," in *Proc. Comput. Imaging IV SPIE Electronic Imaging*, San Jose, CA, USA, Jan. 2006.

[4] J. Bobin, J. L. Starck, and R. Ottensamer, "Compressed sensing in astronomy," *IEEE J. Select. Topics in Signal Process.*, vol. 2, no. 5, pp. 718–726, Oct. 2008.

[5] U. Gamper, P. Boesiger, and S. Kozerke, "Compressed sensing in dynamic MRI," *Magnetic Resonance in Medicine*, vol. 59, no. 2, pp. 365–373, Feb. 2008.

[6] M. F. Duarte, M. A. Davenport, D. Thakhar, J. N. Laska, T. Sun, K. F. Kelly, and R. Baraniuk, "Single pixel imaging via compressive sampling," *IEEE Signal Process. Mag.*, vol. 25, no. 2, pp. 83–91, Mar. 2008.

[7] W. Dai, M. A. Sheikh, O. Milenkovic, and R. G. Baraniuk, "Compressive sensing DNA microarrays," *Eurosip Journal on Bioinformatics and Systems Biology*, 2009.

[8] F. Steinke, M. Seeger, and K. Tsuda, "Experimental design for efficient identification of gene regulatory networks using sparse bayesian models," *BMC systems biology*, vol. 1, no. 1, p. 51.

[9] W. U. Bajwa, J. Haupt, G. Raz, and R. Nowak, "Compressed channel sensing," in *Proc. CISS*, Princeton, NJ, USA, Mar 2008, pp. 5–10.

[10] G. Taubock and F. Hlawatsch, "A compressed sensing technique for OFDM channel estimation in mobile environments: Exploiting channel sparsity for reducing pilots," in *Proc. ICASSP*, Las Vegas, NV, USA, Apr. 2008, pp. 2885–2888.

[11] D. Eiwen, G. Taubock, F. Hlawatsch, H. Rauhut, and N. Czink, "Multichannel-compressive estimation of doubly selective channels in MIMO-OFDM systems: Exploiting and enhancing joint sparsity," in *Proc. ICASSP*, Dallas, TX, USA, Mar. 2010, pp. 3082–3085.

[12] A. Hormati and M. Vetterli, "Compressive sampling of multiple sparse signals having common support using finite rate of innovation principles," *IEEE Trans. Signal Process.*, vol. 8, no. 5, pp. 331–334, May 2011.

[13] J. Meng, H. Li, and Z. Han, "Sparse event detection in wireless sensor networks using compressive sensing," in *Proc. CISS 2009*, Baltimore, MD, USA, 2009, pp. 964–969.

[14] Y. Xie, Y. C. Eldar, and A. Goldsmith, "Reduced-dimension multiuser detection," in *Proc. 46th Annual Allerton Conf. on Commun., Control, and Comp.*, Monticello, IL, USA, Sep. 2010, pp. 584–590.

[15] J. A. Bazerque and G. B. Giannakis, "Distributed spectrum sensing for cognitive radio networks by exploiting sparsity," *IEEE Trans. Signal Process.*, vol. 58, no. 3, pp. 1847–1862, 2010.

[16] H. Li, R. Mao, L. Lai, and R. C. Qiu, "Compressed meter reading for delay-sensitive and secure load report in smart grid," in *Proc. IEEE Int. Conf. Smart Grid Commun.*, 2010, pp. 114–119.

[17] R. Tibshirani, "Regression shrinkage and selection via the lasso," *J. Roy. Statist. Soc. B*, vol. 58, no. 1, pp. 267–288, 1996.

[18] F. Zhang and H. D. Pfister, "On the iterative decoding of high rate ldpc codes with applications in compressed sensing," in *Proc. 46th Annual Allerton Conf. on Commun., Control, and Comp.*, Monticello, IL, USA, Sep. 2008.

[19] W. Bajwa, J. Haupt, A. Sayeed, and R. Nowak, "Compressive wireless sensing," in *Proc. IPSN*, Nashville, Tennessee, USA, Apr. 2006, pp. 134–142.

[20] C. R. Berger, S. Zhou, J. C. Preisig, and P. Willet, "Sparse channel estimation for multicarrier underwater acoustic communication: From subspace methods to compressed sensing," *IEEE Trans. Signal Process.*, vol. 58, no. 3, pp. 1708–1721, Mar. 2010.

[21] M. A. Herman and T. Strohmer, "High-resolution radar via compressed sensing," *IEEE Trans. Signal Process.*, vol. 57, no. 6, pp. 2275–2284, Jun. 2009.

[22] Z. Tian and G. B. Giannakis, "Compressed sensing for wideband cognitive radios," in *Proc. IEEE ICASSP*, 2007, pp. 1357–1360.

[23] I. Jouny, "Compressed sensing for uwb radar target signature reconstruction," in *Proc. IEEE Digital Signal Processing Workshop*, 2009, pp. 714–719.

[24] B. Rankov and A. Wittneben, "Achievable rate regions for the two-way relay channel," in *Proc. IEEE ISIT*, Seatle, WA, USA, Jul. 2006, pp. 1668–1672.

[25] P. Popovski and H. Yomo, "Physical network coding in two-way wireless relay channels," in *Proc. IEEE ICC*, Glasgow, Scotland, Jun. 2007, pp. 707–712.

[26] T. J. Oechtering, I. Bjelakovic, C. Schnurr, and H. Boche, "Broadcast capacity region of two-phase bidirectional relaying," *IEEE Trans. Inform. Theory*, vol. 54, no. 1, pp. 454–458, Jan. 2008.

[27] T. L. Marzetta, "Noncooperative cellular wireless with unlimited numbers of base station antennas," *IEEE Trans. Wireless Commun.*, vol. 9, no. 11, pp. 3590–3600, Nov. 2010.

[28] F. Rusek, D. Persson, B. K. Lau, E. G. Larsson, T. L. Marzetta, O. Edfors, , and F. Tufvesson, "Scaling up MIMO: opportunities and challenges with very large arrays," *IEEE Signal Process. Mag.*, vol. 30, no. 1, pp. 40–60, Jan. 2013.

[29] D. L. Donoho and Y. Tsaig, "Fast solution of ℓ_1-norm minimization problems when the solution may be sparse," *IEEE Trans. Inform. Theory*, vol. 54, no. 11, pp. 4789–4812, Nov. 2006.

[30] M. W. G. Raskutti and B. Yu, "Restricted eigenvalue properties for correlated gaussian designs," *The Journal of Machine Learning Research*, vol. 11, pp. 2241–2259, 2010.

[31] M. Davenport and M. Duarte and Y. Eldar and G. Kutyniok, *Introduction to Compressed Sensing*. Cambridge University Press, 2012.

[32] T. Blumensath and M. Davies, "Iterative hard thresholding for compressive sensing," *Appl. Comput. Harmon. Anal.*, vol. 27, no. 3, pp. 265–274, 2009.

[33] Y. C. Pati, R. Rezaiifar, and P. S. Krishnaprasad, "Orthogonal matching pursuit: Recursive function approximation with applications to wavelet decomposition," in *Proc. 27th Annu. Asilomar Conf. Signals, Systems, and Computers*, Pacific Grove, CA, USA, 1993.

[34] J. A. Tropp, "Just relax: Convex programming methods for identifying sparse signals in noise," *IEEE Trans. Inform. Theory*, vol. 52, no. 3, pp. 1030–1051, Mar. 2006.

[35] Z. Ben-Haim, Y. C. Eldar, and M. Elad, "Coherence-based performance guarantees for estimating a sparse vector under random noise," *IEEE Trans. Signal Process.*, vol. 58, no. 10, pp. 5030–5043, Oct. 2010.

[36] E. V. D. Berg and M. P. Friedlander, "Probing the pareto frontier for basis pursuit solutions," *SIAM Journal on Scientific Computing*, vol. 31, pp. 890–912, 2008.

[37] B. Efron, T. Hastie, I. Johnstone, and R. Tibshirani, "Least angle regression," *Annals of Statistics*, vol. 32, no. 2, pp. 407–499, Apr. 2004.

[38] M. A. T. Figueiredo, R. D. Nowak, and S. J. Wright, "Gradient projection for sparse reconstruction: Application to compressed sensing and other inverse problems," *IEEE Journal of Selected Topics in Signal Processing: Special Issue on Convex Optimization Methods for Signal Processing*, vol. 1, no. 4, pp. 586–597, Dec. 2007.

[39] B. Recht, M. Fazel, and P. Parrilo, "Guaranteed minimum-rank solutions of linear matrix equations via nuclear norm minimization," *SIAM Review*, vol. 52, no. 3, pp. 471–501, Aug. 2010.

[40] B. Negahban and M. J. Wainwright, "Estimation of (near) low-rank matrices with noise and high-dimensional scaling," *The Annals of Statistics*, vol. 39, no. 2, pp. 1069–1097, 2011.

[41] S. Boyd and L. Vandenberghe, *Convex Optimization*. New York, NY, USA: Cambridge University Press, 2004.

[42] H. Rauhut, "Circulant and toeplitz matrices in compressed sensing," in *Proc. SPARS'09: Signal Processing with Adaptive Sparse Structured Representations*, Saint Malo, France, 2009.

[43] C. Douillard and M. Jézéquél, "Iterative correction of inter-symbol interference: Turbo-equalization," *European Trans. Telecomms*, vol. 6, pp. 507–511, Sep./Oct. 1995.

[44] M. Tuchler, A. C. Singer, and R. Koetter, "Minimum mean squared error equalization using a prior information," *IEEE Trans. Signal Process.*, vol. 15, no. 50, pp. 673–683, Mar. 2011.

[45] C. E. Shannon, "Two-way communication channels," in *Proc. 4th Berkeley Symp. Math. Stat. Prob.*, vol. 1, 1961.

[46] S. Katti, I. Maric, A. Goldsmith, D. Katabi, and M. Medard, "Joint relaying and network coding in wireless networks," in *Proc. IEEE ISIT*, Nice, France, Jun. 2007, pp. 1101–1105.

[47] D. Chen and J. N. Laneman, "Modulation and demodulation for cooperative diversity in wireless systems," *IEEE Trans. Wireless Commun.*, vol. 5, pp. 1785–1794, Jul. 2006.

[48] G. Kramer, M. Gastpar, and P. Gupta, "Cooperative strategies and capacity theorems for relay networks," *IEEE Trans. Inform. Theory*, vol. 51, pp. 3037–3063, Sep. 2005.

[49] I. Abou-Faycal and M. Medard, "Optimal uncoded regeneration for binary antipodal signaling," in *Proc. IEEE ICC*, Paris, France, Jun. 2004, pp. 742–746.

[50] L. Lai, K. Liu, and H. E. Gamal, "The three-node wireless network: Achievable rates and cooperation strategies," *IEEE Trans. Inform. Theory*, vol. 52, pp. 805–828, Mar. 2006.

[51] K. S. Gomadam and S. A. Jafar, "Optimal relay functionality for SNR maximization in memoryless relay networks," *IEEE J. Select. Areas in Commun.*, vol. 25, pp. 390–401, Feb. 2007.

[52] M. Elfituri, W. Hamouda, and A. Ghrayeb, "A convolutional-based coded cooperation scheme for relay channels," *IEEE Trans. Veh. Technol.*, vol. 58, no. 2, pp. 655–669, Feb. 2009.

[53] A. Sendonaris, E. Erkip, and B. Aazhang, "User cooperation diversity–part i: System description," *IEEE Trans. Commun.*, vol. 51, no. 11, pp. 1927–1938, Nov. 2003.

[54] A. Sendonaris, E. Erkip, and B. Aazhang, "User cooperation diversity–part ii: Implementation aspects and performance analysis," *IEEE Trans. Commun.*, vol. 51, no. 1, pp. 1939–1948, Nov. 2003.

[55] H. V. Khuong and H. Y. Kong, "LLR-based decode-and-forward protocol for relay networks and closed-form ber expressions," *IEICE Trans. Fundamentals*, vol. E89A, pp. 1832–1841, Jun. 2006.

[56] R. C. Palat, A. Annamalai, and J. H. Reed, "Log-likelihood-ratio based selective decode and forward cooperative communication," in *Proc. IEEE VTC*, Mar. 2008, pp. 615–618.

[57] X. N. Zeng, A. Ghrayeb, and M. Hasna, "Joint optimal threshold-based relaying and ML detection in cooperative networks," *IEEE Commun. Letters*, vol. 16, no. 6, pp. 773–776, Jun. 2012.

[58] X. N. Zeng, A. Ghrayeb, and M. Hasna, "Joint optimal threshold-based relaying and ml detection in network-coded two-way relay channels," *IEEE Trans. Commun.*, vol. 60, no. 9, pp. 2657–2667, Sep. 2012.

[59] S. L. H. Nguyen, A. Ghrayeb, G. Al-Habian, and M. Hasna, "Mitigation error propagation in two-way relay channel with network coding," *IEEE Trans. Wireless Commun.*, vol. 9, no. 11, pp. 3380–3390, Nov. 2010.

[60] G. Al-Habian, A. Ghrayeb, M. Hasna, and A. Abu-Dayya, "Threshold-based relaying in coded cooperative networks," *IEEE Trans. Veh. Technol.*, vol. 60, no. 1, pp. 1223–135, Jan. 2011.

[61] T. M. Duman and A. Ghrayeb, *Coding for MIMO Communication Systems.* Wiley & Sons, 2008.

[62] J. Jose, A. Ashikhmin, T. L. Marzetta, and S. Vishwanath, "Pilot contamination and precoding in multi-cell TDD systems," *IEEE Trans. Wireless Commun.*, vol. 10, no. 8, pp. 2640–2651, Aug. 2011.

[63] J. Hoydis, S. ten Brink, and M. Debbah, "Massive MIMO in UL/DL cellular systems: how many antennas do we need?" *IEEE J. Select. Areas in Commun.*, vol. 31, no. 2, pp. 160–171, Feb. 2013.

[64] S. L. H. Nguyen and A. Ghrayeb, "Precoding for multicell massive MIMO systems with compressive rank-q channel approximation," in *IEEE PIMRC*, London, UK, Sep. 2013.

[65] S. L. H. Nguyen and A. Ghrayeb, "Multicell precoding for downlink massive MIMO based on compressive rank-q channel sensing," *submitted to IEEE Trans. Commun.*, Jun. 2013.

[66] J. Haupt, W. U. Bajwa, G. Raz, and R. Nowak, "Toeplitz compressed sensing matrices with applications to sparse channel estimation," *IEEE Trans. Inform. Theory*, vol. 56, no. 11, pp. 5862–5875, Nov. 2010.

[67] R. S. Varga, *Geršgorin and His Circles, ser. Springer Series in Computational Mathematics*. Berlin, Germany: Springer-Verlag, 2004, no. 36.

[68] W. Xu and B. Hassibi, "Efficient compressive sensing with deterministic guarantees using expander graphs," in *Proc. IEEE ITW*, Tahoe City, CA, USA, Sep. 2007, pp. 414–419.

[69] X. Jiang, Y. Yao, and L. Guibas, "Stable identification of cliques with restricted sensing," in *Proc. NIPS*, Dec. 2009.

[70] F. Parvaresh and B. Hassibi, "Explicit measurements with almost optimal thresholds for compressed sensing," in *Proc. IEEE ICASSP*, Las Vegas, NV, USA, Mar./Apr. 2008, pp. 3853–3856.

[71] R. A. DeVore, "Deterministic construction of compressed sensing matrices," *Journal of Complexity*, vol. 23, no. 4–6, pp. 918–925, Aug.–Dec. 2007.

[72] F. Gao, R. Zhang, and Y.-C. Liang, "Optimal channel estimation and training design for two-way relay networks," *IEEE Trans. Commun.*, vol. 57, no. 10, pp. 3024–3033, Oct. 2009.

[73] G. Gui, Z. Chen, Q. Meng, Q. Wan, and F. Adachi, "Compressed channel estimation for sparse multipath two-way relay networks," *International Journal of the Physical Sciences*, vol. 6, no. 12, pp. 2782–2788, Jun. 2011.

[74] T. Matsumoto, *Iterative (Turbo) Signal Processing Techniques for MIMO Signal Detection and Equalization*. Smart Antenna, State-Of-the-Art, EURASIP Book Series on Signal Processing and Communications, Hindawi, 2005.

[75] P. H. Tan and L. K. Rasmussen, "Asymptotically optimal nonlinear MMSE multiuser detection based on multivariate gaussian approximation," *IEEE Trans. Commun.*, vol. 54, no. 8, pp. 1427–1438, Aug. 2006.

[76] Y. Zhu, D. Guo, and M. L. Honig, "A message-passing approach for joint channel estimation, interference mitigation, and decoding," *IEEE Trans. Wireless Commun.*, vol. 8, no. 12, pp. 6008–6018, Dec. 2009.

[77] P. Schniter, "A message-passing receiver for BICM-OFDM over unknown clustered-sparse channels," *IEEE J. Select. Topics in Signal Process.*, vol. 5, no. 8, pp. 1462–1474, Dec. 2011.

[78] F. R. Kschischang, B. J. Frey, , and H.-A. Loeliger, "Factor graphs and the sum-product algorithm," *IEEE Trans. Inform. Theory*, vol. 47, no. 2, pp. 498–519, Feb. 2001.

[79] N. Letzepis and A. Grant, "Bit error rate estimation for turbo decoding," *IEEE Trans. Commun.*, vol. 57, no. 3, pp. 585–590, Mar. 2009.

[80] B. Raaf, W. Zirwas, K.-J. Friederichs, E. Tiirola, M. Laitila, P. Marsch, and R. Wichman, "Vision for beyond 4G broadband radio systems," in *Proc. IEEE PIMRC*, Toronto, Canada, Sep. 2011, pp. 2369–2373.

[81] J.-A. Tsai, R. M. Buehrer, and B. D. Woerner, "The impact of AOA energy distribution on the spatial fading correlation of linear antenna array," in *Proc. IEEE VTC*, May 2002, pp. 933–937.

[82] H. Q. Ngo, T. L. Marzetta, and E. G. Larsson, "Analysis of the pilot contamination effect in very large multicell multiuser MIMO systems for physical channel models," in *Proc. IEEE ICASSP*, Prague, May 2011.

[83] H. Jin, D. Gesbert, M. Filippou, and Y. Liu, "A coordinated approach to channel estimation in large-scale multiple-antenna systems," *IEEE J. Select. Areas in Commun.*, vol. 31, no. 2, pp. 264–273, Feb. 2013.

[84] S. L. H. Nguyen, A. Ghrayeb, and M. Hasna, "Iterative compressive estimation and decoding for network-channel-coded two-way relay sparse ISI channels," *IEEE Commun. Letters*, vol. 16, no. 12, pp. 1992–1995, Dec. 2012.

[85] M. Biguesh and A. B. Gershman, "Training-based MIMO channel estimation: a study of estimator tradeoffs and optimal training signals," *IEEE Trans. Signal Process.*, vol. 54, no. 3, pp. 884–893, Mar. 2006.

[86] E. J. Candes and Y. Plan, "Tight oracle inequalities for low-rank matrix recovery from a minimal number of noisy random measurements," *IEEE Trans. Inform. Theory*, vol. 57, no. 4, pp. 2342–2359, Apr. 2011.

[87] M. Rudelson and R. Vershynin, "Smallest singular value of a random rectangular matrix," *Communications on Pure and Applied Mathematics*, vol. 62, no. 15, pp. 141–155, Dec. 2009.

[88] M. Davenport, "Sub-gaussian random variables," *Connexions: http://cnx.org/content/m37185/1.6*, Apr. 2011.

[89] T. Tao, *Topics in Random Matrix Theory, Graduate Studies in Mathematics.* AMS, 2012, vol. 132.

[90] S. L. H. Nguyen and A. Ghrayeb, "Compressive sensing-based channel estimation for massive multisuer MIMO systems," in *Proc. IEEE WCNC*, Shanghai, Apr. 2013, pp. 3119–3124.

[91] T. D. Bie and N. Cristianini, "Fast SDP relaxations of graph cut clustering, transduction, and other combinatorial problems," *Journal of Machine Learning Research*, vol. 7, pp. 1409–1436, Dec. 2006.

[92] M. Grant and S. Boyd, "CVX: Matlab software for disciplined convex programming, version 2.0 beta," http://cvxr.com/cvx, Sep. 2012.

[93] M. Grant and S. Boyd, "Graph implementations for nonsmooth convex programs," in *Recent Advances in Learning and Control*, ser. Lecture Notes in Control and Information Sciences. Springer-Verlag Limited, 2008, pp. 95–110, http://stanford.edu/ boyd/graph_dcp.html.

[94] T. Roh, "Interior-point algorithms for sum-of-squares optimization of multidimensional trigonometric polynomials," in *Proc. IEEE ICASSP*, 2007, pp. 905–908.

[95] P. Jain, R. Meka, and I. S. Dhillon, "Guaranteed rank minimization via singular value projection," in *Proc. NIPS*, Vancouver, Canada, Dec. 2010, pp. 937–945.

[96] J. P. Haldar and D. Hernando, "Rank-constrained solutions to linear matrix equations using powerfactorization," *IEEE Signal Process. Letters*, vol. 16, no. 7, pp. 584–587, Jul. 2009.

[97] M. P. Holmes, A. G. Gray, and C. L. Isbell, "Fast SVD for large-scale matrices," in *Workshop on Efficient Machine Learning at NIPS*, 2007.

[98] K. Li, C. Ling, and L. Gan, "Deterministic compressed-sensing matrices: Where Toeplitz meets Golay," in *Proc. ICASSP*, Prague, Czech Republic, May 2011.

[99] D. Baron, S. Sarvotham, and R. G. Baraniuk, "Bayesian compressive sensing via belief propagation," *IEEE Trans. Signal Process.*, vol. 58, no. 1, pp. 269–280, Jan. 2010.

[100] S. D. Babacan, M. Luessi, R. Molina, and A. K. Katsaggelos, "Sparse bayesian methods for low-rank matrix estimation," *IEEE Trans. Signal Process.*, vol. 60, no. 8, pp. 3964–3977, Aug. 2012.